MIXED CONVECTION HEAT TRANSFER IN VERTICAL, HORIZONTAL, AND INCLINED PIPES

by

ANTHONY LAGANA

Department of Mechanical Engineering
McGill University
Montreal, Canada

A Thesis submitted to the Faculty of Graduate Studies and Research
in partial fulfillment of the requirements for the degree
of Master of Engineering

© August 28, 1996

National Library of Canada
Acquisitions and Bibliographic Services
395 Wellington Street
Ottawa ON K1A 0N4
Canada

Bibliothèque nationale du Canada
Acquisitions et services bibliographiques
395, rue Wellington
Ottawa ON K1A 0N4
Canada

Your file Votre référence

Our file Notre référence

The author has granted a non-exclusive licence allowing the National Library of Canada to reproduce, loan, distribute or sell copies of this thesis in microform, paper or electronic formats.

L'auteur a accordé une licence non exclusive permettant à la Bibliothèque nationale du Canada de reproduire, prêter, distribuer ou vendre des copies de cette thèse sous la forme de microfiche/film, de reproduction sur papier ou sur format électronique.

The author retains ownership of the copyright in this thesis. Neither the thesis nor substantial extracts from it may be printed or otherwise reproduced without the author's permission.

L'auteur conserve la propriété du droit d'auteur qui protège cette thèse. Ni la thèse ni des extraits substantiels de celle-ci ne doivent être imprimés ou autrement reproduits sans son autorisation.

0-612-29607-5

Canada

ABSTRACT

An experimental apparatus was designed and constructed for the study of laminar mixed convection heat transfer in vertical, horizontal and inclined tubes. The working fluid was distilled water, with bulk temperatures in the range of 8 °C to 31 °C.

An innovative design allows, for the first time, flow visualization over the entire heated portion of the test section. The key element of this design is a thin, electrically conductive gold-film heater suitably attached to the outside surface of a plexiglas pipe: the gold film is approximately 80% transparent to electromagnetic radiation in the visible wavelength band. This test section was mounted inside a transparent vacuum chamber to insulate it from the environment. A dye injection technique was used to visualize the mixed-convection flow patterns. The apparatus was also designed and instrumented to allow the measurement of both circumferential and axial temperature variations over the heated tube.

The flow-visualization results revealed the following: (i) a steady recirculating flow pattern, followed by laminar flow instability in vertical tubes; (ii) steady spiralling flow patterns in inclined and horizontal tubes, that confirmed earlier numerical predictions. The temperature results agreed qualitatively with earlier published experimental and numerical data. Local and overall Nusselt numbers can be calculated using the data presented, but this is not within the scope of this thesis.

SOMMAIRE

Un nouveau appareil a été conçu et construit pour l'étude de transfer de chaleur en convection mixte laminaire dans des tuyaux verticaux, horizontaux et inclinés. Le fluide utilisé dans l'expérience était l'eau, de temperature moyenne entre 8 °C to 31 °C.

L'appareil permet, pour la première fois, de visualiser l'écoulement à travers la portion réchauffée d'un tuyau. Il comporte une section de chauffage dans laquelle un mince film d'or semi-transparent fournit un flux de chaleur uniforme tout en permettant la visualisation de l'écoulement. La section chauffée, à été ensuite fermée dans un conteneur evacué et transparent. Pour visualiser l'écoulement, de l'encre à été injecté dans le courant de fluide. L'appareil permet aussi la mesure de variations circomférenciales et axiales des temperatures à travers le tuyau réchauffé.

Les résultats obtenus ont révélés, premièrement, qu'une zone de recirculation existe dans l'écoulement des tuyau verticaux, suivit par l'instabilité laminaire, et, deuxièmement, que l'écoulement dans les tuyaux horizontaux et inclinés est en forme de spirale. Les résultats de ces expériences ont confirmés celles de simulations numériques publiées. Les temperatures mesurées étaient en accord qualitativement avec les données experimentales et numériques publiées. La calculation de nombres de Nusselt n'est pas inclue dans les objectifs de cette entreprise.

ACKNOWLEDGEMENTS

I would like to express my gratitude to my supervisor, Professor B. R. Baliga, for suggesting this interesting and challenging project, and for his help and guidance throughout the course of this work.

I would like to thank the Natural Sciences and Engineering Research Council of Canada (NSERC) for financially supporting this research in the form of a Post-Graduate Scholarship awarded to me, and through individual research and equipment grants awarded to Professor B. R. Baliga. The Department of Mechanical Engineering at McGill University granted me a teaching assistantship. The financial help provided by these two institutions was greatly appreciated.

I would like to gratefully acknowledge Alois Hueppin, the Superintendent of the Machine Tool Laboratory, and the Machine Tool Lab Technicians, Antonio Micozzi and Danen Chellan for machining the critical components of the experimental apparatus and their advice. I wish to thank Jack Kelly, and his technicians, Gary Savard, John Boisvert, and Roy Westgate for their technical assistance and advice. I am indebted to George Dedic and George Tewfic of the Instrument Laboratory; their expertise in electronics was invaluable. My sincere thanks go to Nabil Elkouh, my friend and colleague, for his constant help and very useful suggestions. Finally, I would like acknowledge my whole family for their love and support throughout this work.

TABLE OF CONTENTS

LIST OF TABLES

LIST OF FIGURES

NOMENCLATURE

SYMBOL	DESCRIPTION
C_p	specific heat at constant pressure
D	internal diameter of the pipe
E_c	Eckert number $[U_0^2/(q_w^{"}D/k)]$
Gr	Grashof number (based in heat flux, unless otherwise specified) $[\rho^2 g\beta q_w^{"} D^4/\mu^2 k]$
g	acceleration due to gravity, 9.8 m/s^2
h	heat transfer coefficient
I	electrical current applied to the heater
k	thermal conductivity of the fluid, unless otherwise specified
L	length of the heated section of the pipe
Nu	Nusselt number [hD/k]
m	mass flow rate
P_a	applied power to the heater [VI]
P_f	calculated power based on bulk temperature difference $[mC_p\delta T_b]$
Pe	Peclet number [RePr]
Pr	Prandtl number $[\mu C_p/k]$
q	a constant equal to 1.894816
$q_w^{"}$	heat flux applied to the outer surface of the plexiglas pipe

p	pressure
p^*	non-dimensional pressure (see section 2.2.1)
r	radial coordinate
r^*	non-dimensional radial coordinate [r/D]
Re	Reynolds number [$\rho U_0 D/\mu$]
t	time
t^*	non-dimensionalized time [tU_0/D]
T	temperature
T_b	bulk temperature
T_{bi}	inlet bulk temperature
T_{bo}	outlet bulk temperature
T_m	temperature at which water attains its maximum density (4.029325°C)
T_0	reference temperature in the Boussinesq approximation
U	velocity
U_0	mean velocity through the test section
U^*	non-dimensional velocity [U/U_0]
V	voltage applied to the heater; also velocity
z	axial coordinate
z^*	non-dimensional axial coordinate [z/D]

GREEK SYMBOLS

α	tube's angle of inclination, measured with respect to the horizontal
α_t	a constant equal to 9.297173×10^{-6} (°C)$^{-q}$
ß	volumetric thermal expansion coefficient
δT_b	difference between the outlet and inlet bulk temperatures
Θ	circumferential coordinate
Θ^*	dimensionless temperature $[(T_0 - T)/(q_w'' D/k)]$
ϑ^*	dimensionless temperature $[\,\lvert T_m - T \rvert /(q_w'' D/k)]^q$
μ	dynamic viscosity
ρ	density
ρ_m	maximum density of water (999.9720kg/m^3)
ρ_0	density at T_0

SUBSCRIPTS

b	bulk
i	inlet
o	outlet
0	denotes a reference or mean value
w	wall
r	radial component
Θ	circumferential component
z	axial component

CHAPTER 1

INTRODUCTION

1.1 AIMS AND MOTIVATION

The primary objective of the work presented in this thesis was to design, construct and demonstrate the use of an experimental apparatus for the study of laminar mixed convection heat transfer in vertical, horizontal, and inclined tubes of circular cross section. The working fluid was distilled water. The innovative aspect of the work is a design that allows, for the first time, flow visualization over the entire heated portion of the tubes. The apparatus was also designed and instrumented to allow the measurement of both circumferential and axial temperature variations over the heated tubes.

The experimental technique used in this work is based on a thin, semi-transparent, electrically conductive gold-film heater, glued on the outside surface of a plexiglas pipe, and dye injection. In order to ascertain the capabilities of this technique, flow visualization studies were undertaken to obtain qualitative information on upward mixed convection flows in vertical, horizontal and inclined tubes, subjected to an essentially uniform heat flux (UHF) boundary condition. In vertical tubes, these studies revealed the existence of a steady recirculating flow region, followed by regions of ordered and disordered laminar instability. Similar findings have been reported by Bernier and Baliga

[1992a]. In inclined tubes, visual observations of the behaviour of the flow over the entire heated section of the tubes have not been reported in the published literature; thus, the inclined-tube flow visualization results presented in this thesis constitute one of the original contributions of this work.

A number of researchers have used electrically heated thin gold films as essentially transparent sources of uniform heat flux. For example, Baughn et al. [1985] and Hippensteele et al. [1983, 1985] used such films in experimental investigations of forced convection heat transfer in air. Neill [1989] explored the possibilities offered by the gold film technique in the context of steady, laminar natural convection in air. The work of Bernier and Baliga [1992a] represents the first use of this technique with water as the working fluid. They used it to study mixed convection in upward flow of water in vertical tubes. In their design, the gold film is glued to the inside surface of a plexiglas tube, in order to minimize the influence of heat conduction in the wall of the tube. However, their design makes it very difficult to achieve a robust and reliable contact between the gold film and the copper electrodes, that are used to supply electric power to the film. Thus, Bernier and Baliga [1992a] experienced rather frequent, and time consuming, failures of the gold film in their experimental work. One of the aims of this work is to improve the design of Bernier and Baliga [1992a]. Another aim is to extend their results by undertaking experiments with not only vertical tubes, but also inclined and horizontal tubes.

The experimental data obtained in this work could be used to calculate local Nusselt numbers. However, this calculation would require (i) an accurate assessment of wall-conduction redistribution of the heat flux applied via the gold-film heater, possibly using complementary numerical simulations; and (ii) precise inputs of the thermal resistance of the double-sided adhesive tape and the gold film on the outside surface of the plexiglas tube. These tasks are not within the scope of this thesis. Rather, they are suggested as an extension of this work. It should also be noted that fully-developed conditions were not achieved in any of the cases considered here. Hence, overall Nusselt numbers would be case-specific and not particularly useful, so they are not reported in the thesis.

Mixed convection heat transfer is commonly encountered in engineering equipment and in the environment. One example is closed-loop thermosyphons (Japkise, 1973; Bernier and Baliga, 1992c). Other examples include flows in tubes mounted inside flat-plate solar energy collectors (Cheng, 1972b) and in the emergency cooling of nuclear reactors (Zvirin, 1981). The design of such equipment is a multiparameter problem that is best tackled by an astute combination of computer simulations and focused experiments, before the building of prototypes. The experimental apparatus that is the focus of this work is intended to facilitate such complementary experimental/numerical approaches to the design of equipment that involves mixed convection heat transfer.

1.2 INNOVATIVE FEATURES OF THE EXPERIMENTAL APPARATUS

As a part of his doctoral work, M.A. Bernier [1991] designed and constructed an experimental apparatus to study laminar, mixed convection heat transfer in vertical tubes (Bernier and Baliga, [1992a]), with distilled water as the working fluid. That apparatus was later decommissioned and dismantled because of new research priorities and the opening of a new Heat Transfer Laboratory in the Department of Mechanical Engineering at McGill University. The goal in this work was to improve the apparatus designed by Bernier [1991]. In particular, the aim was to make the new apparatus more durable and more versatile than that built by Bernier. Some of the improved features of the new apparatus are briefly discussed in this section.

One of the key objectives in this study was the improvement of a translucent heater that was designed and constructed by Bernier [1991]. In both this study and that of Bernier [1991], a thin semi-transparent, electrically resistive, gold-film was employed to heat a transparent plexiglass tube. In the present study, the film was glued to the *outer* surface of the plexiglass pipe. Bernier [1991], on the other hand, had glued the film to the *inner* surface of the plexiglass tube, allowing it to come into direct contact with the fluid flow and minimize heat loss and conduction redistribution within the tube wall [Bernier and Baliga, 1992a]. However, with Bernier's design, it is very difficult to construct a durable heater, for the following reason: it was necessary to ensure that the two copper electrodes, which were used to power the heater film, did not protrude into

the tube, since its cross-sectional area had to be kept constant. This made it difficult to establish firm and robust contact between the electrodes and the heater film. Thus, the small, but significant, differential thermal expansions of the tube, electrodes and its support structure were enough to break portions of the delicate contact between the electrodes and the heater film. Such breaks decreased the contact area, increased total current density, and caused the film to burn frequently, without warning.

In the present apparatus, the gold-film is glued onto the *outer* surface of the plexiglass pipe, allowing the two copper electrodes to be firmly fastened to it. During the course of the *entire* investigation, burning of the film did not occur. Since the gold-film is glued to the outer surface of the tube, however, conduction redistribution of the applied heat flux in the tube wall is more appreciable than that in Bernier's apparatus. Heat conduction in the walls of tubes conveying fluids, however, has been given ample attention in the literature (Faghri, [1980]; Bernier and Baliga, [1992]; Heggs, [1990]; Laouadi, [1994]), and it is relatively straightforward to account for in numerical simulations. Furthermore, with proper selection of materials and dimensions, the effects of wall conduction can be minimized.

A second enhancement of the apparatus designed by Bernier [1991] was the construction of a transparent vacuum chamber that served to insulate the heated pipe. Bernier and Baliga [1991] used opaque insulation, which was momentarily removed from a portion of the heated pipe-section in order to carry out flow visualization. The

transparent vacuum chamber, incorporated in the present design, allows continuous visualization of flow over the entire length of the uniformly heated tube, something that has not been done prior to this investigation. However, the implementation of this feature of the apparatus required special care in the design of the film heater and the procedures that were used to fix it to the outer surface of the tube, in order to ensure that the film could operate safely in vacuum. Details of the special design are presented later in the thesis (chapter 3).

A third improvement was the mounting of the uniformly heated tube onto an inclinable platform. In all previously published works on laminar mixed convection heat transfer in inclined tubes, opaque pipes were used. Thus there is little or no literature on flow visualization in this area. The translucent heater, inclinable platform, and transparent insulation used in the current apparatus provide an opportunity to fill this void in the literature and enhance the understanding of the aforementioned flows.

1.3 SYNOPSIS OF RELATED INVESTIGATIONS

The purpose of this literature review is to highlight important aspects and findings of previous studies in the area of combined free and forced convection heat transfer in tubes. The review is organized into three categories: the first, second and third of these categories pertain to studies of fluid flow and mixed convection heat transfer in vertical, horizontal, and inclined tubes, respectively. Each of the three above-mentioned categories

is divided into two sub-sections: the first presents experimental studies in the area, while the second treats numerical and theoretical analyses. A summary of the experimental investigations, that highlights their salient features, is presented in Table 1.1.

1.3.1 Vertical Tubes

The results of excellent work on mixed convection heat transfer was published in the early 1940's (Martinelli and Boelter, 1942). Since then, it has been the subject of many investigations, and publications on the subject are quite abundant. Jackson et al. (1989) have provided a comprehensive review that spans fifty years of research and includes works on laminar and turbulent mixed convection in tubes, as well as the transition between these flow regimes.

1.3.1.1 Experimental Investigations

Scheele, Rosen and Hanratty [1960] investigated the effect of natural convection on the transition to turbulence of upward and downward flow of water in a vertical pipe of circular cross-section. A dye injection technique was employed to visualize the flow, and experiments were conducted in a pipe that was subjected to either a uniform wall heat flux or a constant wall temperature. Their Grashof numbers were based on the heat flux to the fluid (for the uniform wall heat flux case), or the difference between the temperatures of the pipe's outer wall and the water at its inlet plane (for the constant wall

temperature case). The flow was allowed to become hydrodynamically fully developed before entering the heated section of the pipe. In each experimental run, they fixed the Grashof number and then recorded the Reynolds number at which transition occurred.

For upward and downward flow, Scheele et al. [1960] reported the occurrence of transition at values of Reynolds numbers that are far lower than those in the corresponding forced convection case, when the Grashof number was high enough to cause the onset of flow reversal. Two years later, Scheele and Hanratty [1962] performed a more extensive study of uniformly heated pipes. Similar experiments were run, but four different values of the length-to-diameter (L/D) ratio were used, as opposed to only one as in their first study. The L/D values were 114 (used by Scheele et al. [1960]), 305, 610 and 762. For upward flow, they reported that, in some cases, the pipe needed to be long enough for small fluctuations in the flow to develop into full scale turbulence. For downward flow, they reported, as did Scheele et al. [1960], that transition to turbulence was initiated by a flow reversal region that appeared near the pipe wall.

It is important to note that Scheele et al. [1960] and Scheele and Hanratty [1962] employed opaque tubes in their study of laminar-turbulent transition in uniformly heated pipes. The motion of the dye could, therefore, only be observed in the vicinity of the outlet plane of the heated sections of their pipes, thus preventing them from visualizing the flow pattern inside most of the heated length.

Metais and Eckert [1964] surveyed the available literature, and presented regime maps for laminar and turbulent flows in both vertical and horizontal tubes with either uniform wall heat flux or constant wall temperature. The parameter on the abscissa of their two-dimensional regime maps is the product of the Grashof number, Gr, based on the difference between the pipe-wall and the fluid bulk temperatures, the Prandtl number, Pr, and the diameter-to-length ratio, D/L; the parameter on the ordinate is the Reynolds number, Re. Their flow regime maps indicate the mode of heat transfer (forced, mixed or free convection) that is dominant for a given value of Re and GrPr(D/L). As expected, free convection dominates when the value of GrPr(D/L) is sufficiently large, whereas an increase in the value of Re augments the effect of forced convection.

Brown and Gauvin [1965] investigated mixed convection heat transfer in upward (aiding) flow of air through a uniformly heated stainless steel tube. The Reynolds number, Re, in their experiment was varied from 385 to 4930, and the Grashof number, Gr, based on the temperature difference between the pipe wall and the fluid in the centre of the tube, ranged from approximately $2X10^5$ to $9X10^6$. The Prandtl number, Pr, was essentially constant at 0.7. For both turbulent and laminar flow, they plotted experimentally determined Nusselt numbers, Nu, versus Gr values, for each value of Re investigated.

The results that Brown and Gauvin [1965] obtained for turbulent flow agreed reasonably well with published correlations for Nu. The heat input to the fluid was quite

high (wall temperatures of up to 950°C were measured), and, consequently, the Grashof numbers were high, thus, their results resemble those published for the case of turbulent pure free convection, with the same Gr and Pr values. Their laminar flow results, however, seem quite sensitive to the particular experimental set-up and do not agree well with published correlations. The causes of such discrepancies are: (i) the thermal boundary condition at the wall was not exactly one of uniform heat flux, since it was necessary for them to leave a space between their heaters wherever a thermocouple port was present; and (ii) the velocity profile of the air at the inlet section of their tube was flat (top-hat shape) as opposed to the parabolic profile that characterized the fully-developed inlet conditions in the works of other researchers.

Using the same experimental apparatus, Brown and Gauvin [1965] published a companion study of mixed convection heat transfer in downward (opposing) flow of air through a uniformly heated tube. The Reynolds number, Re, in their work was varied from 380 to 6900, and the Grashof number, Gr, based on the temperature difference between the wall and the fluid in the centre of the tube, ranged from $1.8X10^5$ to $7.3X10^6$. The Prandtl number, Pr, was once again essentially fixed at 0.7.

As in their study of mixed convection in upward flow, Brown and Gauvin [1965] plotted experimentally determined Nusselt numbers versus Gr values, for each value of Re investigated. For turbulent downward flow, the results they obtained agreed very well with published correlations for turbulent mixed convection in vertical tubes, but deviated

by as much as 45% from the published correlations for the turbulent pure free convection case with the same Gr and Pr values. For laminar downward flow, their results did not agree well with published correlations. The causes of such discrepancies are the same as those mentioned above for their laminar, upward-flow experiments.

Barozzi and Pagliarini [1984] experimentally investigated wall conduction effects on the laminar flow of water in a uniformly heated copper pipe. Their investigation covered a range of Reynolds numbers from 500 to 1900, and relatively low values of applied heat flux, ranging from approximately 3 to 5.4 kWm^{-2}. Results were reported for flow with a fully developed velocity profile at the inlet of the heated section of the pipe, as well as for flows with only partially developed inlet velocity profiles.

Barozzi and Pagliarini [1984] observed that close to the inlet section of the heated pipe, axial wall conduction effects appreciably altered the temperatures in the wall and fluid (compared to those in corresponding cases without axial wall conduction). In addition, their results showed that having a partially developed inlet velocity profile, as opposed to a fully developed one, was only of minor consequence. Their experimental data was used to verify the numerical results they obtained using a finite-element model of their test cases. The following year, Barozzi and Pagliarini [1985] published a numerical study of laminar, forced convection heat transfer in the presence of conduction in a pipe with a uniform heat flux applied to its outer surface. Their results showed that the heat flux on the inner surface of the pipe is approximately uniform when the wall-to-

fluid thermal conductivity and the thickness-to-pipe diameter ratios are small, and the Peclet number is high.

Bernier and Baliga [1992a] developed an experimental technique to visualize the flow of water in a pipe subjected to a uniform wall heat flux. The technique involved the use of a transparent plexiglass pipe, dye injection and a thin, semi-transparent, gold film on a plastic (Mylar) base. The gold/Mylar film was glued to the inside of the pipe, with its gold side facing the plexiglass wall, in order to protect it from the eroding effects of the water. Two copper electrodes were connected to the ends of the film. Electrical current was supplied to the gold-film, through the copper electrodes and ohmic dissipation generated an approximately uniform heat flux. During experiments, a fluorescent dye was injected upstream of the heated portion of the pipe. This dye was illuminated with black light in order to visualize the flow pattern.

Bernier and Baliga [1992a] were able to experimentally observe the presence of recirculation cells and compare them to their numerical predictions: there was good qualitative agreement between the two results. Near the exit of their heated pipe-section, they reported unsteady wave-like motion of the dye filament, something that had not been observed in uniform-heat-flux experiments prior to their study. As was mentioned earlier in this chapter, one of the aims of this work is to enhance and extend the work of Bernier and Baliga [1992a].

1.3.1.2 Numerical and Theoretical Analyses

Theoretical work on mixed convection heat transfer in vertical tubes of circular cross-section was first published by Martinelli and Boelter [1942]. They analyzed fully developed laminar flow in which the density was assumed to vary linearly with temperature. The flow was subjected to a uniform-wall-temperature boundary condition, and the velocity immediately adjacent to the pipe-fluid interface was assumed to vary linearly with distance from the wall. These assumptions rendered the problem amenable to mathematical analysis, and they obtained an explicit equation for the Nusselt number as a function of the Grashof number, Prandtl number, and diameter to pipe-length ratio. The equation obtained by Martinelli and Boelter [1942] was remarkably successful, predicting experimental data with an accuracy of $\pm 20\%$.

Tanaka et al. [1987] used a k-ϵ model of turbulence for low Reynolds number flows to investigate turbulent mixed convection heat transfer in a uniformly heated vertical tube. The flow considered was thermally and hydrodynamically fully developed. The Reynolds number, Re, in their investigation ranged from 1000 to 25 000, and the Grashof number (based on the difference between film and bulk temperatures), Gr, was varied to cover all three regimes of convection: forced, mixed and natural. A flow regime map, similar to that of Metais and Eckert [1964], was plotted, indicating which mode of convection was dominant for a given Re and Gr.

Tanaka et al. [1987] reported lower Nusselt numbers in mixed convection turbulent flows than in pure, forced convection flows of equal Reynolds number. This result was attributed to a sharp decrease in the production of turbulence close to the pipe wall, because of buoyancy effects. Consequently, the Nusselt number was lowered. Tanaka et al. [1987] also ran experiments at Reynolds numbers of 3000 and 5000 over a wide range of Grashof numbers, and the results agreed well with their numerical predictions.

Morton et al. [1989], numerically and experimentally investigated laminar mixed convection heat transfer in a vertical pipe with constant wall temperatures. They considered upward flow, hydrodynamically fully developed at the inlet, undergoing both heating and cooling in a pipe, with one section maintained at a temperature, T_B, warmer than the fluid inlet temperature, T_A, and another, maintained at a temperature, T_C, colder than the inlet temperature of the fluid. Two different cases were studied: in the first (case 1), the flow passed through the cooled section before the heated one, and, in the second (case 2), the flow passed through the heated section before the cooled one. In case 1, the Reynolds and Grashof numbers (based on the temperature difference, $T_A - T_C$) were both fixed, at 25 and 5000, respectively. In case 2, Re and Gr (based on $T_A - T_B$) were again both fixed, at 55 and -50 000, respectively.

Morton et al. [1989] compared their numerical predictions with experimental results. In both cases, a recirculation cell was obtained that began in the heated section

of the pipes. In case 1, the location and size of the recirculation zone was predicted very accurately. In case 2, the recirculation zone occurred further upstream than predicted. The discrepancy was attributed to the effects of axial wall conduction that existed in their experiments, but ignored in their numerical model. In case 1, the effects of axial wall conduction were not considerable because the water in the experiments passed through a cooled section before being heated. The extent of pre-heating of the flow, by heat conducted through the pipe wall, was more appreciable in case 2, where there was no cooling before it entered the heated section.

Jackson et al. [1989] published a thorough literature survey on numerical and experimental works on the subject of mixed convection heat transfer in vertical tubes of circular cross-section. Their survey included studies of both laminar and turbulent flows, of moderate Prandtl numbers, subjected to either a uniform wall temperature or a uniform wall heat flux. Buoyancy-aiding (upward) as well as buoyancy-opposing (downward) flows were considered.

The survey of Jackson et al. [1989] reported that in laminar, mixed convection, upward flow, the Nusselt numbers observed were greater than in the corresponding laminar, pure forced convection case. The reason for this finding was attributed to the increase in velocity of the fluid in the vicinity of the wall, enhancing the convective heat transfer there. In laminar, mixed convection downward flow, the opposite trend prevailed, due to the decrease in velocity near the wall, resulting in reduced convective

heat transfer and lower Nusselt numbers.

Regarding turbulent mixed convection flow, Jackson et al. [1989] reported unexpected trends. In upward flow, the Nusselt numbers were significantly lower than those for the corresponding turbulent, pure forced convection case. In downward flow, the Nusselt numbers were considerably higher than in the pure forced convection case. These unforeseen influences of buoyancy on heat transfer were first noticed in works on fluids near their thermodynamic critical points (Jackson et al., [1975]; Hall and Jackson, [1978]). In the earlier studies of turbulent mixed convection flow of air and water at atmospheric pressure, there was little indication of such results. One explanation suggested that, in the transition from laminar to turbulent flow, a significant modification of the shear stress distribution across the pipe may have caused the unexpected heat transfer results by affecting the production of turbulence. In this context, it is worth noting that as free convection becomes the dominant mode in turbulent, upward mixed convection heat transfer, the Nusselt number becomes higher than that for the corresponding turbulent, pure forced convection case.

Cotton and Jackson [1990] used a low Reynolds number k-ϵ model to investigate turbulent mixed convection in vertical tubes. They considered both ascending and descending, thermally developing flow in pipes that were uniformly heated or subjected to a constant wall temperature. Nusselt number results were plotted versus a "buoyancy parameter," $B_o = (8X10^4Gr)/(Re^{3.425}Pr^{0.8})$, that was varied over three orders of magnitude

(its value ranged from approximately 0.01 to 10).

Cotton and Jackson [1990] found that in downward flow, the Nusselt numbers were significantly higher than those for the corresponding turbulent forced convection case. In upward flow, the Nusselt numbers were considerably lower than those in the pure, forced convection case except when free convection was the dominant mode of heat transfer; in that instance, the Nu values were larger than those in the corresponding forced convection case. The numerical results of Cotton and Jackson [1990] agreed well with corresponding published experimental data, except those on descending flow dominated by natural convection.

Heggs et al. [1990] investigated the effects of wall conduction on mixed convection heat transfer in the flow of water through a vertical tube subjected to a constant outer wall temperature. They considered upward and laminar flow. The Reynolds number, Grashof number (based on the difference between the temperatures of the water at the inlet, and the outer wall of the pipe), and Prandtl number were fixed at 50, -10 000, and 7, respectively. The wall to fluid conductivity ratio, K_r, was varied from 0.5 to 50, and the ratio of the outside to inside radii of the pipe, a/a^*, ranged from 1.1 to 1.4. Heggs at al. [1990] observed that at large values of K_r, a significant amount of heat was conducted upstream of the inlet, within the pipe wall. This axial conduction extended further upstream as the value of a/a^* increased. It pre-heated the water in the tube, and caused flow reversal to occur further upstream than it would have in the

absence of axial wall conduction.

Bernier and Baliga [1992b] have published a numerical investigation of the effects of wall conduction on laminar mixed convection in upward flows through pipes that are uniformly heated on their outer surfaces. The Prandtl number was fixed at 5, and the Grashof number, based on wall heat flux, was set at 5000. Two values of Reynolds numbers were considered: 1 and 10. They presented results for four different values of solid-to-fluid thermal conductivity ratio, K, and three different values of wall thickness-to-pipe diameter ratio, δ. They also conducted a complementary experimental investigation to which they compared their numerical results.

Bernier and Baliga [1992b] found that a significant portion of the applied heat flux on the outside surface of the heated section could be redistributed by axial wall conduction into the upstream and downstream sections of the pipe. The magnitude of the heat lost to the upstream and downstream sections increased monotonically with increase of the solid-to-fluid thermal conductivity ratio and wall thickness-to-pipe diameter ratio. They also found that the axial wall conduction could significantly influence the velocity and temperature profiles inside the fluid. In one case ($Re = 1$, $K = 50$ and $\delta = 0.05$), the axial wall conduction affected the velocity field to such an extent that reversal of flow was observed upstream of the entrance of the heated section. Through flow visualization, Bernier and Baliga [1992b] experimentally verified the presence of flow reversal and the influence of wall conduction on it.

1.3.2 Horizontal Tubes

Work on mixed convection heat transfer in horizontal tubes of circular cross-section was well under way by the 1960's, and excellent experimental data was published by Mori [1966], Petukhov [1969], and others. The following literature review offers a selection of the many papers available on the subject, focusing on important findings and aspects relevant to the current investigation.

1.3.2.1 Experimental Investigations

Jackson et al. [1961] investigated mixed convection heat transfer in a horizontal tube subjected to a constant wall temperature. The working fluid was air and the flow was both hydrodynamically and thermally developing. The product of the Grashof number (based on the log-mean temperature difference) and Prandtl number, GrPr, ranged from $1.1X10^6$ to $2.2X10^6$. The Graetz number, Gz, was varied from 60 to 1300. A correlation for the laminar flow Nusselt number as a function of GrPr and Gz was developed. Their results indicated that laminar-to-turbulent transition occurred at a Reynolds-Prandtl product, RePr, of approximately 2450. A correlation for the turbulent flow Nusselt number as a function of Re and Pr was also developed.

Brown and Thomas [1965] performed an experimental investigation of mixed convection heat transfer in laminar flow through horizontal tubes. The working fluid was

water, and a constant-wall-temperature boundary condition was used. The Reynolds number in their experiment was varied from 200 to 1500 and the Grashof number, based on the difference between the pipe wall and average fluid bulk temperatures, ranged from $4X10^4$ to $480X10^4$. They derived a new correlation for Nusselt number, as a function of the Graetz and Grashof numbers, that fit their water data to within $\pm 8\%$. Furthermore, their equation fit the majority of the published data, irrespective of fluid, to within $\pm 50\%$, which was comparable to the accuracy of the best previous correlations.

McComas and Eckert [1966] studied mixed convection heat transfer in air flowing through a horizontal tube with a constant wall heat flux. The flow was laminar and was allowed to become hydrodynamically fully developed before entering the heated section of the pipe. The Reynolds number in their experiment ranged from 100 to 900, and the Grashof number, based on the difference between pipe-wall and fluid bulk temperatures, was varied from approximately 0.1 to 1000.

McComas and Eckert [1966] reported higher Nusselt numbers than in the corresponding, pure, forced convection case. This was because the velocities near the wall of the tube were larger than in the corresponding forced convection case. The lighter, warmer fluid, near the heated wall, moved upward, whereas the colder fluid of higher density, in the central portion of the tube cross-section, moved downward. The superposition of this secondary flow onto the main flow resulted in a spiral trajectory of the fluid particles as they moved through the tube, ascending near the wall, toward the

top, and descending in the central portion. McComas and Eckert [1966] also observed that the length of the thermally developing section was approximately the same as that for the corresponding pure, forced convection case.

Mori et al. [1966] experimentally investigated mixed convection heat transfer in air flowing through a uniformly heated horizontal tube. Velocity and temperature profiles were measured in laminar and turbulent flows over a relatively wide range of the parameter ReRa (where Re is the Reynolds number and Ra is the Rayleigh number based on axial temperature gradient). Furthermore, the effects of buoyancy on the local Nusselt number, and the Reynolds number at which laminar-to-turbulent transition occurs (Re_{crit}) were studied.

When the product of the Reynolds and Rayleigh numbers (ReRa) was greater than $1x10^4$ and the flow was laminar, Mori et al. [1966] observed the secondary flows described by McComas and Eckert [1966]. Since the pipe-wall temperature was higher than the fluid bulk temperature, the fluid near the wall was warmer and lighter than the fluid nearer to the central portion of the tube, and it moved upward. Two upward flows along the pipe wall, one on either side of the vertical diametric surface, met at the top of the tube, and moved downward in its central portion. This created two symmetrical recirculation cells, or vortices, in the vertical cross-section of the tube, and were photographed by Mori and Futugami [1967]. The velocity and temperature profiles were, therefore, very different from those in the corresponding, pure, forced convection case.

The gradients of both these profiles were quite large near the pipe wall, and the locations of the maximum velocity and temperature shifted downward below the longitudinal axis of the tube.

For values of ReRa as low as $1X10^3$ in laminar flow, Mori et al. [1966] reported higher local Nusselt numbers than in the corresponding, pure, forced convection case. They proposed a correlation for the local Nusselt number as a function of ReRa. In addition, they observed that the non-dimensionalized, fully developed temperature and axial velocity profiles for different flows, with equal values of ReRa, collapsed onto the same curves. For turbulent flow, Mori et al. [1966] conducted similar experiments and found that the dominant mode of heat transfer was forced convection. The effect of the secondary flow on the temperature and velocity profile was very small, and essentially no effect on the Nusselt number was observed. Lastly, when the intensity of turbulence at the inlet of the pipe was low, Mori et al. [1966] found that the critical Reynolds number, Re_{crit}, decreased with increasing Rayleigh number, whereas, when the intensity of turbulence at the inlet was high, Re_{crit} increased with increasing Rayleigh number.

Shannon and Depew [1968] experimentally investigated mixed convection heat transfer in laminar flow of water through a horizontal tube with uniform wall heat flux. The flow was allowed to become hydrodynamically fully developed, and was maintained at approximately 0°C until it entered the heated section of the pipe. The water was, therefore, heated past its density inversion point as it flowed through the tube. The

Reynolds number, in their experiment, was varied from 120 to 2300, and local Grashof number, based on the difference between the pipe-wall and the fluid bulk temperatures, was varied up to $2.5x10^5$.

In the fully developed region, Shannon and Depew [1968] reported Nusselt numbers as much as 2½ times greater than in the corresponding pure, forced convection case. The difference between the pipe-wall and calculated fluid bulk temperatures was constant, as expected in fully developed flow. It should be noted that in the experimental runs at high Grashof numbers, the local Nusselt number, Nu, monotonically increased with axial distance along the tube. In the runs at low Grashof numbers, sizable experimental errors existed and no reliable conclusions were drawn. In the thermally developing region, Shannon and Depew [1968] obtained local Nu values that were very similar to that of the pure, forced convection case.

Petukhov et al. [1969] investigated mixed convection heat transfer in water flowing through a horizontal tube subjected to a constant wall heat flux. The Rayleigh number in their experiment, Ra, based on heat flux, ranged from $2X10^5$ to $4X10^5$, and the Reynolds number, Re, was varied from 50 to the critical value, Re_{crit}. Furthermore, the flow was allowed to become hydrodynamically fully developed before entering the heated test section. They found that the presence of mixed convection in horizontal tubes leads to higher values of the critical Reynolds number than in the corresponding, pure forced convection case. They also observed that the length of the thermally developing

section in the mixed convection flow was approximately the same as that for the corresponding, pure forced convection case.

In their investigation, Petukhov et al. [1969] also conducted experiments on mixed convection heat transfer in upward, flow of water through uniformly heated, vertical tubes. The Rayleigh number, based on longitudinal temperature gradient, ranged from 250 to 6500, and the Reynolds number, from 250 to Re_{crit}. Experiments were run with hydrodynamically fully developed flow at the inlet of the heated section, as well as with developing flow. In both cases, similar results were obtained. At some location downstream of the inlet, the wall temperature and the local Nusselt number were observed to vary in an "unexpected", but axially symmetric fashion. Petukhov et al. [1969] did not discuss the characteristics of that peculiar flow, but they were most probably observing the presence of flow reversal.

It is important to note that Petukhov et al. [1969] employed opaque tubes in their investigation, and inferred laminar-turbulent transition indirectly from significant changes, along the tube, in values of the local measured Nusselt number. Petukhov [1970] has published additional details in a comprehensive article on the study of forced convection heat transfer in turbulent pipe flow, in the series, "Advances in Heat Transfer".

Morcos and Bergles [1975] experimentally investigated mixed convection heat

transfer in laminar flow of water through uniformly heated horizontal tubes. The Rayleigh number in their experiment, based on the average wall-to-bulk fluid temperature difference, was varied from approximately $2X10^4$ to $1X10^6$, and the Reynolds number ranged from about 20 to 500. Results were obtained for two pipes: one made of stainless steel and the other made of glass. The product, $k_w t$, of the metal tube (where k_w is the thermal conductivity, and t is the wall thickness) was roughly seven times larger than that of the glass tube.

Morcos and Bergles [1975] reported that values of the Nusselt numbers, Nu, for mixed convection flows increased with increasing Rayleigh number, and were considerably higher than those in the corresponding, pure, forced convection case. Furthermore, they observed higher Nusselt numbers in the metal tube than in the glass tube, suggesting that Nu is affected by the product, $k_w t$. The Nusselt number was found to depend primarily on the Rayleigh number, but by using both ethylene glycol and water as working fluids, Morcos and Bergles [1975] also noticed a dependence of Nu on the Prandtl number of the fluid.

Abid et al. [1994] performed experimental and numerical investigations of laminar, mixed convection heat transfer in uniformly heated horizontal pipes. The working fluid was water, and the flow was allowed to become fully developed before entering the heated section. Using infrared thermography, they measured the temperature distribution in the pipe wall, and reported substantial circumferential variations. In any

given cross-section perpendicular to the longitudinal axis of the pipe, the temperature was a maximum at the top of the pipe and monotonically decreased to a minimum at the bottom. This result is due to the fact that warmer fluid moves up along the wall, whereas the relatively colder fluid moves down to replace it in the lower portion of the tube. The results of their numerical analysis confirmed their experimental observations, and also confirmed the existence of the secondary flows, described earlier by McComas and Eckert [1966] and photographed by Mori and Futugami [1967].

1.3.2.2 Numerical and Theoretical Analyses

Faris and Viskanta [1969] used perturbation analysis in terms of a power series of the ratio, Gr/Re^2 (where Gr is the Grashof number based on the bulk-to-wall temperature difference, and Re is the Reynolds number), to calculate the velocity and temperature fields of laminar flow inside a uniformly heated horizontal pipe. The flow under consideration was thermally and hydrodynamically fully developed, and the density was assumed to vary only in the buoyancy terms (the Boussinesq approximation). In their analysis, the individual influences of the ratio Gr/Re^2, the Prandtl number, Pr, and a parameter $\Gamma = PeGr_z/\sqrt{Re}$ (Pe is the Peclet number and Gr_z is a Grashof number based on the axial temperature gradient) were considered.

Faris and Viskanta [1969] obtained a distorted velocity field similar to the one described by McComas and Eckert [1966]: a spiral trajectory of the fluid particles,

ascending near the wall, toward the top, and descending in the central portion as they moved through the pipe. In any cross-section perpendicular to the longitudinal axis of the pipe, two symmetrical recirculation cells were reported, in which flow rose next to the pipe wall and descended in the pipe's central region. Furthermore, the temperature and velocity profiles obtained by the perturbation analysis agreed reasonably well with the experimental data of Mori et al. [1966]. Faris and Viskanta [1969] obtained values of the Nusselt number, Nu, that were substantially higher than in the corresponding pure, forced convection case. They also demonstrated, that the average Nu could be significantly influenced by Pr and Γ.

Newell and Bergles [1970] used a finite-difference, numerical technique with successive over (or under) relaxation of the dependent parameters to numerically investigate mixed convection heat transfer in horizontal pipes. The flow under consideration was laminar, thermally as well as hydrodynamically fully developed and subjected to a uniform wall heat flux. Axial wall conduction was ignored, but circumferential conduction in the pipe wall was included in their analysis. Results were obtained for two pipes: one whose thermal conductivity was the same as the fluid, and one whose thermal conductivity was infinitely large compared to that of the fluid.

Newell and Bergles [1970] obtained a flow pattern similar to the one described by Faris and Viskanta [1969], characterized by the spiral motion of the fluid particles as they moved through the tube. The velocity distributions were qualitatively similar to

those obtained by Mori et al. [1966]. When using the pipe with the thermal conductivity equal to that of the fluid, they found that the wall temperature was significantly higher at the top of the tube than it was at the bottom, as observed by Abid et al. [1994]. In addition, Newell and Bergles [1970] developed useful design correlations for Nusselt number, friction factor, and circumferential variation of wall temperature as functions of the Prandtl number, and the parameter $GrPr_w$, respectively: here, Gr is the Grashof number based on the difference between the average pipe-wall and fluid bulk temperatures, and Pr_w is the Prandtl number evaluated at the average pipe-wall temperature.

Faghri and Sparrow [1980] performed a numerical analysis of laminar, forced convection in a pipe. The Peclet number was low enough to make the axial conduction effects appreciable in the pipe wall as well as in the fluid itself. The pipe was subjected to a uniform wall heat flux. Furthermore, the wall of the pipe was relatively thin, so radial temperature variations across the thickness were negligible. The extent of axial heat conduction was governed by two parameters: the Peclet number, Pe, and a conduction parameter, ß, equal to the product of the solid-to-fluid thermal conductivity ratio and the thickness-to-radius ratio.

Faghri and Sparrow [1980] found that axial conduction in the wall carried a substantial amount of heat upstream into the unheated portion of the pipe for low values of Pe and large values of ß. This resulted in a preheating of both the wall and the fluid

in the upstream region, sometimes as far back as twenty radii from the entrance of the region subjected to the heat flux. Furthermore, they found that the local Nusselt number began to exhibit fully developed characteristics some distance upstream of the heated section of the pipe.

Huiren and Songling [1991] employed a low Reynolds number k-ϵ model to study the effect of inlet turbulence intensities on forced convection heat transfer in transitional pipe flow. A constant wall temperature boundary condition was used, and the flow at the inlet was laminar with a flat velocity profile. The values of the Reynolds number, Re, in their investigation, ranged from 1000 to 10000, and the inlet turbulence intensity, Tu_i, of the flow was varied from 0.1 to 8.0%. The pipe was long enough so that the flow, in all cases studied, could become fully developed.

The results obtained by Huiren and Songling [1991] indicated that flows with Reynolds numbers under 1850 do not undergo laminar to turbulent transition even when the inlet turbulence intensity is relatively large (Tu_i = 8.0%). For flows with Reynolds numbers greater than 2608 and lower than 4809, their numerical model indicated that the average Nusselt number varies appreciably with inlet turbulence intensity. When the Reynolds number was less than 2068, however, the average Nusselt number was not significantly influenced by the inlet turbulence intensities. Likewise, the Nusselt number for flows with Reynolds number greater than 4809 was unaffected by the inlet levels of turbulence intensity, and it could be calculated with commonly used correlations for

turbulent flow.

1.3.3 Inclined Tubes

Published work on mixed convection heat transfer in inclined, circular cross-section tubes dates from 1966, when Iqbal and Stachiewicz used perturbation analysis to calculate velocity and temperature fields for laminar, fully-developed, upward flow and uniform heat flux. Since then, the problem has been investigated experimentally by several research groups, but the published results cover a rather limited range of the independent parameters. The literature contains a comparable number of numerical studies, but once again, they are far from being exhaustive. In addition, one of the conclusions drawn by Iqbal and Stachiewicz [1966] is supported by one publication, but contradicted by four others.

1.3.3.1 Experimental Investigations

Sabbagh et al. [1976] investigated mixed convection heat transfer in laminar, upward flow of air through a circular cross-section copper tube with constant wall heat transfer rate per unit axial length and circumferentially uniform wall temperature. The effect of tube inclination was studied for slope angles (α) ranging from the horizontal orientation ($\alpha = 0°$) to the vertical ($\alpha = 90°$). Their Reynolds number, Re, ranged from 740 to 1204, but their Rayleigh number, Ra, based on axial temperature gradient, was

fixed at 40.8.

For $\alpha = 0°$, Sabbagh et al. [1976] found that both the velocity and temperature profiles in the tube were influenced significantly by the secondary flow resulting from the effects of buoyancy. The maximum velocity and temperature occurred at positions below the tube centre line. As they increased the slope angle, however, both profiles progressed toward axial symmetry and the effect of the secondary flow lessened. When the tube was in the vertical position (α=90°), the velocity and temperature profiles were axially symmetric to within experimental accuracy. They also found that, for fixed values of Re and Ra, the Nusselt number decreased monotonically with tube inclination, and, therefore, the maximum Nusselt number occurred in the horizontal position.

Barozzi et al. [1985] performed a similar investigation of laminar, upward flow of water through a circular copper tube with the same thermal boundary conditions: uniform wall heat transfer rate per unit axial length and circumferentially constant wall temperature. The effect of tube inclination was studied for angles ranging from the horizontal position ($\alpha = 0°$) to $\alpha = 60°$, and they too observed a monotonic drop in the Nusselt number with increasing slope angle, α.

Barozzi et al. [1985] found that the influence of the inclination angle on the Nusselt number decreased as the Reynolds number was varied from, approximately, 500 to 1500. Due to the rather narrow range of Rayleigh number (Ra) explored, however,

they did not draw any conclusions regarding the dependence of Nusselt number on Ra. In their experiment, the influence of wall conduction effects on the heat transfer characteristics was very difficult to estimate because of the peculiar geometry of the test section. Two copper fins, containing grooves in which electrical wires were inserted, were brazed to their tube. The fins were insulated along with the tube; their purpose was to provide the electrical current that was used to heat the test section.

Lavine et al. [1989] have also performed an experimental investigation of mixed convection in a circular, inclined tube. Unlike the two previous studies, however, the working fluid in their experiment (water) flowed in a downward (buoyancy-opposing) direction, and a constant-wall-temperature boundary condition was used at the outer wall of the tube. The angle of inclination was varied from $\alpha = 0°$ to 80°, and the Reynolds number, from 100 to 3500. The Grashof number, based on the difference between the temperatures of the outer wall of the tube and the water at the inlet, was varied from 1.0×10^6 to 7.0×10^6. Their results revealed the presence of flow reversal regions (except at $\alpha = 0°$) near the pipe wall and an optimal tilt angle, generally small (less than twenty degrees), that produced a maximum flow reversal length. They also observed that the inclination of the tube influenced the transition to turbulence.

For a tilt angle, α, of 10° and Grashof number at least 5.12×10^6, Lavine et al. [1989] observed transition to turbulence when the Reynolds number was as low as 300. For lower values of Grashof number and the same tilt angle, the transition phenomenon

behaved as it would have in the pure forced convection case. As they increased the angle of inclination to $\alpha = 45°$ and 80°, however, transition to turbulence was observed when Re was as low as 300 regardless of the Grashof number. This early occurrence of turbulence was believed to be induced by vortical motion generated in the interface between the flow reversal region and main flow. Early transition occurred when the vortical motion was observed to propagate into the main flow.

Leong et al. [1991] studied mixed convection in laminar flow of water through an inclined, circular tube in a buoyancy-opposing direction. The flow was allowed to become hydrodynamically fully developed before entering the heated test section. A uniform heat flux was imposed on the tube wall, axially as well as circumferentially. Two values of Grashof number, based on wall heat flux, were used. The Reynolds number was varied between 432 and 1296. Their investigation considered only small angles of inclination, where, in accordance with the findings of Lavine et al. [1989], they expected the strongest flow reversals.

Through flow visualization, Leong et al. [1991] confirmed the presence and strength of flow reversals. For fixed values of Gr and Re, their experiments indicated the existence of a minimum circumferentially-averaged Nusselt number when the angle of inclination was between 0° and 10°, corresponding to the range of tilt angles in which the flow reversal length was the largest. Since their test section was opaque, however, flow visualization was only performed in an unheated transparent portion of the tube

(where the flow developed before entering the heated section), and was carried out solely to determine the extent of the flow reversals.

1.3.3.2 Numerical and Theoretical Analyses

Using perturbation analysis in terms of power series of Rayleigh numbers, Iqbal and Stachiewicz [1966] calculated the velocity and temperature fields in upward, laminar flow inside an inclined circular tube with axially and circumferentially uniform heat flux. Fluid properties were assumed, constant except for the variation of density in the buoyancy terms (the Boussinesq approximation) and only hydrodynamically and thermally fully developed flow was considered. In their analysis, the Rayleigh number was the dominant parameter affecting the velocity field, temperature field and Nusselt number, but the Prandtl and Reynolds numbers also influenced these results independently.

The results of Iqbal and Stachiewicz [1966] revealed temperature and velocity profiles qualitatively similar to those found by Sabbagh et al. [1976]. Maximum temperature and velocity occurred at positions below the centre line of the tube, in agreement with Sabbagh's [1976] experimental results. Depending upon the value of the Prandtl number, however, Iqbal and Stachiewicz [1966] found that the two maxima could be located above the centre line for certain tube inclinations. As the inclination angle was increased, the distortion of the velocity and temperature profiles was reduced, until they became axially symmetric in the vertical position. Furthermore, they showed that, for

any combination of Rayleigh, Reynolds and Prandtl numbers, the maximum Nusselt number occurred when the inclination angle, α, was between 20° and 60°, contradicting the experimental results of both Sabbagh [1976] and Barozzi [1985].

Iqbal and Stachiewicz [1967] extended their theoretical investigation of the same problem one year later by considering the effect of the temperature dependence of density throughout their governing equations. They found that the introduction of variable density had an insignificant effect on the temperature profiles and Nusselt number, confirming the validity of the Boussinesq approximation. The velocity field, on the other hand, varied along the axial length of the tube in accordance with the density changes.

Cheng and Hong [1972a] employed a combination of the boundary vorticity method and the line iterative relaxation method to obtain a numerical solution for upward, laminar flow in an inclined tube subjected to uniform wall heat transfer rate per unit axial length and circumferentially constant wall temperature. The flow under consideration was thermally as well as hydrodynamically fully developed. Fluid properties were assumed constant except for the density variations in the buoyancy terms (the Boussinesq approximation).

The results obtained by Cheng and Hong [1972a] indicated that for any combinations of Rayleigh, Reynolds and Prandtl numbers, the Nusselt number varied monotonically with tube inclination. Therefore, the maximum Nu did not occur when the

inclination angle was *between* 20° and 60°. They concluded that the perturbation method used by Iqbal and Stachiewicz [1966] was invalid. Furthermore, their velocity and temperature profiles matched quite closely those obtained by Sabbagh et al. [1976]. In addition, they found that if the Rayleigh number, for a fixed α, Re and Pr, was high enough, a flow reversal region occurred, roughly in the middle of the cross-section. It is worth noting that Cheng and Hong [1972a] observed that the Nusselt number decreased with increasing tube inclination at high values of ReRa, but at low ReRa, the Nusselt number was seen to increase with increasing tube inclination.

Cheng and Hong [1972b] produced a companion solution to that of Cheng and Hong [1972a], using the same combination of numerical methods for upward, hydrodynamically and thermally developed, laminar flow in inclined tubes with axially and circumferentially uniform heat flux. Their results affirmed those in their above-mentioned paper. Furthermore, their Nusselt number values were significantly different from those of Iqbal and Stachiewicz [1966].

Orfi, Galanis and Nguyen [1990] numerically investigated the effects of tube inclination on the mixed convection heat transfer in laminar, upward flow inside a circular cross-section tube with axially and circumferentially uniform heat flux. The numerical technique employed to solve the problem was based on the SIMPLER method (Patankar, 1980), and the flow under consideration was both hydrodynamically and thermally fully developed.

Orfi, Galanis and Nguyen [1990] reported the same qualitative trends in the dependence of velocity and temperature profiles on angle of inclination as did the aforementioned authors. Concerning the effect of tube inclination on Nusselt number, however, they obtained a curious result. When the natural convection effects were small (Gr values were low), they observed a monotonic decrease in Nusselt number as the tube inclination increased, and thus found no optimum tilt angle, between 20° and 60°, for which the Nusselt number was a maximum. When the natural convection effects were larger (Gr values were higher), however, there was a definite optimum inclination between α = 20° and 60° for which Nu reached a maximum, supporting the conclusion of Iqbal and Stachiewicz [1966].

Laouadi, Galanis and Nguyen [1994] continued the investigation of Orfi, Galanis and Nguyen [1990]. Laouadi et al. [1994] numerically studied the effects of conduction in the pipe wall on upward, laminar flows in inclined pipes, uniformly heated on the outer surface. The Grashof number, based on heat flux was varied from $5X10^4$ to $1X10^6$, and the Reynolds number was fixed at 500. The flow under consideration was thermally fully developed, and three different tube inclinations were studied: α = 0° (horizontal), α = 30° and α = 60°. They presented results for three different values of the wall-to-fluid thermal conductivity ratio, k_p = 0.1, 10 and 1000, and two different values of outer-to-inner tube radius ratio, r_o/r_i = 1.05 and 1.5.

Laouadi et al. [1994] found that the effects of wall conduction become appreciable

for large values of k_p and r_o/r_i. According to their results, conduction in the pipe wall increases the intensity of the secondary motion that is induced by the effects of buoyancy.

It is important to note that Laouadi et al. [1994] and Cheng and Hong [1972a] reported that the flow pattern inside inclined tubes is similar to that found in horizontal tubes. That is, it consists of a comparable, spiral-like motion of the fluid particles as they move through the tube.

1.4 SURVEY OF THE THESIS

This thesis has five chapters and is organized as follows. In Chapter 1, the objectives of the thesis were discussed. The current knowledge on mixed convection in vertical, horizontal and inclined tubes, with or without conduction in the pipe wall, was also discussed in the this chapter. In Chapter 2, the governing equations, the flow patterns that have been previously reported in uniformly heated tubes, and the effects of wall conduction are all reviewed. The experimental apparatus and procedure are described in detail in Chapter 3. The results of flow visualization and the temperature measurements are presented and discussed in Chapter 4. Finally, in Chapter 5, the contributions of the thesis are summarized and recommendations for future work are made.

CHAPTER 2

THEORETICAL CONSIDERATIONS

2.1 INTRODUCTION

The present investigation focuses on unsteady or steady, laminar, Newtonian fluid flow and heat transfer in vertical, horizontal, and inclined tubes of circular cross-section, under the influence of gravity. A schematic illustration of the problem is given in figure 2.1. A cylindrical-polar coordinate system (r,Θ,z) is used to describe the fluid flow and heat transfer characteristics and their spatial variations. The z-coordinate is directed along the longitudinal axis of the pipe, and directed upward (opposite to the gravitational acceleration vector, g) when the tube is vertical. The tube is subjected to a uniform wall heat flux and heated over a length of approximately 57 diameters. The fluid flow at the inlet plane of the heated portion of the pipe was fully developed.

This chapter is organized as follows. Section 2.2 examines the governing equations and non-dimensional parameters. Sections 2.3, 2.4 and 2.5 discuss the flow patterns that have been reported in vertical, horizontal and inclined tubes, respectively. Section 2.6 considers flows of water near its density inversion temperature. Finally, section 2.7 discusses the effect of wall conduction in the pipe when the heat flux is applied to its outermost surface.

2.2 LAMINAR FLOW ANALYSIS

2.2.1 Governing Equations

The velocity, pressure and temperature fields in the fluid are governed by the continuity, Navier-Stokes, and energy equations. These equations are available in any standard fluid dynamics and heat transfer text book, for example, in Appendix B, of Frank M. White's book, *Viscous Fluid Flow*, 2nd ed., 1991. The following dimensionless variables are introduced

$$
\begin{aligned}
r^* &= \frac{r}{D} \qquad z^* = \frac{z}{D} \\
U_z^* &= \frac{U_z}{U_0} \qquad U_r^* = \frac{U_r}{U_0} \qquad U_\theta^* = \frac{U_\theta}{U_0} \\
\theta^* &= \frac{[T_0 - T]}{[q_w'' D/k]} \qquad t^* = \frac{tU_0}{D} \\
p^* &= \frac{p + \rho_0 g(z\sin\alpha + r\sin\theta\cos\alpha)}{\rho_0 U_0^2}
\end{aligned}
\tag{1}
$$

where D is the diameter of the pipe, α is the angle of inclination of the longitudinal axis of the pipe measured from the horizontal plane, and U_0 is the mean axial velocity of the fluid. The Boussinesq approximation is invoked. Thus, in all terms except the buoyancy term, the density is set equal to a constant reference value

$$\rho = \rho_0 \tag{2}$$

In the buoyancy term, the following approximation is made

$$\rho = \rho_0 - \rho_0 \beta [T - T_0] \quad . \tag{3}$$

Here, β is the volumetric thermal expansion coefficient; T_0 is equal to the mean of the inlet and outlet bulk temperatures ($T_0=[T_{bi}+T_{bo}]/2$); and ρ_0 is the density of the fluid at T_0.

The continuity, r-momentum, Θ-momentum, z-momentum, and energy equations can be cast in the following non-dimensionalized forms, respectively,

$$\frac{1}{r^*}\frac{\partial (r^* U_r^*)}{\partial r^*} + \frac{1}{r^*}\frac{\partial U_\theta^*}{\partial \theta} + \frac{\partial U_z^*}{\partial z^*} = 0 \tag{4}$$

$$\frac{\partial U_r^*}{\partial t^*} + U_r^* \frac{\partial U_r^*}{\partial r^*} + \frac{U_\theta^*}{r^*}\frac{\partial U_r^*}{\partial \theta} - \frac{U_\theta^{*2}}{r^*} + U_z^* \frac{\partial U_r^*}{\partial z^*} = - \frac{\partial p^*}{\partial r^*} + \frac{\mu}{\rho_0 U_0 D}[\nabla^{*2} U_r^* - \frac{U_r^*}{r^{*2}} - \frac{2}{r^{*2}}\frac{\partial U_\theta^*}{\partial \theta}] + [\frac{g_r \beta q_w'' D^2/k}{U_0^2}]\Theta^* \tag{5}$$

$$\frac{\partial U_\theta^*}{\partial t^*} + U_r^* \frac{\partial U_\theta^*}{\partial r^*} + \frac{U_\theta^*}{r^*}\frac{\partial U_\theta^*}{\partial \theta} + \frac{U_r^* U_\theta^*}{r^*} + U_z^* \frac{\partial U_\theta^*}{\partial z^*} = -\frac{1}{r^*}\frac{\partial p^*}{\partial \theta} + \frac{\mu}{\rho_0 U_0 D}[\nabla^{*2} U_\theta^* - \frac{U_\theta^*}{r^{*2}} + \frac{2}{r^{*2}}\frac{\partial U_r^*}{\partial \theta}] + [\frac{g_\theta \beta q_w'' D^2/k}{U_0^2}]\Theta^* \tag{6}$$

$$\frac{\partial U_z^*}{\partial t^*} + U_r^* \frac{\partial U_z^*}{\partial r^*} + \frac{U_\theta}{r^*}\frac{\partial U_z^*}{\partial \theta} + U_z^* \frac{\partial U_z^*}{\partial z^*} = - \frac{\partial p^*}{\partial z^*} + \frac{\mu}{\rho_0 U_0 D}[\nabla^{*2} U_z^*] + [\frac{g_z \beta q_w'' D^2/k}{U_0^2}]\Theta^* \tag{7}$$

$$\frac{\partial \Theta^*}{\partial t^*} + U_r^* \frac{\partial \Theta^*}{\partial r^*} + \frac{U_\theta^*}{r^*}\frac{\partial \Theta^*}{\partial \theta} + U_z^* \frac{\partial \Theta^*}{\partial z^*} = \frac{K}{\rho_0 U_0 D\ C_p}[\nabla^{*2}\Theta^*] +$$
$$\frac{\mu}{\rho_0 U_0 D}\frac{U_0^2}{C_p[q_w'' D/k]}\Big[\,2\Big(\Big(\frac{\partial U_r^*}{\partial r^*}\Big)^2 + \Big(\frac{1}{r^*}\Big(\frac{\partial U_\theta^*}{\partial \theta} + U_r^*\Big)\Big)^2 + \Big(\frac{\partial U_z^*}{\partial z^*}\Big)^2\Big)$$
$$+ \Big(\frac{\partial U_\theta^*}{\partial z^*} + \frac{1}{r^*}\frac{\partial U_z^*}{\partial \theta}\Big)^2 + \Big(\frac{\partial U_z^*}{\partial r^*} + \frac{\partial U_r^*}{\partial z^*}\Big)^2 +$$
$$\Big(\frac{1}{r^*}\frac{\partial U_r^*}{\partial \theta} + r^*\frac{\partial}{\partial r^*}\Big(\frac{U_\theta^*}{r^*}\Big)\Big)^2\,\Big] \qquad (8)$$

where

$$\nabla^{*2} = \frac{1}{r^*}\frac{\partial}{\partial r^*}\Big(r^*\frac{\partial}{\partial r^*}\Big) + \frac{1}{r^{*2}}\frac{\partial^2}{\partial \theta^2} + \frac{\partial^2}{\partial z^{*2}}\ . \qquad (9)$$

The components of the gravity vector in cylindrical coordinates are

$$g_r = g\cos\alpha\sin\theta \qquad g_\theta = g\cos\alpha\cos\theta \qquad g_z = g\sin\alpha \qquad (10)$$

As was stated earlier, α is the angle of inclination of the longitudinal axis of the tube measured from the horizontal plane.

2.2.2 Dimensionless Parameters

The dimensionless parameters that appear in the non-dimensionalized equations are

$$Re = \frac{\rho_0 U_0 D}{\mu}; \qquad \alpha$$

$$Gr = \frac{g\beta\,[q_w''\,D^4/k]}{[\frac{\mu}{\rho_0}]^2} \qquad (11)$$

$$Pr = \frac{\mu C_p}{k}; \qquad Ec = \frac{U_0^2}{C_p[q_w''\,D/k]}$$

Re, Gr, Pr and Ec are the Reynolds, Grashof, Prandtl and Eckert numbers, respectively. The Grashof number is a measure of the ratio of the buoyancy forces and the viscous forces acting within the fluid. The Gr/Re^2 term,

$$\frac{Gr}{Re^2} = \frac{g\beta q_w''\,D^2/k}{U_0^2}, \qquad (12)$$

that appears on the right-hand sides of the momentum equations, is, therefore, a measure of the ratio of the buoyancy forces and the inertia force (recall that the Reynolds number approximates the ratio of the inertia and the viscous forces). The Gr/Re^2 parameter thus indicates the strength of the free convection effects relative to the imposed forced convection effects.

If the value of the Gr/Re^2 parameter is very much less than 1, then the last terms in the momentum equations are negligible and the problem reduces to that of pure forced convection. On the other hand, if the Gr/Re^2 parameter is much greater than 1, then the buoyancy terms dominate and the problem becomes one of pure natural convection. When the values of the Gr/Re^2 parameter lie somewhere between those two extremes, the forced and free convection effects become comparable in magnitude, and the problem is said to involve mixed convection. In many mixed convection flows, including those considered in this thesis, the Eckert number, Ec, is much less than 1, and the viscous dissipation terms in the energy equation may be ignored.

2.2.3 Boundary, Inflow and Outflow Conditions

In the problem of interest, the tube is subjected to a uniform wall heat flux over its outer surface. At the inlet of the heated tube, the temperature is essentially constant over the cross-sectional area, and a Poiseuille velocity profile prevails. At the outlet of the heated tube, there exists strictly outflow; that is, no flow enters the heated tube from the outlet. In developing flow problems, an additional dimensionless parameter appears: the length to diameter ratio, L/D.

If wall conduction effects were included in the analysis, two additional non-dimensional parameters would be involved: the ratio of the outer and inner radii of the pipe, r_o/r_i; and the ratio of the thermal conductivities of the pipe wall and the fluid, k_w/k_f.

2.3 FLOW PATTERNS IN VERTICAL TUBES

In the case of upward flow in vertical tubes, the fluid closer to the tube wall heats up and becomes lighter than the fluid nearer to the centre of the pipe. The lighter fluid accelerates relative to the heavier one and gives rise to larger velocities near the wall of the pipe. The heat transfer rate is therefore enhanced, and this situation is accordingly called mixed convection heat transfer in the presence of buoyancy-aiding flow. Various possible axial velocity profiles are qualitatively sketched in figure 2.2.

As the fluid closer to the wall accelerates, the fluid nearer to the centre of the pipe must decelerate in order to satisfy the equation of continuity. The axial velocity therefore increases close to the wall, and reduces in the central portion of the pipe. For larger wall heat fluxes, the lighter fluid will accelerate until the velocity profile becomes saddle-shaped, as shown in figure 2.2(c). If sufficient heat is supplied (Gr/Re^2 is very large) and the pipe is long enough, the flow in the central portion of the tube will decelerate until it reverses direction, and a flow reversal region, called a recirculation cell, is created. The cell is axisymmetric and located in the central portion of the pipe when the tube is vertical and the flow is steady. In order to satisfy the continuity equation, the fluid located closer to the wall, and outside the recirculation cell, moves upward at a much larger rate than it would have in the corresponding pure forced

convection case.

Prior to this investigation, the laminar, upward flow inside a vertical, uniformly heated tube was assumed to remain steady and axisymmetric. A stable recirculation cell was believed to prevail undisturbed. In this study, however, unsteadiness of the flow was detected some distance downstream of the onset of flow reversal. This unsteady phenomenon is discussed, in greater detail, in chapter 4.

In the case of downward flow, the fluid closer to the wall heats up and becomes lighter than the fluid nearer to the centre of the cross-section. The buoyancy forces, however, act in a direction *opposite* to that of the primary forced flow. The lighter flow therefore decelerates relative to the heavier one and gives rise to smaller velocities near the wall of the pipe. The heat transfer rate is therefore decreased, and this situation is accordingly called mixed convection heat transfer in the presence of buoyancy-opposing flow.

If sufficient heat is applied (Gr/Re^2 is very large) and the pipe is long enough, the velocity of the fluid near the wall will reverse direction. Scheele and Hanratty [1962] reported that a stable, asymmetric, laminar flow reversal region is possible, in the vicinity the wall of the pipe, if the Reynolds number is small. Otherwise, if the Reynolds number is large, the reversed flow quickly induces transition to turbulence.

2.4 FLOW PATTERNS IN HORIZONTAL TUBES

In horizontal tubes, the direction of the forced convection current is transverse to that of the gravity vector. In this case, the warmer fluid, close to the pipe wall, moves upward along both lateral sides of the pipe until the two streams meet at the top of the tube, merge, and pushed downward into the central portion of the pipe. This occurs as the main flow is forced through the tube and is being heated. Two symmetrical recirculation cells appear in any vertical cross-section perpendicular to the longitudinal axis of the pipe, as shown in Figure 2.3(a). The superposition of this secondary flow onto the main forced flow results in a spiral trajectory of the fluid particles as they move through the tube, ascending near the wall toward the top, and descending in the central portion, as shown in Figure 2.3(b). If the flow is steady, the spiral eventually acquires a fixed shape, not varying with axial distance, and the flow can be considered fully developed.

2.5 FLOW PATTERNS IN INCLINED TUBES

In flow through inclined tubes, the gravity vector can be resolved into two components: one parallel to the longitudinal axis of the pipe ($g\sin\alpha$) and the other

transverse to it ($g\cos\alpha$). In the case of upward flow, the longitudinal component will cause the warmer flow close to the wall to accelerate in the z-direction, as in vertical pipes. The transverse component will induce the lighter fluid to climb along the pipe-wall as in horizontal tubes. If the two components are comparable in magnitude and the buoyancy forces in the fluid are appreciable, they combine to create a flow field that has features in common with those in vertical and horizontal tubes.

No experimental studies involving visualization of upward flows in inclined tubes have been conducted. The flow patterns that occur have only been studied numerically. Sabbagh [1976] and Barozzi [1985] conducted experimental investigations, but neither performed any flow-visualization studies.

Cheng and Hong [1972] and Laouadi et al. [1994] undertook numerical investigations of the problem and, according to their results, the flow patterns in inclined tubes (with α = 30°, 45° or 60°) are similar to those found in horizontal tubes; that is, spiral trajectories of the fluid particles exist in inclined pipes as in horizontal ones. In one particular numerical run, with α = 45°, a very low Reynolds number, and a large applied heat flux, Cheng and Hong [1972] reported the occurrence of a flow reversal region in the central portion of the pipe. These results, however, were not confirmed by experiments. Furthermore, they assumed that the flow was steady throughout.

Does unsteadiness exist in inclined-tube flows as it does in vertical tubes? An

answer to this question will be sought in this work. One of the objectives of this study was to experimentally investigate the pattern of upward flows in uniformly heated inclined tubes. This was carried out, and the results are presented and discussed in chapter 4.

In the case of downward flow, the longitudinal component of the gravity vector decelerates the lighter fluid closer to the wall, as in downward flow in vertical tubes, and the effects of the two components of the gravity vector combine to create a complex flow field. A single flow reversal region was observed experimentally by Leong et al. [1991] at an angle of inclination as low as 10°. The recirculation cell was stable and located at the top of the pipe, next to the wall. This author has found no numerical investigations, in the literature, of downward mixed-convection flow in inclined tubes.

2.6 WATER NEAR ITS DENSITY INVERSION TEMPERATURE

The density of water near 4°C does not vary linearly with temperature, but exhibits an extremum. Thus, the Boussinesq approximation invoked in section 2.2 is not valid. Consequently, the governing equations are non-dimensionalized with the following modifications.

The density is kept constant and set equal to its maximum value (which occurs at T_m = 4.029325°C) in all terms, except in the buoyancy term;

$$\rho = \rho_m = 999.9720\ kg\text{-}m^{-3}. \qquad (13)$$

In the buoyancy term, the following approximation is used:

$$\rho = \rho_m - \rho_m \alpha_1 |T - T_m|^q \ . \qquad (14)$$

In this equation, which is taken from the work of Kukulka, Gebhart and Mollendorf, [1978], q = 1.894816 and $\alpha_1 = 9.297173 \times 10^{-6}$ $(°C)^{-q}$ (Elkouh and Baliga, 1995).

In order to obtain a suitable non-dimensionalization of the governing equations, the dimensionless variables introduced in section 2.2.1 are used, and an additional one is included:

$$\vartheta^* = \left(\frac{|T - T_m|}{q_w'' D/k}\right)^q \ . \qquad (15)$$

In the resulting non-dimensionalization, the continuity and energy equations are identical to those given in section 2.2.1. The r-momentum, Θ-momentum, and z-momentum equations, however, take the following forms:

$$\frac{\partial U_r^*}{\partial t^*} + U_r^* \frac{\partial U_r^*}{\partial r^*} + \frac{U_\theta^*}{r^*}\frac{\partial U_r^*}{\partial \theta} - \frac{U_\theta^{*2}}{r^*} + U_z^* \frac{\partial U_r^*}{\partial z^*} =$$
$$- \frac{\partial p^*}{\partial r^*} + \frac{\mu}{\rho_m U_0 D}\left[\nabla^{*2} U_r^* - \frac{U_r^*}{r^{*2}} - \frac{2}{r^{*2}}\frac{\partial U_\theta^*}{\partial \theta}\right] + \tag{16}$$
$$+ \left[\frac{g_r \alpha_1 (q_w'' D/k)^q D}{U_0^2}\right] \vartheta^*$$

$$\frac{\partial U_\theta^*}{\partial t^*} + U_r^* \frac{\partial U_\theta^*}{\partial r^*} + \frac{U_\theta^*}{r^*}\frac{\partial U_\theta^*}{\partial \theta} + \frac{U_r^* U_\theta^*}{r^*} + U_z^* \frac{\partial U_\theta^*}{\partial z^*} =$$
$$- \frac{1}{r^*}\frac{\partial p^*}{\partial \theta} + \frac{\mu}{\rho_m U_0 D}\left[\nabla^{*2} U_\theta^* - \frac{U_\theta^*}{r^{*2}} + \frac{2}{r^{*2}}\frac{\partial U_r^*}{\partial \theta}\right] + \tag{17}$$
$$+ \left[\frac{g_\theta \alpha_1 (q_w'' D/k)^q D}{U_0^2}\right] \vartheta^*$$

$$\frac{\partial U_z^*}{\partial t^*} + U_r^* \frac{\partial U_z^*}{\partial r^*} + \frac{U_\theta}{r^*}\frac{\partial U_z^*}{\partial \theta} + U_z^* \frac{\partial U_z^*}{\partial z^*} =$$
$$- \frac{\partial p^*}{\partial z^*} + \frac{\mu}{\rho_m U_0 D}\left[\nabla^{*2} U_z^*\right] + \tag{18}$$
$$+ \left[\frac{g_z \alpha_1 (q_w'' D/k)^q D}{U_0^2}\right] \vartheta^* \quad .$$

The terms that appear in the momentum equations are identical to those listed in section 2.2.2, except for the buoyancy terms. The dimensionless buoyancy parameters now assume a different form:

$$\frac{Gr}{Re^2} = \frac{g \alpha_1 (q_w'' D/k)^q D}{U_0^2}, \tag{19}$$

where the Grashof number, Gr, is given by,

$$Gr = \frac{g\alpha_1 (q_w'' D/k)^q D^3}{[\frac{\mu}{\rho_m}]^2} . \qquad (20)$$

If the Gr/Re^2 term is negligible, the free convection currents that arise are weak and their effect insignificant. If, on the other hand, the Gr/Re^2 term is very large, the free convection dominates. At intermediate values of Gr/Re^2, mixed convection is obtained.

The literature, however, does not discuss how the heat transfer characteristics are affected by the presence of natural convection currents in cold water near 4°C. Neither does it contain any work on the visualization of such flows.

It may be inferred, however, that the flow fields that arise may be notably different from those discussed in the previous sections. The density of water increases as the temperature is increased until it reaches a maximum at 4.029325°C, after which it begins to decrease with increasing temperature. Hence, the warmer fluid near the heated wall may not be lighter than the cooler fluid near the center of the pipe until it is heated past 4.029325°C. Warmer fluid may, consequently, decelerate relative to colder fluid until it reaches a certain temperature, and then accelerate. Whether or not the heat transfer is enhanced or diminished relative to that of the pure, forced convection case, and whether or not stable recirculation cells form, are questions that have not been answered in the published literature.

2.7 THE EFFECTS OF WALL CONDUCTION

In laminar, mixed convection flow inside a tube uniformly heated on the outer surface, heat conduction in the pipe-wall may have an important influence on both the velocity and temperature fields in the fluid. The parameters that the determine the extent of the wall conduction in a particular experimental run, with fixed Reynolds (Re) and Grashof (Gr) numbers, are the ratio of the wall and fluid thermal conductivities, k_w/k_f, and the ratio of the outer and inner tube radii, r_o/r_i.

A thicker tube wall of higher thermal conductivity will allow more heat to conduct within its wall than a thinner tube wall of lower conductivity. Furthermore, a fluid of higher thermal conductivity will draw more heat from the pipe than a fluid of lower conductivity, thereby reducing conduction effects within the tube wall.

The amount of heat conducted in the wall increases with increased Gr/Re ratio (Bernier and Baliga, [1992b]). For a given tube and a fixed Reynolds number, a larger applied heat flux will create larger temperature gradients in its wall, and more heat conduction will occur.

In vertical tubes, the temperature fields in the fluid and pipe-wall are axisymmetric. In horizontal and inclined tubes, the temperature fields in the fluid and in the pipe are three-dimensional.

When axial conduction in a tube is significant, a sizable portion of the heat flux applied on the outer surface of the pipe is redistributed upstream and downstream of its heated section. Axial wall conduction, therefore, pre-heats the water before it enters the heated portion of the pipe. In vertical tubes, flow reversal occurs upstream of its point of inception in the absence of wall conduction. Pre-heating of the fluid also causes the spiralling motion, discussed in section 2.4, to begin further upstream than it otherwise would.

Tangential wall conduction in horizontal and inclined tubes affects the secondary, buoyancy-induced motion, since the temperature field of the inner wall of the pipe is more uniform than what it would have been in the absence of the wall conduction. Laouadi et al. [1994] performed a numerical investigation of the problem for horizontal tubes ($\alpha = 0°$) and tubes with an angle of inclination, α, of 30° from the horizontal. According to their results, conduction in the pipe-wall increases the intensity of the symmetrical recirculation cells that occur in the pipe's cross-section, and, therefore, the spiralling motion becomes more pronounced.

CHAPTER 3

EXPERIMENTAL APPARATUS AND PROCEDURES

3.1 INTRODUCTION

An inclinable, translucent test section was designed and constructed for the present investigation. A thin, semi-transparent gold-film glued onto the outer surface of a plexiglas pipe was used as an electrical heating element. A transparent vacuum chamber served to insulate the pipe and the heating element. A dye injection technique was used to visualize the flow patterns. The translucency of the test section permitted flow visualization to be carried out over its entire heated length. Calibrated thermocouples were used to measure circumferential as well as axial temperature variations. In addition, the entire test section was designed so that it could be disassembled and reassembled with relative ease.

This chapter is organized as follows. In the next section, the various elements of the experimental apparatus are described. Section 3.3 is devoted to a discussion of the design and construction of the heated test section. Section 3.4 describes the techniques used for temperature, average velocity, and power measurements, as well as the data acquisition system used in this investigation. The flow visualization technique is discussed in section 3.5, and the experimental procedure is outlined in section 3.6.

3.2 OVERALL DESIGN

The experimental apparatus used in this study is presented schematically in Figure 3.1 and photographically in Figure 3.2. It includes a distilled water, a vacuum, and a dye injection circuit. The distilled water was used as the heat transfer fluid. Therefore, the distilled water circuit is also referred to as the working-fluid circuit. The entire distilled water circuit had a volumetric capacity of approximately 120 litres.

For ease of discussion, the heated section of the plexiglas pipe, over which flow visualization and temperature data were acquired, is also referred to as the "test section".

In the working-fluid circuit, water flowed into the heated test section from a constant head tank, securely fastened to the ceiling of the laboratory. A pump (March MFG., Pump model TE-5.5C-MD) continuously drew water from a 20L constant-temperature bath (Neslab, model RTE-221) and fed it into the constant head tank. After flowing through the heated test section, the water was returned to the constant temperature bath.

As can be seen in the photographs of Figure 3.2, the apparatus was attached to a metal frame which consisted of robust steel channels (Unistrut, model P1000 and P4100 channels) and fittings (Unistrut angle and flat plate fittings) that could be easily

assembled.

All the flexible tubes in the assembly (3/4" i.d. X 1 1/8" o.d. reinforced PVC) were insulated with two layers of half-inch foamed plastic pipe insulation (Armaflex, manufactured by Armstrong, k = 0.04 W/m°C): this black-coloured insulation is clearly visible in Fig. 3.2(a). The pipe insulation was slit in the longitudinal direction in order to facilitate its installation on the flexible tubes, and glued in place using a special adhesive (Armstrong adhesive #520).

The constant-temperature bath was capable of maintaining the set water temperature to within ± 0.02°C. The entire apparatus was insulated very well in order to minimize the effects of ambient temperature variations. Thus the temperature of the water, at the inlet of the heated section of the plexiglas pipe, could be maintained essentially constant (within ± 0.05°C) throughout the duration of an experimental run.

3.2.1 The Test Section and Vacuum Circuit

As can be seen in Fig. 3.1, in the working-fluid circuit, water flowed, from a constant head tank, under the influence of gravity, into the test section. After travelling through the heated plexiglas pipe, it was either returned to the constant-temperature bath or to a graduated cylinder that was used to measure the mass flow rate by the so-called stopwatch-bucket method. The flow rate through the test section was controlled by a ball

valve (used for coarse adjustments) installed far upstream of the inlet to the heated section of the plexiglas pipe, and a gate valve (used for fine adjustments) located downstream of the test section. These valves are shown in Figure 3.1.

A section of plexiglas pipe, 3/4" i.d. X 1" o.d., and 1.65 m (5 feet, 5 inches) long, was used to build the heated test section. It was connected to flexible tubes by coupling flanges on both its ends, as shown in Figure 3.3(a). The coupling flanges were designed to minimize flow disturbances, and to accommodate thermocouples and a dye-injection needle.

A procedure was devised to glue a semi-transparent electrically conductive gold-film (Courtaulds Performance Film, AUARE-14) onto the outer surface of the pipe, over 1.14 m (45 inches) of its length. During the experiment, electrical current was fed through copper electrodes fastened to both ends of this gold film, uniformly heating the outer surface of the plexiglas tube. The whole set-up is shown schematically in Figure 3.3, and the gluing procedure is described in detail in section 3.3 of this chapter.

The gold-film section of the 1" o.d. plexiglas pipe was enclosed inside a larger plexiglas pipe, 3 1/2" i.d. X 4" o.d. and approximately 1.22 m (4 feet) long. The annular chamber between these pipes was closed at both ends by round, Lexan caps. All joints were sealed using Wynn's precision O-rings. The annular space was connected to a vacuum pump (Edwards, Pump model EMF-8) using brass pressure fittings (Laurentian

Valve and Fittings, Swagelock models) installed in the Lexan cap, and thick Tygon vacuum tubing. The vacuum circuit is illustrated in Figure 3.3.

The air in the annular space between the inner and outer plexiglas tubes was then evacuated down to approximately 200 mbars, in order to minimize heat loss from the 1" o.d. plexiglas pipe. The annular vacuum chamber was connected to a bourdon-type dial pressure gauge (Edwards Dial Capsule Gauge CG16K) through the top Lexan cap. The entire test section and annular vacuum chamber assembly were then mounted onto an inclinable platform, as shown in Figure 3.1.

In order to reduce radiation heat transfer losses, the outer plexiglas tube was enclosed in a specially designed insulation and a thermal blanket. The insulation consisted of a styrofoam casing, protected by a layer of 3M duct tape and coated on its inner surface with reflective aluminium foil. It was designed so that it could be easily and quickly removed when flow visualization was to be carried out. The insulation and thermal blanket are shown in the Figure 3.2(e), (f) and (g). The radiation heat transfer losses, and the reasons for not using a radiation shield inside the annular vacuum chamber, are discussed further in chapter 4.

The bottom coupling flange of the heated plexiglas tube housed a dye injection needle and a thermocouple that was used to measure the inlet bulk temperature. The top coupling flange accommodated a thermocouple that was used to measure the outlet bulk

temperature of the distilled water. The inner diameter of each of the flanges was machined to 0.75", in order to match the inner diameter of the plexiglas and PVC tubing. The cross-sectional area of the water conduit was thus constant through the test section and coupling flanges. The water flow entering the test section was therefore essentially undisturbed. Enough length of pipe from the dye injection needle to the inlet of the test section was provided for the flow to become fully developed.

Immediately after the exit of the plexiglas pipe from the annular vacuum chamber, and just before the upper coupling flange, a plexiglas mixing cup was attached, as shown in Figure 3.3(a). The mixing cup was filled with marbles. Its purpose was to mix the water thoroughly before it came into contact with the thermocouple in the upper coupling flange. Adequate mixing of the water, after it left the heated test section, rendered its temperature essentially uniform. Thus the thermocouple in the upper coupling flange provided an accurate reading of the outlet bulk temperature of the distilled water.

During experiments, the lower and upper coupling flanges, the mixing cup, and adjacent tubing were well insulated by several layers of pink Fibreglass insulation, as shown in Figure 3.2(e), (f) and (g). The pink Fibreglass was put inside protective, plastic bags in order to facilitate its installation and removal.

When water is heated, its capacity to contain dissolved air diminishes. Thus, as the distilled water flowed through the heated section of the plexiglas pipe, some of the

dissolved air was released: this air collected in bubbles and pockets behind the valves and in the mixing cup. If these bubbles and pockets of air were allowed to become too large, they altered the flow rate of the distilled water through the test section. It was, therefore necessary to purge this air from the apparatus periodically (at least once a day, during the experimental runs). The air was purged by running a very high flow rate of water through the test section, until no air bubbles and pockets were observed to exit the tube along with the water. In addition, the mixing cup was outfitted with two drainage ports from which air bubbles could be expelled.

The apparatus is designed to accommodate an appropriate flowmeter at the location where the distilled water is returned from the test section to the constant temperature bath. Such a flowmeter would facilitate the measurement and control of the distilled water's flow rate. However, it would also imposed considerable additional hydraulic resistance in the water circuit. This additional hydraulic resistance would reduce the maximum flow rate attainable and diminish the effectiveness of the aforementioned air purging technique. A flowmeter bypass line was therefore installed, as shown in Figure 3.1, through which the purging of air could be effectively executed, even with the flowmeter in place.

3.2.2 The Distilled-Water or Working-Fluid Circuit

In the working-fluid circuit, distilled water is pumped from a 20L constant-temperature water bath to the bottom of a constant head-tank, anchored firmly to the ceiling of the laboratory, on a levelled metal support. The flow rate to the constant-head tank was controlled by a ball valve, located upstream of the tank and downstream of the pump outlet. A bypass tube was also installed, using a T-junction, upstream of the ball valve, in order to return the excess water flow rate from the pump back into the constant-temperature bath. A second ball valve was located in the bypass line to control the return water rate. The entire set-up is shown schematically in Figure 3.1.

The dimensions of the constant-head tank were 40 cm wide X 60 cm long X 40 cm high. Thus it could hold approximately 100 litres of water. The tank was insulated on all sides with 25 mm thick Styrofoam insulation and several layers of pink Fibreglass insulation. The pink Fibreglass was put inside protective, plastic bags in order to facilitate its installation and removal. Small openings in the top cover exposed the inside of the constant-head tank to ambient air, so that the pressure at the upper surface of the water inside the constant-head tank would be maintained atmospheric.

A square cross-section plexiglas tube, 10 cm X 10 cm and 32 cm long, was fixed to the bottom surface of the constant-head tank, over an opening that was connected to the constant temperature bath by a flexible PVC tube. The flow rate of the distilled water

into the constant-head tank was always maintained at a value greater than through the test section. Thus, when the water level in the constant-head tank reached a height of 32 cm, it overflowed into the square cross-section tube and returned to the constant-temperature bath. In this manner, the water level in the constant-head tank was maintained at a fixed height throughout the experiments.

As described above, and shown in Figure 3.1, water flowed under the influence of gravity from the constant-head tank through the test section, and back to the constant-temperature bath.

Two one-way check valves were placed between the water pump and the constant-head tank, and a solenoid valve was located downstream of the test section. These valves were installed in order to prevent the water in the constant-head tank from flowing back into the constant-temperature bath if an unexpected power outage occurred and shut off the water pump during the experiments.

In order to minimize air entrainment into the distilled-water circuit, simple nozzles and diffusers were constructed using plastic water funnels, and filtering cloth. They were inserted into the respective inlets and outlets of the tubes entering the constant-temperature bath and served to calm the flow. They are shown in Figure 3.2(b). Gurgling of the water in the bath was, therefore, effectively eliminated and this, in turn, dramatically reduced the amount of air bubbles that collected in the test section during

the experiment.

3.3 DESIGN AND CONSTRUCTION OF THE GOLD-FILM TEST SECTIONS

One of the main objectives of this investigation was to construct a translucent test section that is both well insulated and subjected to a uniform wall heat flux. The transparency of the heated pipe section was necessary in order to obtain flow visualization data over its entire length. As was stated earlier, this objective was achieved by enclosing a plexiglas pipe inside a transparent, insulating vacuum chamber, and by using a clear, flexible and electrically conductive gold film as the heating element. The procedure that was used to construct the gold-film test section will now be described.

3.3.1 Characteristics of the Gold Film

The thin, translucent gold film used in this study is commercially available in flat sheets and manufactured by Courtaulds Performance Films (Canoga Park, California) under the brand name AUARE-14. It consists of a thin, transparent polyester film on which a translucent, very thin coat of gold is applied by means of vacuum deposition. The gold coat is then protected from abrasion by overlaying a clear ceramic layer onto it. The characteristics of the gold film used in this investigation are the following, as determined by Bernier [1991]:

1. Overall thickness:

   0.13 mm (0.005 inches).

2. Gold layer thickness:

   estimated at approx. 20 Angstroms, based on data provided
   the manufacturer.

3. Mean electrical resistivity

   Approximately 13 Ω/square.

4. Variation in electrical resistivity over the film surface:

   ±6.2%, Neill [1989].

5. Transparency to light:

   80% ±10%.

6. Maximum allowable operating temperature:

   100°C.

3.3.2 Construction Procedures

Two gold-film test sections were built for this study, both are 1.067 m (42 and 7/16 inches) long. These two test sections are shown photographically in Figure 3.4. One was outfitted with 19 thermocouples and used for temperature measurements as well as flow visualization data, while the other was left bare and used exclusively for flow visualization data. The former will be henceforth referred to as test section no. 1 and the

latter, as test section no. 2. Without thermocouples, test section no. 2 provided a completely unobstructed view of the flow patterns that were highlighted by the dye-injection technique.

The gold-film was glued to the outer surface of the plexiglas pipe, as opposed to its inner surface as was done by Bernier [1991]. This allowed for enhanced contact between the gold film and the two copper electrodes situated at its ends. Installation of the gold film on the outside of the pipe permitted the two electrodes to be firmly fixed to the electrically conductive surface of the film, and this increased its operational life-span considerably.

Before the gold-film was mounted onto the plexiglas pipe, a protective coating of 3M #853 single-sided adhesive tape was applied onto its gold (conductive) side. The back of the gold-film (the polyester side) was uniformly overlaid with 3M #9469PC double-sided tape. It was then cut to the required dimensions and carefully wrapped around the plexiglas pipe.

The procedure for constructing the heated test sections consisted of three major steps: (i) cutting of the gold film and application of the proper adhesive tapes to it; (ii) gluing of the gold film to the plexiglas pipe; (iii) provision of electrical connections from the gold film to the power supply; and (iv) installation the thermocouples onto test section no. 1. Details of this construction procedure are discussed in the following pages

of this section.

3.3.2.1 Cutting of the Gold Film and Application of Adhesives

The gold film used in this study was cut from a sample roll 45.7 cm (18 inches) wide and 15.25 m (50 feet) long. First, strips of film measuring approximately 15.2 cm (6 inches) wide and 1.22 m (4 feet) long were cut. These dimensions are larger than those of the final piece of the gold film that was mounted onto the plexiglas pipe. The larger dimensions of the first cuts were necessary for proper application of the adhesive tapes.

The gold side of the film was covered completely by 3M #853 single-sided adhesive tape over 1.078 m (42 and 7/16 inches) of its length. At the extremities of the film, enough of the gold side was left bare to allow for proper attachment of copper electrodes. Double-sided 3M #9469PC tape was then very carefully applied over the entire length of the polyester side of the film. Meticulous care was exercised, especially in the application of the double-sided tape, to make sure that no air gaps or bubbles existed between or underneath the individual strands of tape. Pockets of air between the gold film and the plexiglas pipe would cause a non-uniform distribution of the applied heat flux. This would deteriorate the overall performance of the test section in vacuum.

Following the aforementioned application of the adhesive tapes, the gold film was

cut to the exact dimensions required for proper mounting onto the plexiglas pipe. Its final length, including the exposed gold surface necessary for the attachment of the electrodes was 1.14 m (45 inches). Its width was reduced to approximately 1 millimetre less than the outer circumference of the pipe (1" o.d. $\pm$.005"), in order to ensure that no portion of it overlapped after mounting onto the plexiglas pipe.

The techniques used in the application of both types of adhesive tapes are illustrated schematically in Figures 3.5 and 3.6. As a necessary precaution, the exposed gold film pieces were always handled with clean surgical gloves or protected in saran wrap.

3.3.2.2 Gluing of the Gold Film to the Plexiglas Pipe

Bernier [1991] performed tests to measure the variation in the resistance of a gold-film section bent over a pipe of radius 3/8". The results of those tests indicated that the change in resistance due to the bending was of the order of $\pm 1\%$ or less and, therefore, considered acceptable.

A 90° L-bar, approximately 1.5 m (5 feet) long was securely fastened to a large plywood board. A longitudinal edge of the prepared gold-film section was then aligned up against the vertical shoulder of the L-bar, with its adhesive side up and exposed. The plexiglas pipe was then pressed against the vertical shoulder of the L-bar and firmly

pushed onto the adhesive side of the film. The technique is illustrated in Figure 3.7.

Once preliminary adhering contact was made between the pipe and gold film, they were moved onto a clean rubber mat. The gold film was then completely wrapped around the pipe. The latter was slowly rolled over the former while maintaining constant downward pressure. A long, thin bead of epoxy (Devcon, 2-Ton epoxy glue) was finally applied over the two opposite longitudinal edges of the gold film which were now almost touching each other on the outer wall of the pipe. This prevented the gold film from unwrapping and releasing itself from the plexiglas surface during the experiments. The technique is illustrated in Figure 3.8.

3.3.2.3 Electrode Construction

The design of the copper electrodes is shown in Figure 3.9. The semi-circular contact surfaces of the electrodes were machined to a diameter .008 inch larger than the outer diameter of the exposed extremities of the gold-film test section. Strands of 3M electrically-conductive Scotch brand tape were applied to the contact surfaces of the electrodes to ensure that they fit snugly onto the test section. The two halves of each electrode were bolted together and solidly glued to the exposed extremities of the gold film. The glue used was Tra-Duct conductive silver epoxy adhesive, #2902. The electrode and test-section assembly is shown photographically in Figure 3.10.

3.3.2.4 Thermocouple Installation onto Test Section No.1

A total of nineteen thermocouples were installed onto the test section. Sixteen thermocouples were glued directly onto its protective layer of 3M #853 single-sided tape. They were arranged in diametrically opposed pairs that formed two symmetrical rows that ran longitudinally along the test section, as portrayed in Figure 3.11. One thermocouple was fixed to each of the two electrodes, glued inside a drilled 1/8"-hole, and a final thermocouple was glued to the plexiglas pipe just upstream of the first (inlet) electrode. All thermocouples were glued using Devcon, 2-Ton epoxy: their locations with respect to the electrodes are shown in Figure 3.11.

As a protective measure, the thermocouple beads were covered by a dab of Omegabond 101 thermally conductive epoxy (Omega Engineering, Inc.) immediately after their calibration. They were eventually stuck to the test section using the Devcon, 2-Ton epoxy, in order to ensure a strong and reliable attachment.

Once the beads were glued to the test section, the thermocouple wires were orderly arranged and supported on a cage that was inserted into the vacuum chamber with the test section. The cage was constructed out of four long, thin (¼" o.d.) plexiglas rods, and two flexible plastic strips (4.2 cm x 30 cm). It is sketched, along with the test section assembly, in Figure 3.3(b) and shown photographically in Figure 3.12. The thermocouple wires were thus prevented from unnecessarily obstructing the view of, and

touching, the gold-film test section.

Using two similar plastic strips (4.2 cm X 30 cm), two supporting collars were made on which nineteen thermocouple connectors (Omega Engineering Inc., subminiature connectors, SMP-E-MF) were glued using Devcon, 2-Ton epoxy. The connectors provided a removable coupling between the thermocouples installed onto the test section inside the annular vacuum chamber, and the thermocouple lead wires that were passed through a hole drilled into each Lexan cap of the vacuum chamber (see Figure 3.3). The thermocouple lead wires coming out of the Lexan caps were connected to the data acquisition system. The two supporting collars and adjoining wiring are shown in Figure 3.12.

3.4 SUPPORTING EQUIPMENT AND DATA ACQUISITION SYSTEM

The acquisition of temperature data, the powering up of the gold-film section, and the measurements of the applied voltage and currents were managed by a computer-controlled data acquisition system (Hewlett-Packard, model 3478A). The supporting equipment consists of a DC power supply (Xantrex, model XKW 300-3.5), an IBM compatible 286 personal computer, and two multimeters. Each of the devices were fitted with an HP-IB computer interface card. Twenty-two chromel-constantan thermocouples (Omega Engineering Inc. TT-E-30) were fabricated, calibrated, and used in the experiments. The entire set-up, including all electrical connections, is shown

schematically in Figure 3.13. A computer program, written in Microsoft Quick Basic 4.5, was coded, tested, and used for all computer-control and data acquisition tasks.

3.4.1 Temperature Measurements

As was stated above, twenty-two 30-gauge chromel-constantan (Type E; Omega Engineering Inc., TT-E-30); thermocouples were used in this investigation. They were all fabricated in-house, employing the technique described by Neill, [1989]. Out of these twenty-two thermocouples, nineteen were located on the test section and employed inside the vacuum chamber (see Figure 3.11). Two thermocouples were installed within the coupling flanges, and used to measure inlet and outlet bulk temperatures (shown in Figure 3.3(a)). One was kept outside the apparatus and used to measure ambient temperature.

The thermocouples were individually calibrated against a quartz thermometer (Hewlett-Packard, model 2804A), employing the method described by Stathopoulos [1990]. With this method, the uncertainty in the temperatures measured by the calibrated thermocouples is $\pm 0.05°$ (Stathopoulos, [1990]). The thermocouples were all connected to the data acquisition unit, which was, in turn, interfaced with the IBM compatible 286 personal computer. The output voltages of all thermocouples were read and stored on appropriate data-files. In order to mitigate the influence of noise in the thermocouple readings, each thermocouple voltage was read sixty times. The arithmetic mean of these

sixty readings was then recorded. Preliminary tests had indicated that the average of forty or more readings produced essentially invariant average values.

In the final series of experiments, in order to assist in the estimation of energy losses, fifteen uncalibrated, 30 gage, Type-E thermocouples were used to measure temperatures of the 4" o.d. plexiglas pipe, mixing cup, coupling flanges and adjacent tubing. A mechanical thermocouple multiplexer (Omega Digicator, thermocouple indexer) was used to manually read the thermocouples. Based on the data provided by the manufacturer (Omega), the temperatures measured with these thermocouples were estimated to be accurate to within $\pm 0.1°$.

3.4.2 Circumferential Indexing of the Thermocouples

The thermocouples installed on the test section were arranged in diametrically opposed pairs and formed two longitudinal rows, as was mentioned in the section 3.3.2.4. It was desired, however, to take readings of temperatures at several angular positions along the entire circumference of the tube.

As shown in Figure 3.3(a), the 1" o.d. plexiglas pipe was kept in place inside the top and bottom flanges by O-ring seals (Wynn's Precision O-rings). Thus, the pipe could be rotated relative to the flanges. Furthermore, the sliding joints between the 1" o.d. plexiglas pipe and the two Lexan end caps of the annular vacuum chamber were sealed

with O-ring seals (also shown in Figure 3.3(a)). Therefore, it was possible to circumferentially index the thermocouples fixed to the 1" o.d. plexiglas pipe by incrementally rotating the pipe, about its longitudinal axis, relative to the fixed flanges and Lexan caps.

The following procedure was used to obtain temperature data at three different angular locations, for each combination of the water flow rate through the test section, the inlet bulk temperature, and the power applied to the gold-film heater: i) take temperature readings of all the thermocouples in their current configuration, after steady-state is achieved; ii) rotate the 1" o.d. plexiglas pipe (and, therefore, the thermocouples glued to it) 45° clockwise, allow the apparatus enough time to reacquire steady state, and take temperature readings of all thermocouples in their new configuration; iii) rotate the pipe and its thermocouples, clockwise, 45° more, allow steady state to be regained, and take temperature readings of all thermocouples one last time. This procedure is also outlined in Figure 3.14.

A protractor was carefully aligned and fastened onto the inclinable platform on which the test section was supported. The plane of the protractor was kept perpendicular to the longitudinal axis of the 1" o.d. plexiglas pipe. A pointer was then aligned and fastened onto the portion of the pipe adjacent to the protractor. The pointer and the protractor were used to determine the angular position of the thermocouples. The protractor-pointer calibration is illustrated in Figure 3.14(a) and shown photographically

in Figure 3.14(b).

The steady-state fluid flow and heat transfer phenomena under study are either symmetric about a vertical plane passing through the longitudinal axis (flows in horizontal and inclined tubes) or axisymmetric about the longitudinal axis (the steady part of flows in vertical tubes). Therefore, data over half of the circumference is, theoretically, all that is needed to study the full circumferential variation of temperature.

3.4.3 Average Velocity and Power Measurements

The average velocity of the water moving through the tube was measured by the so-called stopwatch-bucket method. When it was desired to measure the flow rate, a graduated cylinder was held at the outlet of the tube returning the fluid from the test section to the water bath. A stopwatch was then used to measure the rate at which water filled the cylinder. The calculated volume flow rate was then divided by the inner cross-sectional area of the plexiglas pipe to obtain the average velocity of the water.

The voltage and current applied to the gold-film heater were measured by using two multimeters (Hewlett Packard, model 3478A), one connected in parallel and the other in series with the gold-film section. The values were read and stored on data-file by the IBM compatible 286 computer with which the multimeters were interfaced. The electrical resistance of the gold-film section was obtained by dividing the measured

voltage by the measured current, while the power applied to it was obtained by multiplying the two.

3.4.4 Condition for Steady State

In each run of the experiment, steady-state conditions were considered to have been achieved when the readings from the inlet and outlet bulk-temperature thermocouples, as well as the outputs of all the other thermocouples on the test section varied by less than $\pm 1\%$ over a period of ten minutes.

3.5 FLOW VISUALIZATION INSTRUMENTATION AND PROCEDURE

In this investigation, the dye injection method, as described by Bernier [1991], was employed for the flow visualization studies. An injection apparatus was constructed specifically for this experiment and will now be described.

Flow visualization was carried out by injecting a fluorescent dye (Cole Palmer Instrument Co., Water Soluble Fluorescent Liquid Dye #298-17) into the water just before it entered the heated test section. The dye was prepared by dissolving approximately 13 drops (1.25 ml) of concentrated dye in 900 ml of distilled water. Thus, the dye solution was almost completely composed of water, and it could be considered neutrally buoyant. Furthermore, the molecular diffusion rate of the dye was small enough

to allow clear visualization of the injected filaments. Nevertheless, this concentration of the dye solution was strong enough to yield flow visualization photographs of good contrast, as will be demonstrated in Chapter 4.

The dye injection apparatus is illustrated schematically in Figure 3.15 and photographically in Figure 3.16. It consists of a copper reservoir connected to the dye injection needle (shown in Figure 3.3(a)), a nitrogen-filled pressure cylinder, a venting port, a filling tube, and a pressure gauge. The flexible tubing used was 3/8" o.d. reinforced PVC, and the solid tubing was 1/4" o.d. copper. The valves were Nupro brass needle valves, and all pipe fittings were Swagelock.

The injection needle is a 1/16" o.d. stainless steel pipe, carefully bent to an angle of 90°, and installed into the inlet coupling flange as shown in Figure 3.3(a). It was positioned at the geometric centre of the pipe cross-section. During the flow visualization experiments, the brass reservoir was partially filled with dye and pressurized with nitrogen. When visualization of the flow was desired, the injection valve was opened and dye was introduced into the water. The dye injection needle extended 3 and 1/4 inches longitudinally through the water conduit: this length was enough to allow the injected dye solution to attain the local fluid temperature before being released into the water.

During the flow visualization experiments, the dye was illuminated using two four-foot long, 40 Watt black lights (Sylvania Blacklight Blue F40/BLB) mounted onto

the inclinable platform on either side of the test section. Two long aluminium shades, that can be seen in the photographs of Figure 3.2, directed the light onto the test section. Photographs were taken using a Minolta X-570 camera, with the laboratory, aside from the illumination of the dye, in total darkness. Very good photographic results were obtained using Kodak, 1000 ASA Royal Gold film.

In most cases, flow visualization was carried out by continuously injecting a thin filament of the dye solution into the test section. However, in some experiments with the test section in the vertical configuration, the test section was flooded with the dye solution for a short period of time (typically 15 seconds). This flooding technique gave a clearer and more complete definition of recirculation cells than did the dye filament technique. During the visualization experiments in which the dye filament technique was used, the dye solution reservoir was pressurized to approximately 8 p.s.i. gauge. In order to flood the flow field with dye, however, it was necessary to pressurize it to roughly 15 p.s.i. gauge.

Once dye was injected into the water, the outlet of the tube that returned the water from the test section to the constant-temperature bath was removed from the bath and placed into a 2- litre container. The dye-contaminated water was completely expelled from the working-fluid circuit and new distilled water was used to replace it.

3.6 SYNOPSIS OF THE EXPERIMENTAL PROCEDURE

The following step-by-step procedure was used during each experimental run with the test section outfitted with thermocouples (test section no. 1).

1. The test section was adjusted to the desired orientation: vertical, horizontal or inclined.

2. The distilled water flow rate through the test section was set, and the desired amount of electrical power was applied to the gold-film heater.

3. The apparatus was then allowed to reach steady state; this required at least six hours. The experiment, however, was allowed to run overnight.

4. Voltage outputs from all thermocouples were recorded. The flow rate as well as the applied voltage and current were measured. The thermocouples glued to the gold-film were then indexed 45°.

5. At this stage, any air bubbles or pockets in the distilled water circuit were purged. Immediately after this purging operation, the distilled water flow rate was set to its previous value, and at least an additional five hours were allocated for the apparatus to regain steady state.

6. Voltage outputs from all thermocouples were recorded. The flow rate, as well as the applied voltage and current, were measured and recorded. The thermocouples glued to the gold-film were then indexed an additional 45°.

7. The apparatus was again allowed to reacquire steady state. Since the test section, mixing cup and flanges were already warm, this typically required three to four hours.

8. Voltage outputs from all thermocouples were again recorded. The flow rate, as well as the applied voltage and current, were measured and recorded.

9. Dye was injected into the test section, the insulation covering the outer tube of the annular vacuum chamber was removed, and the blacklights were turned on. The lights in the laboratory were shut off, and photographs of the test section were taken. During flow visualization, the dye-contaminated water flowing through the test section was allowed to empty into an external container (a 2L graduated cylinder). New distilled water was poured into the constant-temperature water bath, to replace the expelled dye-contaminated water.

10. The power supply to the gold-film heater was shut off, and the distilled water circuit was purged of air bubbles and pockets.

If only flow visualization experiments were desired to be carried out, the bare test section (test section no.2) was used. Furthermore, the indexing part of step 4 would not be performed, and steps 5 to 8 would not be executed.

CHAPTER 4

RESULTS AND DISCUSSION

4.1 INTRODUCTION

As was mentioned in Chapter 1, the main objective of this work was to design, construct, and demonstrate the use of an experimental apparatus for the study of laminar mixed convection heat transfer in a straight tube of circular cross section, with its longitudinal axis positioned at several different angles of inclination to the horizontal plane. The design and construction of this apparatus, and the related instrumentation and experimental procedures were explained in Chapter 3. In this chapter, the capabilities of this apparatus are demonstrated by presenting and discussing some illustrative flow visualization photographs and temperature data. These results also cast some light on mixed convection phenomena that have, hitherto, not received much attention in the literature. Since the literature contains few and limited results of fluid flow patterns that characterize mixed convection in uniformly heated tubes, the dye injection experiments were of particular interest and emphasis is placed on them. Temperature data were also acquired, and are presented and discussed in this chapter.

The chapter is organised as follows. Section 4.2 presents and discusses the flow visualization results obtained using test section no. 2. Section 4.3 presents and discusses

the temperature results acquired using test section no. 1; flow visualization was carried out for these runs as well, and the results are included in the presentation. Finally, section 4.4 examines the experimental errors and their sources.

4.2 FLOW VISUALIZATION RESULTS

Thirty-five flow visualization runs were carried out using test section no.2. The pertinent data for each run are documented in tables A.1 to A.5. The Grashof number used, Gr, is based on the applied heat flux; its expression in terms of fluid properties and heat flux is given in Appendix A. Fluid properties used in the calculation of Re and Gr were evaluated at a mean bulk temperature, equal to the arithmetic average of the inlet and outlet bulk temperatures. Table A.5 contains the overall electrical resistance of the gold-film heater in each flow-visualization run.

The flow visualization runs were performed in order to gain a better understanding of the phenomena under study, and also to add to the mixed-convection results in the literature, as was discussed in section 4.1. Photographs were taken of the injected dye patterns in the test section. These photographs are documented in figures A.1 to A.35 of Appendix A. Through the flow visualization results, it was confirmed that the steady flow patterns existing inside the heated tube were symmetric about the vertical plane passing through the longitudinal axis of the tube.

4.2.1 A Note on the Reported Bulk Temperatures

During the flow visualization runs, the thermocouple in the outlet coupling flange, employed to read outlet bulk temperatures, sometimes gave readings that appeared incorrect. It was discovered that the mixing cup was not adequately mixing the water, and thus its temperature was not rendered uniform before it contacted the thermocouple. This was corrected by filling the cup to capacity with glass marbles (the effectiveness of the porous bed of marbles is discussed in section 4.4).

However, this problem was not totally corrected until all of the flow visualization runs were completed. Therefore, for the thirty-five flow-visualization runs reported in this section, the outlet bulk temperature was calculated, iteratively, using the inlet bulk temperature, the power applied, and the property relations proposed by Kukulka et al. [1978]. In these calculations, it was assumed that the heat losses from the test section to the ambient air and laboratory surroundings were negligible. The validity of this assumption is discussed in section 4.4.

4.2.2 Flow Visualization in Vertical Tubes

Five runs were carried out with the tube in the vertical orientation ($\alpha = 90°$). The measured inlet bulk temperature, the calculated outlet bulk temperature, the flow rate, the applied power, the calculated Reynolds and Grashof numbers, and the Gr/Re^2

ratio for each of these runs are documented in table A.1. The flow visualization photographs of these runs are presented in figures A.1 to A.5.

The results in figures A.1 to A.5 show three distinguishable zones in the heated tube. These three different zones constitute three distinct regimes of flow that were observed over the length of the tube. They are shown schematically in figure 4.1.

The first distinct zone is a stable recirculating fluid flow pattern, that occurs downstream of the inlet cross section. A similar stable recirculating flow pattern has been previously photographed by Bernier and Baliga [1992]. The second distinct zone contains a wave-like fluctuation of the injected dye filament, unsteady with time, but laminar and remarkably sinusoidal in nature. It can be seen very clearly in figure A.2, extending over more than twenty-five tube diameters in length. This flow feature will be henceforth referred to, in this thesis, as the "laminar instability".

In the investigation of Bernier and Baliga [1992], the laminar instability occurred very close to the outlet of their heated tube, and thus only its onset was photographed. Nevertheless, its presence was noted and identified as a possible laminar-turbulent transition zone. Scheele and Hanratty [1962] also photographed a stable recirculation zone and a similar instability in upward flow inside a tube subjected to a constant-wall-temperature boundary condition. They too identified it as a laminar-turbulent transition zone. However, the flow visualization photographs obtained in this work clearly show

that the fluid flow in this zone remains laminar.

The third fluid flow pattern consists of an irregular and disorderly motion of the dye occurring downstream of the laminar instability zone. In the third zone, the filament of dye, which remains undivided in the first and second zones, separates into many thin filaments. The thin dye filaments gradually depart from the orderly wave-like motion and become entangled. The flow, however, seemed to remain laminar, since the observable filaments of dye, though erratically intertwined, did not break up and diffuse, as is characteristic of turbulent flow. Eventually, however, the dye does diffuse and individual filaments are difficult to discern. This author suspects that this third zone is a precursor to laminar-turbulent transition. This assertion, however, can only be confirmed by a more exhaustive experimental investigation.

The stable recirculation cell and the laminar instability can be seen in the photographs of figures A.1 to A.5. The best photographs were obtained in run #2, shown in figure A.2. The flow rate in this run was the lowest one investigated in this work: thus, the flow patterns, delineated by the injected dye, are very clear. The third zone, with the irregular motion of the dye, was difficult to photograph as clearly as the first two zones, but it is adequately observable in figure A.2.

An expected result is clearly seen in the photographs presented in figures A.1 to A.5. In the runs with high values of Gr/Re^2, the natural convection effects are strong,

and the recirculation cell begins closer to the inlet cross section than in the runs with low Gr/Re^2 values.

A multitude of miniature air bubbles can be seen, along the inside of the test section, in the photograph of run #1, in figure A.1. Run #1 was carried out before the flow calmers (discussed in section 3.2.2 and shown photographically in figure 3.2(b)) were installed. After the difficulty with the air bubbles was encountered in run #1, the flow calmers were conceived and implemented. As can be seen in all the other photographs, in figures A.2 to A.5, the formation of air bubbles was effectively controlled by these modifications to the original design of the experimental apparatus.

4.2.3 Flow Visualization in Horizontal Tubes

Six flow visualization runs were carried out with the tube in the horizontal orientation ($\alpha = 0°$). The measured inlet bulk temperature, the calculated outlet bulk temperature, the flow rate, the applied power, the calculated Reynolds and Grashof numbers, and the Gr/Re^2 ratio for each of these six runs are documented in table A.2. The photographs of the flow patterns in the runs are shown in figures A.6 to A.11.

The photographs in figures A.6 to A.11 show a spiralling flow pattern. Similar flow patterns have been photographed by Mori and Futugami [1967]. The filament of dye, injected along the centerline of the tube, drops downward immediately after it enters

the heated section of the pipe, and, as it approaches the pipe wall, splits into two similar streams. The two streams then climb along the sides of the tube in a spiralling pattern, as was discussed in section 2.4, merge when they reach the top of the tube, and form a single dye filament once again. This flow-pattern will henceforth be referred to, in this thesis, as the "helix". It can observed in the photographs of figures A.6 to A.11. In all runs, the flow remained laminar and steady throughout the tube.

In the photographs of figures A.6 and A.10, as the reconstituted dye filament drops again, downstream of the first helix, some dye can be seen rising along the sides once more, forming a second observable helix. Downstream of the second helix, the dye becomes diffuse, and subsequent helices were difficult to discern. The photographs of figures A.6 and A.10 correspond to runs #14 and #18, in which the Gr/Re^2 values were considerably higher than those of the other horizontal runs. The natural convection effects were thus stronger (relative to their respective forced convection currents) in runs #14 and #18, and two helices were able to form before the dye became diffuse.

In the runs with lower Gr/Re^2 values, the natural convection effects were weaker, and only the first helix was clearly distinguishable. The observed helices in runs #15, #16, #17, #19 were longer and more elongated than the helices of runs #14 and #18.

The experiments with the tube in the horizontal position are especially prone to the accumulation of air bubbles inside the heated tube, as is observable in the

photographs of figures A.8(a) and A.9. With the pipe in the horizontal orientation, minute air bubbles that would normally flow out of the tube, propelled by buoyancy forces, collect at the top and grow. In this work, the problem was controlled by monitoring the experiment closely, and carrying out the dye injection and photography soon after steady-state conditions was reached. The air-bubble purging procedure described in Chapter 3 was also used regularly.

4.2.4 Flow Visualization in Inclined Tubes

Twenty-four flow visualization runs were carried out with the tube at angles of inclination in the range $0° < \alpha < 90°$. Five different angles of inclination were investigated: $\alpha = 30°$, 45°, 60°, 76°, and 87°. The twenty-four runs are presented in this section in two groups, since each group displayed characteristics particular to itself. The first group will be referred to as the "tilted-tube runs", which includes angles of inclination of 30°, 45°, and 60°. The second group, which will be referred to as the "near-vertical runs," includes angles of inclination of 76° and 87°.

The measured inlet bulk temperature, the calculated outlet bulk temperature, the flow rate, the applied power, the calculated Reynolds and Grashof numbers, and the Gr/Re^2 values for the tilted-tube runs are presented in table A.3, and those of the near-vertical runs are given in table A.4.

4.2.4.1 The Tilted-Tube Runs: α = 30°, 45°, and 60°

This group consists of seventeen runs. The flow-visualization photographs of these runs are shown in figures A.12 to A.28. Figures A.12 to A.19 contain the photographs pertaining to the 45° inclination. The photographs in figures A.20 to A.25 correspond to the photographs of the 60° inclination, and figures A.26 to A.28 contain the photographs that were obtained with the 30° inclination.

The flow patterns portrayed in figures A.12 to A.28 qualitatively confirm the numerical results reported by Laouadi et al. [1994] and Cheng and Hong [1972a]. A spiralling flow pattern, similar to the one photographed in the horizontal tubes, is evident in the photographs for all seventeen runs. This flow pattern can be clearly observed in the oblique-view photographs of figures A.21(b), A.22(a) and A.26(b). The other photographs display frontal views of this flow pattern. As in the horizontal-tube cases (α = 90°), in all cases considered, the flow remained steady and laminar throughout the test section. In contrast, for the vertical-tube cases (α = 90°), laminar-instability was encountered in all cases considered. Thus, in the inclined-tube and horizontal-tube cases, the component of the gravity vector, perpendicular to the longitudinal axis of the tube ($g\cos\alpha$) creates the spiral flow pattern and suffices to stabilize the flow.

As was expected, the observed helices in the runs with lower Gr/Re^2 values are longer and more elongated than those in the runs with higher Gr/Re^2 values. A lower

Gr/Re^2 value leads to weaker natural convection effects and the result is a less pronounced helix.

4.2.4.2 The Near-Vertical Runs: $\alpha = 76°$ and $87°$

Seven near-vertical flow-visualization runs were carried out. The photographs corresponding to these runs are shown in figures A.29 to A.35. Figures A.29 to A.32 contain the photographs pertaining to the 76° inclination, and figures A.33 to A.35 contain the photographs corresponding to the 87° inclination.

The fluid flow patterns obtained with both inclinations exhibited features similar to those generated in the tilted-tube runs. The observed helices, however, were much longer, for comparable values of Gr/Re^2, than those of their horizontal- and tilted-tube counterparts. This, of course, is because the component of gravity perpendicular to the longitudinal axis of the tube was much less in the near-vertical runs than that in the horizontal- and tilted-tube runs. Consequently, the component of the buoyancy force that causes the fluid to rise transversely along the sides of the tube is weaker, and a less pronounced helix is formed.

As in the horizontal- and tilted-tube cases, the flow in the runs with the 76° inclination remained steady and laminar throughout the tube. In run #26, the Gr/Re^2 value was very high. The photograph in figure A.29(a), which corresponds to run #26,

shows a slightly distorted helix. The helix begins even before the inlet to the heated section. This was due to the fact that for this run, the applied heat flux was very large and the flow rate was rather low, allowing for appreciable axial wall conduction effects. Furthermore, because the copper electrode is asymmetric, the wall conduction effect in the vicinity of the inlet to the test section is *not* symmetric. As a result, a stable recirculation cell formed on the right side of the tube, and the helix is distorted, as seen in figure A.29(b)). However, no flow instability or unsteadiness occurred. Thus, again, it is seen that the component of the gravity vector perpendicular to the longitudinal axis of the tube (gcos76°) suffices to stabilize the flow in tubes with the 76° inclination.

In runs with the 87° inclination, flow instability was observed. A jagged waviness in the dye filament occurred downstream of the inlet, at the top of the heated tube, and is seen in the photographs of figures A.33(c) and A.34(c). Upstream, faint ripples of dye broke off from the body of the helix and climbed upwards; they are seen in the photographs of figures A.33(d) and A.34(c).

In the runs with the 87° inclination, run #32 had a Gr/Re^2 value that was high compared to those of the other two runs for the same inclination. As is seen in the flow visualization photograph of figure A.35, run #32 exhibited flow features similar to those encountered in both the vertical tube runs and the horizontal- and tilted- tube runs. An axisymmetrical recirculation cell was observed in the centre of the tube (as seen in figure A.35(d)), around which extended a helix, symmetrical and intact (as seen in figure

A.35(b)). Further along the length of the tube, the laminar instability appeared, wave-like and remarkably sinusoidal (as seen in figure A.35(c)).

4.3 RESULTS OF THE TEMPERATURE RUNS

Three experimental runs were carried out using test section no.1. This test section was equipped with thermocouples, as discussed in section 3.3.2.4. Therefore, these runs will be referred to as the "temperature runs." In this section, some of the results of these temperature runs are compared with published results.

In the first temperature run, #38, the tube was horizontal, $\alpha=0°$; in the second run, #39, the tube was inclined, $\alpha=45°$; and in the third run, #40, the tube was vertical, $\alpha=90°$. In all three runs, the full experimental procedure outlined in section 3.6 was executed. The results of the temperature runs are documented in Appendix B.

In table B.1, the following data pertaining to the temperature runs are presented: the measured inlet and outlet bulk temperatures; the measured flow rate, Q, applied voltage, V, and current, I; the applied power input (P_a = V*I); the calculated rate of heat transfer to the fluid ($P_f = mC_p\delta T_b$), based on the measured bulk temperature difference; and the percentage difference between the calculated and applied power inputs ($|P_a - P_f| / P_a)*100$.

The angle of inclination from the horizontal, α, the Reynolds number, Re, and Grashof number, Gr, and the ratio Gr/Re^2 for each temperature run are tabulated in Table B.2. Table B.2 also contains the value of the outlet bulk temperature, calculated iteratively, using the measured inlet bulk temperature, the power applied, $P_a = V*I$, and the property relations proposed by Kukulka et al. [1978]. The fluid properties used in the calculation of Re and Gr were evaluated at the mean bulk temperature, equal to the arithmetic average of the measured inlet bulk temperature and the calculated outlet bulk temperature.

In Tables B.3 to B.5, the actual temperature readings, obtained from the thermocouples attached to the gold-film heater during each of the three temperature runs, are presented. For ease of documentation, run #38 and run #39 have been subdivided into three cases (denoted A, B and C), corresponding to three angular positions of the two diametrically opposed lines of thermocouples attached to the gold-film heater. Since the time-mean temperature measurements for flow in a vertical tube were axisymmetric (in run #40) the thermocouples were circumferentially indexed only twice. Thus, run #40 is only divided into two cases: #40-A and #40-B. The overall electrical resistance of the gold-film heater in each case is tabulated in Table B.6.

As was stated earlier, the thermocouples attached to the gold-film heater were arranged in two longitudinal and diametrically-opposed lines (as shown in Figure 3.11). Using the cylindrical-polar coordinate system (discussed in section 2.2) with origin at the

inlet of the heated tube and the z-axis aligned with the longitudinal axis, the location of a thermocouple on the surface of the gold-film is specified by the azimuthal angle, Θ, and its distance, z. The temperature readings and their respective polar coordinates (Θ and z) are tabulated in Tables B.3 to B.5. The coordinate, z, is tabulated in non-dimensional form, z/L, where L is the length of the test section, 42 and 7/16 inches.

The flow visualization photographs taken during the runs #38, #39 and #40, are displayed in figures B.1, B.2 and B.3, respectively. A spiral flow pattern of the dye is evident in figures B.1 and B.2, corresponding to the horizontal-tube ($\alpha = 0°$) and the inclined-tube ($\alpha = 45°$) run, respectively. In Figure B.3 which pertains to the vertical-tube ($\alpha = 90°$) run, a recirculation cell can be seen (in figure B.3(a)); downstream of this recirculation cell, the laminar instability occurs (seen in figure B.3(b)); in figure B.3(b), downstream of the wave-like laminar instability, the disorderly motion of the dye, discussed in section 4.2.2, can also be observed.

The temperature readings tabulated in Tables B.3 to B.5 are plotted in figures B.4 to B.6. Figures B.4, B.5 and B.6 contain graphs for runs #38, #39 and #40, respectively. The temperature readings are graphed on polar plots, one for each axial location along the test section where readings were taken. For each run, the readings for the different cases, or different angular positions of the thermocouple, are graphed on the same plot. Hence, the circumferential variation of the temperatures can be easily examined. In this context, it is useful to note the following information for runs #38, 39 and 40. In the

three cases of run #38, the flow rate differed by ± 0.05 cm^3/s and the power applied by roughly $\pm 0.08\%$: thus, the Gr/Re^2 values varied by 6.2% above and 4.2% below the mean. Among the three cases of run #39, the power applied did not vary and the flow rates differed by only $\pm .01$ cm^3/s: thus, the Gr/Re^2 values varied by less than 1% about their mean. In the two cases of run #40, the two flow rates were equal as well as the power applied: thus, the Gr/Re^2 values were also equal.

Abid et al. [1994] and Laouadi et al. [1994] reported significant circumferential variations in the temperature of uniformly heated horizontal and inclined tubes. In a given cross-section, perpendicular to the longitudinal axis of the tube, the temperature was a maximum at the top of the pipe and monotonically decreased to a minimum at the bottom. This reported trend is due to the spiral flow patterns that occur: warmer fluid moves upward along the wall of the tube, whereas colder fluid moves downward in the central regions. The results for runs #38 and #39, graphed in figures B.4 and B.5, respectively, show these trends too.

In the case of vertical tubes, the time-mean temperature field is axisymmetric, as documented by Bernier and Baliga [1992]. In run #40, the first five thermocouples, located at the axial distances of z/L = 0.093, 0.205, 0.317, 0.429, and 0.541, were situated upstream of the unsteady, laminar instability. The readings obtained form these thermocouples are axisymmetric to within ± 0.53°C.

Graphs of the temperature readings versus axial distance along the tube are shown in figures B.7, B.8 and B.9, which correspond to runs #38, #39 and #40, respectively. In all three runs, the temperatures increased with axial distance, but a clear linear trend did not occur. The axial variation of the temperatures depends significantly on the extent of the wall conduction effects, since readings were taken on the outer surface of the gold-film heater, which, in turn, was attached to the outer surface of the pipe wall.

4.4 EXPERIMENTAL ERRORS AND UNCERTAINTIES

In this section, the following sources of experimental errors and uncertainty are discussed: (i) radiation losses from the gold-film heater; (ii) wall conduction effects; (iii) the effectiveness of the mixing cup; (iv) the sensitivity of the results to changes in the ambient temperature; (v) the accuracy of the temperature readings; and (iv) the uniformity of the electrical resistance of the gold-film heater.

4.4.1 Radiation Losses

An upper bound on the radiation losses from the gold-film heater will be calculated for run #40. This will also allow the estimation of the radiation losses in runs #38, and #39, because the temperatures and applied power in the runs were comparable to those of run #40.

During run #40, the test section was fully insulated, as discussed in section 3.2.1, and the average reading from the four thermocouples installed on the outer surface of the 4" o.d. plexiglas pipe (section 3.4.1) was 28.6°C (the variation about their mean was small: $\pm 1.5°$). In order to estimate the radiation losses from the gold-film heater, the following conservative assumptions were made: (i) the gold-film heater and the inner surface of the 4" o.d. plexiglas pipe radiated as black bodies (thus, their emissivity was set equal to one); (ii) the temperature of the outer surface of the gold-film was uniform and equal to 40°C; and (iii) the temperature of the 4" o.d. plexiglas pipe was uniform and equal to 28°C. Furthermore, one-dimensional radial heat transfer was assumed to prevail. Under these conditions, the radiation losses amounted to 7.04% of the total power applied to the gold-film heater.

Since the gold-film heater does not actually radiate as a black body, the real radiation losses in run #40 were substantially less than 7.04%. In this context, it should be noted that Neill [1989] estimated the emissivity of the gold-film as 0.2.

Since the measured temperatures and the applied power in runs #38 and #39 were comparable to those of run #40, the radiation losses in all three runs were similar in magnitude. This can be easily confirmed by calculations similar to those indicated above for run #40.

During the flow visualization runs, the outer surface of the 4" o.d. plexiglas pipe

was not insulated. If it is assumed, for run #40, that the outer-surface temperature of the 4" o.d. pipe was uniform and equal to the ambient value of 20°C, the black-body radiation losses would amount to 11.28% of the total power applied to the gold-film heater. Once again, since the gold-film heater does not actually radiate as a black body, the real losses would be substantially less than 11.28%. It is reasonable to assume that since, in all but four of the thirty-five runs, the power applied was less than, or almost equal to, that of run #40. Only in runs #12 (α=45°), #19 (α=0°), #25 (α=60°), and #29 (α=76°) was it greater than that of run #40 (roughly 145 watts).

This author recommends that a researcher intending to use this apparatus in the future undertake the task of implementing an effective radiation shield. A clear view of the flow in the test section is desired. Thus, the material of the radiation shield would have to (i) be transparent enough in the visible wavelength range to allow satisfactory photographs to be taken; and (ii) have a low transmissivity to the thermal radiation. Different translucent materials would have to be selected, tested, and their performance assessed.

4.4.2 Wall Conduction Effects

The experimental apparatus that was designed and constructed in this work is intended to eventually generate results that can be used to ascertain the accuracy of numerical models of the mixed convection phenomena. A companion numerical

investigation can account for the presence of wall conduction with relative ease. Thus, wall conduction effects are not a source of experimental uncertainty, but an element of the phenomena under study. Nonetheless, an appraisal of the extent of the wall conduction will be presented.

Laouadi et al. [1994] numerically investigated the effects of heat conduction in the pipe wall on upward, laminar flows in horizontal and inclined pipes. According to Laouadi et al. [1994], the effects of wall conduction in tubes with an outer-to-inner radius ratio of 1.5 are negligible if the ratio between wall and fluid conductivities, K_p, is 0.1 or less. The wall conduction effects become significant in pipes with a K_p of 10. The Grashof number in the investigation of Laouadi et al. [1994], based on heat flux at the solid-fluid interface, varied from $5X10^4$ to $1X10^6$, and the Reynolds number was fixed at 500.

In this investigation, the plexiglas tube used has an outer-to-inner radius ratio of 1.33 and a K_p of approximately 0.3. The Grashof number, based on the heat flux generated by the gold-film heater, was varied from $5.85X10^4$ to $3.54X10^5$, and the Reynolds number ranged from 24.13 to 215.7. Thus, a rudimentary comparison with the results of Laouadi et al. [1994] suggests that wall conduction effects, in the present investigation, are present but not significant.

4.4.3 The Effectiveness of the Mixing Cup

In Table B.1 the applied power ($P_a = V*I$), the calculated rate of energy gain of the fluid ($P_f = mC_p\delta T_b$), based on the measured bulk temperature difference, and the percentage difference between the two, $(|P_a - P_f|/P_a)*100$, are tabulated. In the three horizontal-tube cases, #38-A, #38-B and #38-C, the differences, $(|P_a - P_f|/P_a)*100$, are 7.66%, 9.44%, and 8.63%, respectively. In the three inclined-tube cases with $\alpha=45°$, #39-A, #39-B and #39-C, the differences are 5.94%, 4.24%, and 4.35%, respectively. In the two vertical-tube cases, #40-A and #40-B, the differences are 1.88% and 2.03%.

Thus, the marble-filled mixing cup became more effective as the angle of inclination increased toward 90° (vertical). In section 4.2.3, it was remarked that air pockets tended to collect at the top of the horizontal tube. This difficulty is also encountered at the top of the mixing cup, and in the interstices between the marbles. These air bubbles reduce the effectiveness of the mixing in the cup. Air bubbles and pockets collect more quickly in the horizontal-tube cases since they are not subjected to buoyancy forces in the direction of flow through the tube and mixing cup. Thus, the difficulty is more pronounced in the horizontal-tube cases than in the inclined- and vertical-tube cases.

4.4.4 Sensitivity to Ambient Temperature Changes

The ambient temperature in the laboratory was controlled by a 33,000 BTU air conditioning unit. During an entire experimental run, the temperature in the laboratory varied by less than $\pm 1.5°$ about a mean value of 20° Celsius. Correspondingly, the inlet and outlet bulk- temperature readings varied by less than $\pm 0.05°$. Furthermore, due to the thermal inertia of plexiglas pipe, the related variations in the temperature readings of the gold-film heater were imperceptible.

4.4.5 Uncertainty in the Temperature Readings

As was discussed in section 3.4.1, the uncertainty in the temperatures measured by the calibrated thermocouples was less than $\pm 0.05°C$. The calibration procedure used in this work is the same as that developed by Stathopoulos [1990], who also rated the uncertainty in the corresponding temperature measurements as less than $\pm 0.05°C$.

It should be noted that one of two thermocouples situated at the distance $z/L=0.765$ gave anomalously low temperature readings. For instance, in run #40, the thermocouple readings at $\Theta = 90°$ and 0° were notably lower than their counterpart readings at $\Theta = 270°$ and 180°. Since all calibrations were verified before the installation of the thermocouples, the cause of this difficulty seems to be damage to the thermocouple during the installation procedure. In the graphs of figures B.7(a), B.8(a),

and B.9(a), the readings obtained from this defective thermocouple were not included.

4.4.6 Uniformity of the Electrical Resistance of the Gold Film

The nominal electrical resistance of the gold film at room temperature was rated at 13.54 Ω/square by Neill [1989]. He also determined that the resistance of the gold film was uniform to within ±6.2%. However, if a six-inch wide strip of gold film was cut from the central region of an eighteen-inch wide spool, as was done in this investigation, Bernier [1991] found that the gold-film resistivity was uniform to within ±3%.

The resistivity of the gold film was found to vary negligibly with temperature. In run #11, in which the applied power was the lowest out of all the runs (19.07 watts), the measured overall electrical resistance of the gold-film heater was 175.47Ω. In run #12, in which the applied power was the highest out of all the runs (145.58 watts), the measured overall electrical resistance of the gold-film heater was 179.56Ω. Thus, the variation of the overall electrical resistance of the gold-film heater in all runs about the mean of those two values is less than ±1.15%.

CHAPTER 5

CONCLUSION

The main contribution of this work is discussed first in this chapter. Following that, a summary of the results is presented. Finally, some ideas for extensions of this work are presented in the concluding section of the chapter.

5.1 MAIN CONTRIBUTION

An experimental apparatus for the study of mixed convection heat transfer in vertical, horizontal and inclined tubes was designed and constructed. The test section consisted of a plexiglas pipe which was heated uniformly by a translucent gold-film electrical heater. A transparent vacuum chamber was used to insulate the test section. This allows, for the first time, flow visualization over the entire length of a uniformly heated tube. The apparatus was also designed to allow the study of both circumferential and axial temperature variations over the heated tube.

The gold-film heater was fixed to the outside surface of the plexiglas tube. Innovative techniques were developed for the cutting, gluing, and powering of the gold-film heating element. The gold-film heater performed continuously, in a vacuum, over a period of several months, without burning. In contrast, with the earlier design of

Bernier and Baliga [1992a], in which the gold-film was fixed to the inside surface of the plexiglas tube, the heating element burned up quite frequently.

Flow calmers (see section 3.2.2) were installed in the apparatus so that the ingestion of air was greatly minimized. Thus, the accumulation of air bubbles in the test section was effectively eliminated in the inclined- and vertical-tube runs, and kept at tolerable levels in the horizontal-tube runs. The apparatus was also designed to allow it to be periodically flushed in order to remove any residual air pockets (see section 3.2.1).

5.2 SUMMARY OF THE RESULTS

Flow visualization results were obtained for seven angles of inclination, measured with respect to the horizontal: 0°, 30°, 45°, 60°, 76°, 87°, and 90°. Thirty-five experimental runs were carried out over a range of Gr/Re^2 values from 6 to 200. Temperature data, over the circumference and axial length of the heated tube, were obtained for three angles of inclination: 0°, 45° and 90°.

The flow visualization experiments in vertical tubes revealed recirculation zones in all cases considered. Similar recirculation zones had been predicted and detected in an earlier investigation (Bernier and Baliga, [1992]). A zone of laminar instability was detected downstream of the stable recirculation zone. In this zone of laminar instability, unsteady, wave-like fluctuations of the injected dye filament occurred. In one case, the

laminar instability zone extended extending over twenty-five tube diameters in length. The laminar instability zone was followed by a region of unsteady, disorderly flow, which may be a precursor to laminar-turbulent transition.

In inclined tubes, the flow visualization experiments revealed spiral-like flow patterns. Such flow patterns were predicted numerically by Laouadi et al. [1994]. Laminar flow instability was not detected in the tubes with the following angles of inclination, measured with respect to the horizontal: 0°, 30°, 45°, 60° and 76°. In these cases, the component of the gravity vector perpendicular to the longitudinal axis of the tube ($g\cos\alpha$) suffices to stabilize the flow.

Laminar instability and spiral-like flows were detected in tubes with the 87° inclination. In one particular run, a stable recirculation cell, very similar to those detected in vertical tubes, was observed as well.

Results of the circumferential variation of temperature qualitatively confirmed the published data of Laouadi et al. [1994]. In inclined and horizontal tubes, the minimum temperature occurred at the bottom of the tube, and monotonically increased until the top of the tube. The temperatures increased with axial distance along the tube.

5.3 PROPOSED EXTENSIONS OF THIS WORK

The following extensions of this work are suggested:

1. Only upward mixed-convection flows in vertical and inclined tubes were considered in this work. However, with minor modifications of the distilled water (or working-fluid) circuit, the experimental apparatus could be used to study downward mixed-convection flows in vertical and inclined tubes.

2. The radiation losses from the gold-film heater were estimated to be less than 11.28% for the cases considered in this work. These losses could be reduced by employing radiation shields inside the annular vacuum chamber around the heated test section. Such shields would have to be constructed of materials that have high transmissivity to electromagnetic radiation in the visible wavelength band, 0.4μm to 0.7μm, and very low transmissivity outside this wavelength band.

3. With the values of Grashof number, Gr, Reynolds number, Re, and length-to-diameter ratio of the test section, L/D, considered in this work, it was not possible to generate fully turbulent mixed convection flows. However, a plexiglas tube with a smaller diameter, and hence

higher L/D value, could be used to construct a new heated test section. Such a test section would allow the investigation of laminar-turbulent transition and fully turbulent mixed convection.

4. In this work, the bulk temperature of the distilled water at the inlet was maintained at 8°C or higher. However, in cold climates, such as that in Canada, mixed convection in water often occurs near its density inversion temperature (approximately 4°C). The cooling capacity of the constant-temperature bath used in this investigation is not high enough to achieve inlet bulk temperatures less than 4°C. It would be worthwhile to obtain a more powerful constant-temperature bath, and investigate mixed convection in the vicinity of the density inversion temperature.

In conclusion, the author hopes that this thesis has contributed, at least in a modest manner, to an improved understanding of mixed convection phenomena in tubes. He also hopes that the experimental apparatus that was designed and constructed in this work will continue to be used in complementary experimental/numerical approaches to the design of mixed-convection heat transfer equipment.

REFERENCES

Abid, C., Papini, F., Ropke, A., and Veyret, D., Etude de la Convection Mixte dans un Conduit Cylindrique. Approches Analytique/Numérique et détermination expérimentale de la Température de Paroi par Thermographie Infrarouge, **Int. J. Heat Mass Transfer**, vol. 37, no. 1, pp. 91-101, 1994.

Barozzi G.S. and Pagliarini, G., Experimental Investigation of Coupled Conduction and Laminar Convection in a Circular Tube, **Int. J. Heat Mass Transfer**, vol. 27, no. 12, pp. 2321-2329, 1984.

Barozzi, G.S. and Pagliarini, G., A Method to Solve Conjugate Heat Transfer Problems: The Case of Fully Developed Laminar Flow in a Pipe, **ASME Journal of Heat Transfer**, vol. 107, pp. 77-83, 1985.

Barozzi, G.S., Zanchini, E. and Mariotti, M., Experimental Investigation of Combined Forced and Free Convection in Horizontal and Inclined Tubes, **Meccanica**, vol. 20, no. 1, pp. 18-27, 1985.

Baughn, J.W., Takahashi, R.K., Hoffman, M.A., McKillop, A.A, Local Heat Transfer Measurements Using an Electrically Heated Thin Gold-Coated Plastic Sheet, **ASME Journal of Heat Transfer**, vol. 107, pp. 953-959, 1985.

Bernier, M.A., **Investigation of a Closed Loop Thermosyphon**, Ph.D. Thesis, McGill University, 1991.

Bernier, M.A. and Baliga, B.R., Visualization of Upward Mixed-Convection Flows in Vertical Pipes Using a Thin Semitransparent Gold-Film Heater and Dye Injection, **Int. J. Heat and Fluid Flow**, vol. 13, no. 3, 1992a.

Bernier, M.A. and Baliga, B.R., Conjugate Conduction and Laminar Mixed Convection in Vertical Pipes for Upward Flow and Uniform Wall Heat Flux, **Numerical Heat Transfer**, Part A, vol. 21, pp. 313-332, 1992b.

Bernier, M.A. and Baliga, B.R., A 1-D/2-D Model and Experimental Results for a Closed-Loop Thermosyphon with Vertical Heat Transfer Sections, **International Journal of Heat and Mass Transfer**, vol. 35, pp. 2969-2982, 1992c.

Brown C.K. and Gauvin W.H., Combined Free and Forced Convection Flow, I. Heat Transfer in Aiding Flow, **Can. J. Chem. Eng.**, vol. 43, no. 6, pp. 306-312, 1965.

Brown C.K. and Gauvin W.H., Combined Free and Forced Convection Flow, II. Heat Transfer in Opposing Flow, **Can. J. Chem. Eng.**, vol. 43, no. 6, pp. 313-318, 1965.

Brown, A.R. and Thomas, M.A., Combined Free and Forced Convection Heat Transfer For Laminar Flow in Horizontal Tubes, **J. Mech. Engng Sci.**, vol. 7, no. 4, pp. 440-448, 1965.

Cheng, K.C. and Hong, S.W., Combined Free an Forced Laminar Convection in Inclined Tubes, **Appl. Sci. Res.**, vol. 27, pp. 19-38, 1972a.

Cheng, K.C. and Hong, S.W., Effect of Tube Inclination on Laminar Convection in Uniformly Heated Tubes for Flat-Plate Solar Collectors, **Solar Energy**, vol. 13, pp. 363-371, 1972b.

Cotton, M.A. and Jackson, J.D., Vertical Tube Air Flows in the Turbulent Mixed Convection Regime Calculated Using a Low-Reynolds-Number k-ϵ Model, **Int. J. Heat Mass Transfer**, vol. 33, no. 2, pp. 275-286, 1990.

Elkouh, N. and Baliga, B.R., Effect of Variable Properties on Natural Convection in Water Near its Density Inversion Temperature, **Proc. 30th National Heat Transfer Conference**, Portland, U.S.A., August 6-8, vol. 11, pp. 53-59, 1995.

Faghri, M. and Sparrow, E.M., Simultaneous Wall and Fluid Axial Conduction in Laminar Pipe-Flow Heat Transfer, **ASME Journal of Heat Transfer**, vol. 102, pp. 58-63, 1980.

Faris, G.N. and Viskanta, R., An analysis of Laminar Combined Forced and Free Convection Heat Transfer in a Horizontal Tube, **Int. J. Heat Mass Transfer**, vol. 12, pp. 1295-1309, 1969.

Gebhart. B. and Mollendorf, J.C., Buoyancy-Induced Flows in Water Under Conditions in Which Density Extrema May Arise, **J. of Fluid Mech.**, vol. 89, pp. 673-707, 1978.

Hall, W.B. and Jackson, J.D., Heat Transfer Near the Critical Point. Keynote Lecture, **Proc. 6th Int. Heat Transfer Conf.**, Toronto, Canada, 1978.

Heggs, P.J., Ingham, D.B. and Keen, D.J., The Effects of Heat Conduction in the Wall on the Development of Recirculating Combined Convection Flows in Vertical Tubes, **Int. J. Heat Mass Transfer**, vol. 33, no. 3, pp. 517-528, 1990.

Hippensteele, S.A., Russell, L.M., Stepka, F.S., Evaluation of a Method for Heat Transfer Measurements and Thermal Visualization Using a Composite of a Heater Element and Liquid Crystals, **ASME Journal of Heat Transfer**, vol. 105, pp. 184-189, 1983.

Hippensteele, S.A., Russel, L.M., Torres, F.J., Local Heat-Transfer Measurements on a Large Scale-Model Turbine Blade Airfoil Using a Composite of Heater Element and Liquid Crystals, **ASME Journal of Engineering for Gas Turbines and Power**, vol. 107, pp. 953-960, 1985.

Huiren, Z. and Songling, L., Numerical Simulation of Transitional Flow and Heat Transfer in a Smooth Pipe, **Int. J. Heat Mass Transfer**, vol. 34, no. 10, pp. 2475-2482, 1991.

Incropera F. P. and Dewitt, D.P., **Introduction to Heat Transfer**, Second Edition, John Wiley & Sons, 1990.

Iqbal, M. and Stachiewicz, J.W., Influence of Tube Orientation on Combined Free and Forced Laminar Convection Heat Transfer, **ASME Journal of Heat Transfer**, vol. 88, pp. 109-116, 1966.

Iqbal, M. and Stachiewicz, J.W., Variable Density Effects in Combined Free and Forced Convection in Inclined Tubes, **Int. J. Heat Mass Transfer**, vol. 10, pp. 1625-1629, 1967.

Jackson, T.W., Spurlock, J.M. and Purdy, K.R., Combined Free and Forced Convection in a Constant Temperature Horizontal Tube, **A.I.Ch.E. Journal**, vol. 7, no. 1, pp. 38-41, 1961.

Jackson, J.D., Hall, W.B., Fewster, J., Watson, A. and Watts, M.J., Heat Transfer to Supercritical Pressure Fluids, UKAEA, Harwell, **Report No. AERE R 8158, 1975.**

Jackson, J.D., Cotton, M.A. and Axcell, B.P., Studies of Mixed Convection in Vertical Tubes, **Int. J. Heat and Fluid Flow**, vol. 10, no. 1, pp. 2-15, 1989.

Japkise, D., Advances in Thermosyphon Technology, in **Advances in Heat Transfer**, edited by Irvine, T.F., and Hartnett, J.P., vol. 9, pp. 1-111, Academic Press, New York, 1973.

Kukulka, D.J., Gebhart, B. and Mollendorf, J.C., Thermodynamic and Transport Properties of Pure and Saline Water, **Advances in Heat Transfer**, vol. 18, pp. 325-363, 1987.

Laouadi, A., Galanis, N. and Nguyen C.T., Laminar Fully Developed Mixed Convection in Inclined Tubes Uniformly Heated on their Outer Surface, **Numerical Heat Transfer**, Part A, vol. 26, pp. 719-738, 1994.

Lavine, A.S., Kim, M.Y. and Shores, C.N., Flow Reversal in Opposing Mixed Convection Flow in Inclined Pipes, **ASME Journal of Heat Transfer**, vol. 111, pp. 114-120, 1989.

Leong, K.C., Chan, S.K. and Phua, L.H., Experimental Investigation of Buoyancy-Opposing Mixed Convection in an Inclined Tube, **Proc. 32nd Heat Transfer and Fluid Mechanics Institute**, Sacramento, U.S.A., June 6&7, pp. 141-156, 1991.

Martinelli, R.C. and Boelter, L.M.K., The Analytical Prediction of Superposed Free and Forced Viscous Convection in a Vertical Pipe, **University of California, Publications in Engineering**, vol. 5, pp. 23-58, 1942.

McComas, S.T. and Eckert, E.R.G., Combined Free and Forced Convection in a Horizontal Circular Tube, **ASME Journal of Heat Transfer**, vol. 88, pp. 147-153, 1966.

Metais, B. and Eckert, E.R.G., Forced, Mixed, and Free Convection Regimes, **ASME Journal of Heat Transfer**, vol. 86, pp. 295-296, 1964.

Morcos, S.M. and Bergles, A.E., Experimental Investigation of Combined Forced and Free Laminar Convection in Horizontal Tubes, **ASME Journal of Heat Transfer**, vol. 97, pp. 212-219, 1975.

Mori, Y., Futugami, K., Tokuda, S. and Nakamura, M., Forced Convective Heat Transfer in Uniformly Heated Horizontal Tubes (1st Report - Experimental Study on the Effect of Buoyancy), **Int. J. Heat Mass Transfer**, vol. 9, pp. 453-463, 1966.

Mori, Y. and Futugami, K., Forced Convective Heat Transfer in Uniformly Heated Horizontal Tubes (2st Report - Theoretical Study), **Int. J. Heat Mass Transfer**, vol. 10, pp. 1801-1813, 1967.

Morton, B.R., Ingham, D.B., Keen, D.J. and Heggs, P.J., Recirculating Combined Convection in Laminar Pipe Flow, **ASME Journal of Heat Transfer**, vol. 111, pp. 106-113, 1989.

Neill, W.S., **Local Natural Convection Heat Transfer Measurements Using a Thin Gold-Film Technique**, M. Eng. Thesis, McGill University, 1989.

Newell, P.H., Jr. and Bergles, A.E., Analysis of Combined Free and Forced Convection for Fully Developed Laminar Flow in Horizontal Tubes, **ASME Journal of Heat Transfer**, vol. 92, pp. 83-93, 1970.

Orfi, J., Galanis, N. and Nguyen, C.T., Laminar Incompressible Flow With Mixed Convection in an Inclined Pipe, **Proc. IASTED Int. Symposium. Modelling, Simulation and Optimization**, Calgary, Canada, May 22-24, pp. 127-130, 1990.

Patankar, S.V., **Numerical Heat Transfer and Fluid Flow**, Hemisphere Publishing Corporation, 1980.

Petukhov, B.S., Polyakov A.F. and Strigin, B.K., Heat Transfer in Tubes with Viscous-Gravity Flow, **Heat Transfer - Soviet Research**, vol. 1, no. 1, pp. 24-31, 1969.

Petukhov, B.S., Heat Transfer and Friction in Turbulent Pipe Flow with Variable Physical Properties, **Advances in Heat Transfer**, vol. 6, pp. 503-564, 1970.

Sabbagh, J.A., Aziz, A., El-Ariny, A.S. and Hamad, G., Combined Free and Forced Convection in Inclined Circular Tubes, **ASME Journal of Heat Transfer**, vol. 98, pp. 322-324, 1976.

Scheele G.F., Rosen, E.M. and Hanratty, T.J., Effect of Natural Convection on Transition to Turbulence in Vertical Pipes, **Can. J. Chem. Eng.**, vol. 38, pp. 67-73, 1960.

Scheele G.F. and Hanratty, T.J., Effect of Natural Convection on Stability of Flow in a Vertical Pipe, **J. of Fluid Mech.**, vol. 14, pp. 244-256, 1962.

Shannon, R.L. and Depew, C. A., Combined Free and Forced Laminar Convection in a Horizontal Tube with Uniform Heat Flux, **ASME Journal of Heat Transfer**, vol. 90, pp. 353-357, 1968.

Stathopoulos, N., **Design and Implementation of an Automatic System for Thermocouple Calibration**, Mechanical Laboratory II Report, McGill University, 1990.

Tanaka, H., Maruyama, S. and Hatano, S., Combined Forced and Natural Convection Heat Transfer for Upward Flow in a Uniformly Heated, Vertical Pipe, **Int. J. Heat Mass Transfer**, vol. 30, no. 1, pp. 165-174, 1987.

White, F.M., **Viscous Fluid Flow**, Second Edition, McGraw-Hill Inc., 1991.

Zvirin, Y., Jeuck III, P.R., Sullivan, C.W. and Duffey, R.B., Experimental and Analytical Investigation of a Natural Circulation System with Parallel Loops, **ASME Journal of Heat Transfer**, vol. 103, pp. 645-652, 1981.

TABLE AND FIGURES

	Year	L/D RATIO	Boundary Condition	Flow Regime	Inlet Profile	Working Fluid	Flow Direction	Incl. Angle, α
Scheele	1960	140	CWT	Tr	HFD	WATER	↑ & ↓	90°
Scheele	1960 1962	114 305 610 762	UHF	Tr	HFD	WATER	↑ & ↓	90°
Petukhov	1969	80	UHF	L & Tr	HFD & HD	WATER	↑	90°
Brown	1965	23	UHF	L & Tu	FLAT	AIR	↑ & ↓	90°
Barozzi	1984	100	UHF	L	HFD & HD	WATER	↑	90°
Tanaka	1987	110	UHF	Tu	HD	N_2	↑	90°
Jackson	1961	31	CWT	L&Tr&Tu	HD	AIR	→	0°
Brown	1965	36 72 108	CWT	L	HFD	WATER	→	0°
McComas	1966	71	UHF	L	HFD	AIR	→	0°
Mori	1966	197	UHF	L&Tr&Tu	HFD	AIR	→	0°
Shannon	1968	787	UHF	L	HFD	WATER	→	0°
Petukhov	1969	99	UHF	L & Tr	HFD	WATER	→	0°
Morcos	1975	107	UHF	L	HFD	Eth.Glyc. & Water	→	0°
Morcos	1975	179	CHACT	L	HFD	Eth.Glyc. & Water	→	0°
Abid	1994	208	UHF	L	HFD	WATER	→	0°
Sabbagh	1976	115	CHACT	L	HD	AIR	↑	0°-90°
Barozzi	1985	83	CHACT	L	HD	WATER	↑	0°-60°
Lavine	1989	40	CWT	L&Tr&Tu	HD	WATER	↓	0°-80°
Leong	1991	44	UHF	L	HFD	WATER	↓	0°-20°

Legend:
L/D Ratio: Length-to-diameter ratio of the pipe's heated section.
UHF: Axially and circumferentially uniform wall heat flux.
CWT: Constant wall temperature.
CHACT: Constant wall heat flux per unit axial length and circumferentially constant wall temperature.
L: Laminar flow.
Tr: Transitional flow.
Tu: Turbulent flow.
HFD: Hydrodynamically fully developed inlet velocity profile.
HD: Hydrodynamically developing inlet velocity profile.
FLAT: Flat (uniform) inlet velocity profile.
↑: Upward (buoyancy-aiding) flow.
↓: Downward (buoyancy-opposing) flow.
→: Horizontal flow.

Table 1.1: Summary of Published Experimental Work of Mixed Convection Heat Transfer in Vertical, Horizontal, and Inclined Tubes.

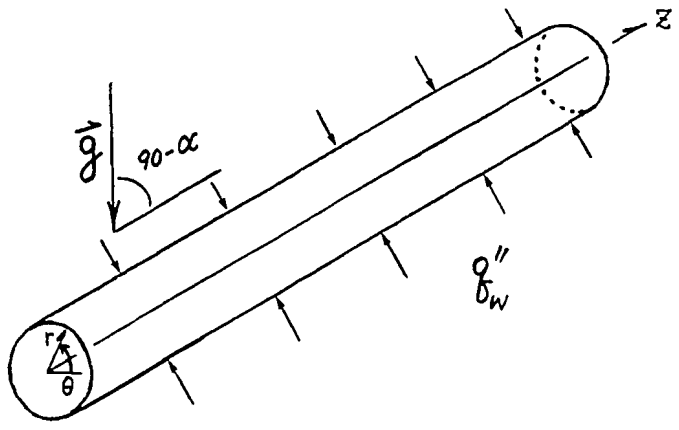

Fig 2.1: Schematic Illustration of the Problem of Interest.

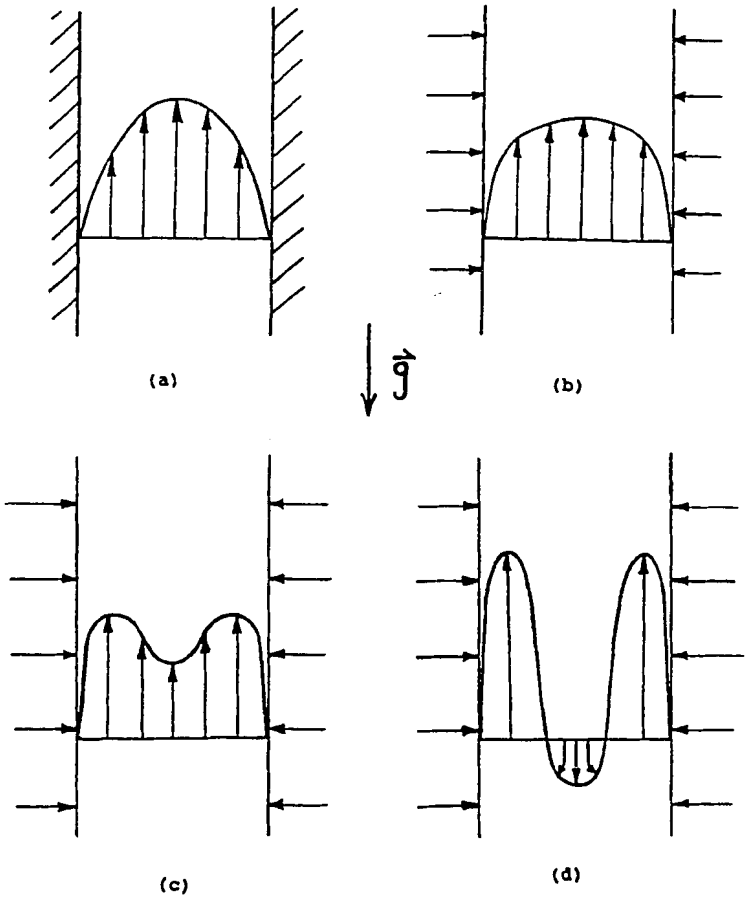

Figure 2.2: Qualitative Sketches of Flow Profiles Inside a Vertical Uniformly Heated Tube: (a) Poiseuille velocity profile at the inlet: (b) and (c) downstream of the inlet, the fluid closer to the wall accelerates, while the fluid in the central portion of the cross section decelerates: (d) further upstream, flow reversal may occur if the applied heat flux is large enough.

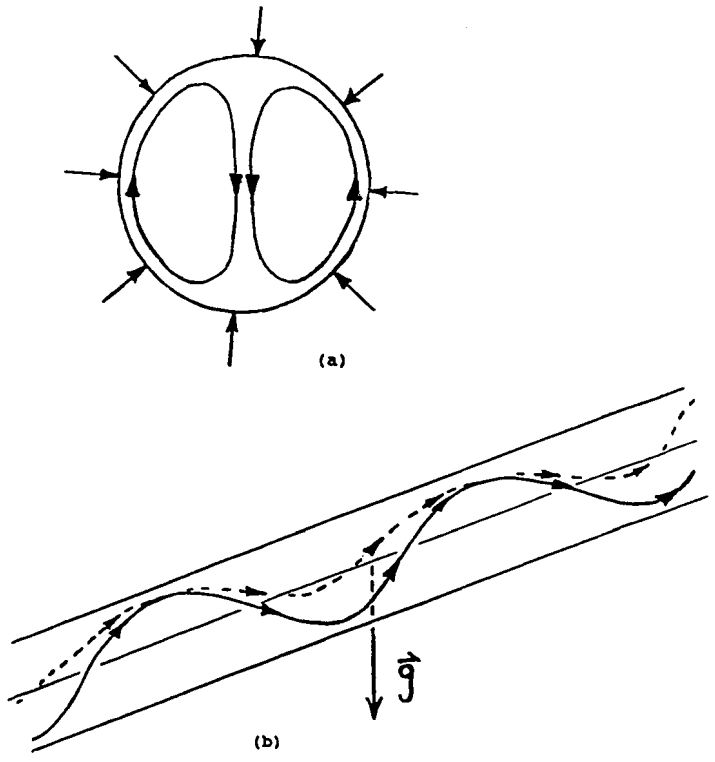

Figure 2.3: Qualitative Sketches of Flow Profiles Inside a Horizontal Uniformly Heated Tube: (a) two stable and symmetrical recirculation cells occur in the cross-section of the tube; (b) spiral motion of the fluid occurs as it moves through the tube.

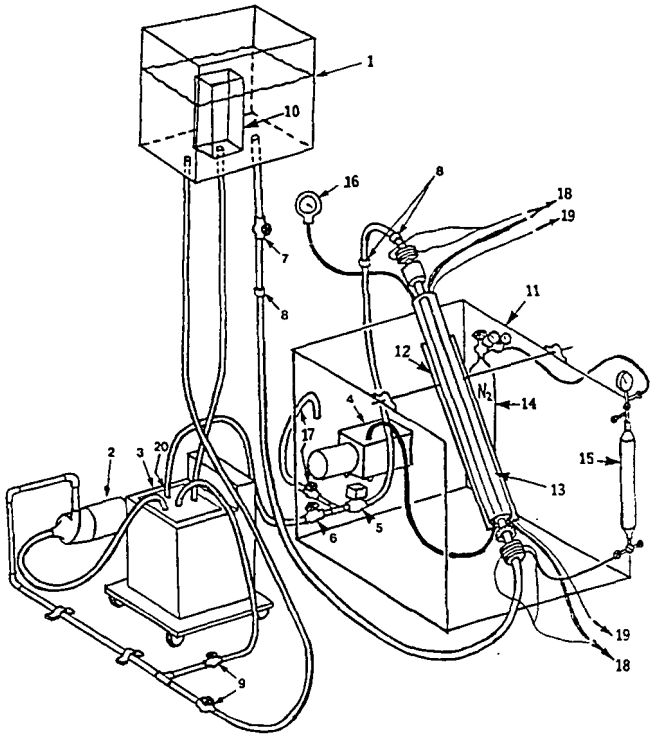

Figure 3.1: Schematic of the Experimental Apparatus: (1) constant head tank; (2) water pump; (3) constant-temperature water bath; (4) vacuum pump; (5) solenoid valve; (6) fine adjustment gate valve; (7) coarse adjustment ball valve; (8) pipe connectors; (9) ball valves; (10) inner tank (for overflow); (11) metal frame; (12) inclinable platform; (13) test section and vacuum chamber; (14) pressurized nitrogen cylinder; (15) dye injection apparatus; (16) vacuum pressure gauge; (17) bypass gate valve and pipe; (18) thermocouple wires (to data acquisition system); (19) electrical lead wire (to power supply); (20) exit of the primary fluid circuit.

(a) (b)

Figure 3.2: Photographs of the Experimental Apparatus; photographs showing, in (a), the waterbath, PVC tubing insulated with black Armaflex, and surrounding equipment; in (b), the flow calmers in the waterbath.

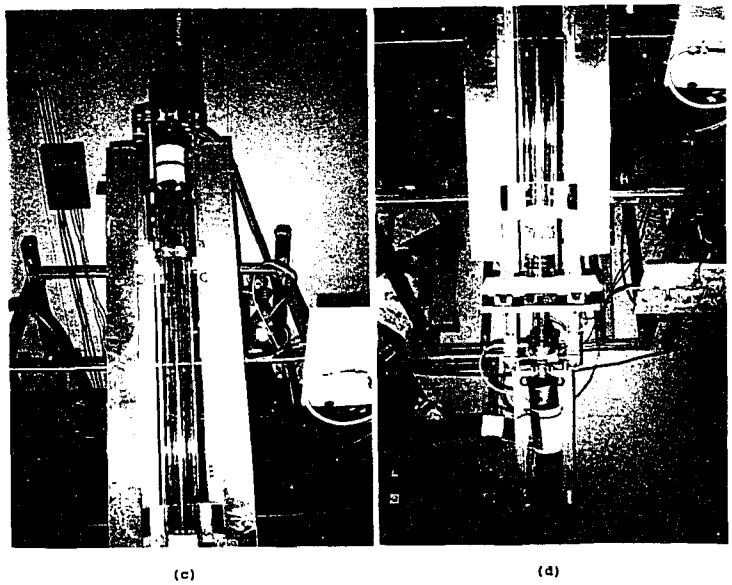

(c) (d)

Figure 3.2 (cont'd): Photographs of the Experimental Apparatus; photographs of the test section and vacuum chamber, inclined 45° to the horizontal, showing, in (c), their top portion without insulation, displaying the mixing cup and the outlet coupling flange; in (d), their bottom portion displaying the inlet coupling flange with dye injection port. Also visible, inside the vacuum chamber, are the purple thermocouple connectors and their white supporting collar (compare with figure 3.3(b)). The two long aluminium sheets on either side of the test section are shades covering two 4'-long blacklight bulbs.

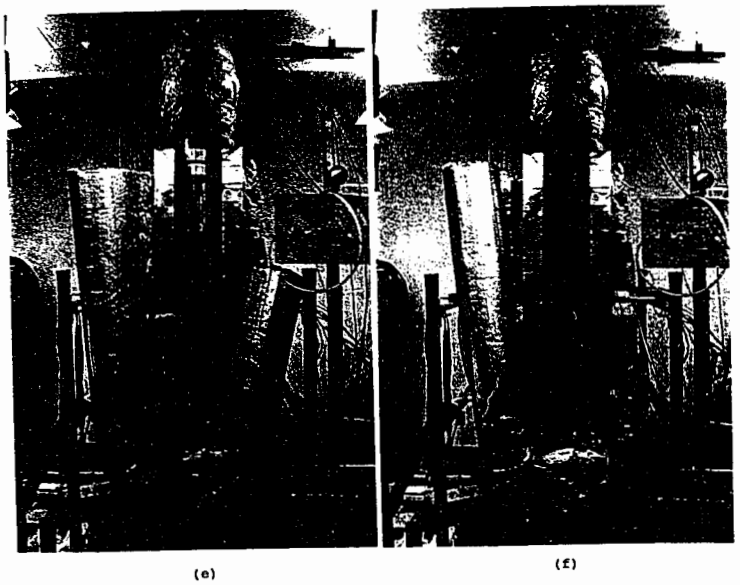

(e) (f)

Figure 3.2 (cont'd): Photographs of the Experimental Apparatus; photographs of the test section and vacuum chamber, vertically aligned, showing, in (e) both the thermal blanket and styrofoam insulation off; in (f) the styrofoam insulation on; and finally, in (g), on the following page, the thermal blanket on. Also visible is the insulation of the mixing cup and coupling flanges.

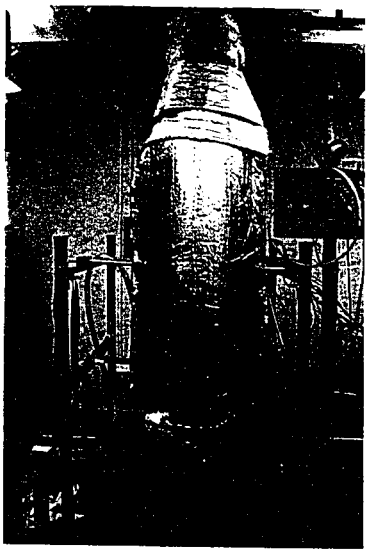

Figure 3.2(g): Photograph of the Experimental Apparatus, Completely Insulated.

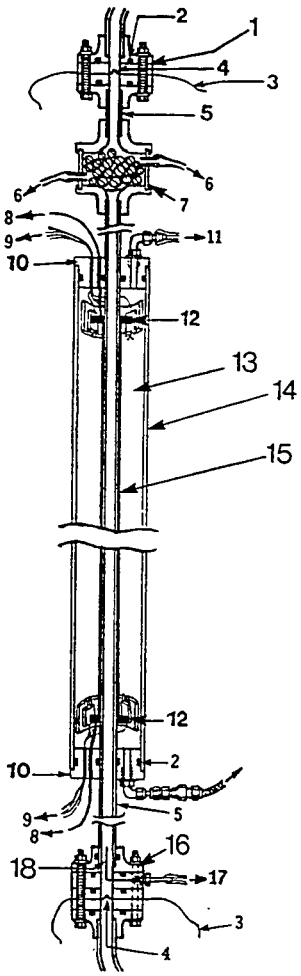

No.	Part
1	Outlet Coupling Flange
2	O-Ring Seal
3	Thermocouple Lead Wire
4	Thermocouple
5	1" o.d. Plexiglass Pipe
6	Draining Port (Closed by Ball Valve)
7	Mixing Cup and Marbles
8	Electrical Lead Wire (to Power Supply)
9	Thermocouple Wire (to Data Acquisition System)
10	Lexan Cap
11	Elbow and Hose (to Vacuum Pressure Gauge)
12	Copper Electrodes
13	Annular Vacuum Chamber
14	4" o.d. Plexiglass Pipe
15	Gold-Film (Test) Section
16	Inlet Coupling Flange
17	Needle Mount and Pipe (to Dye Injection Needle)
18	Dye Injection Needle

Figure 3.3(a): Schematic of the Test Section and Surrounding Pieces.

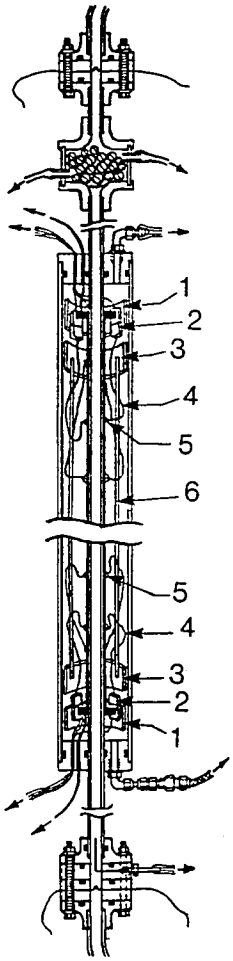

No.	Part
1	Supporting Collar for Thermocouple Connectors
2	Thermocouple Connector (Male and Female Joined)
3	Supporting Collar for Thermocouple Cage
4	Thermocouple Wire
5	Thermocouple
6	¼" Plexiglass Rods (the Thermocouple Cage)

Figure 3.3(b): Schematic of the Test Section. Including the Thermocouples and the Supporting Thermocouple Cage.

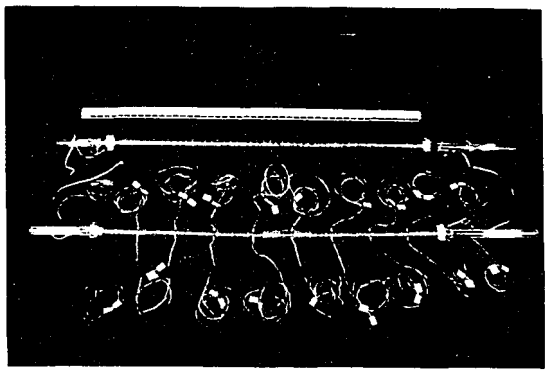

(a)

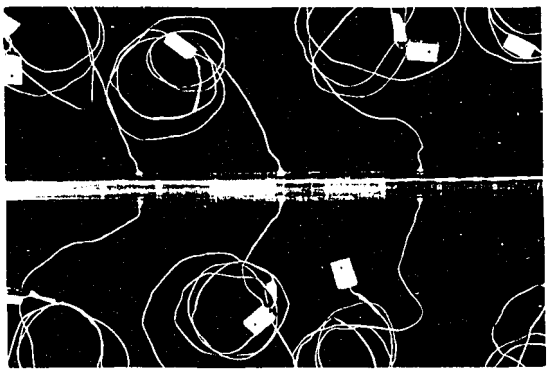

(b)

Figure 3.4: Photographs of Gold-Film (Test) Sections; photographs showing, in (a), a 4' scale (top), test section no. 2 (middle), and test section no. 1 (bottom); in (b), close-up of thermocouples glued to test section no. 1.

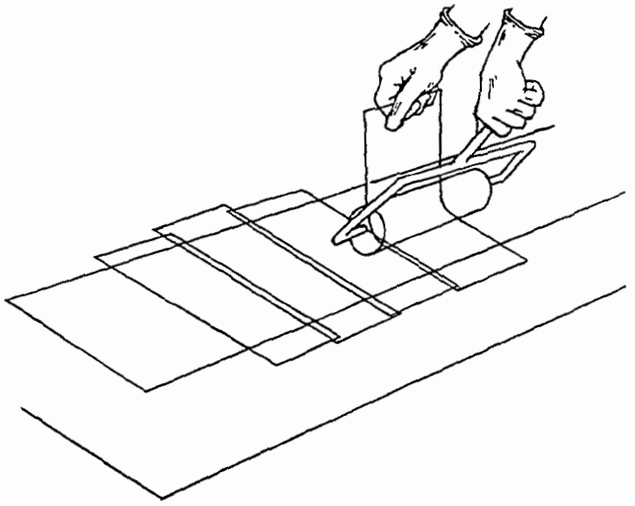

Figure 3.5: Application of Single-Sided Adhesive Tape. The tape is applied using a roller. A slight overlap between the individual strands of tape is allowed in order to ensure that none of the gold film is left bare. The tape is applied slowly and carefully in order to avoid or minimize the air gaps that form underneath it.

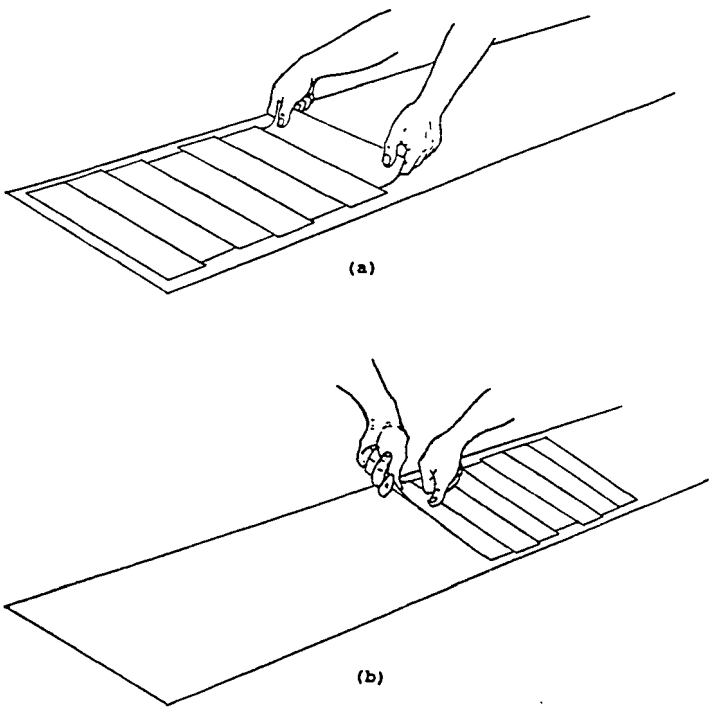

Figure 3.6: Application of Double-Sided Adhesive Tape: (a) the edge of a strand of tape is placed alongside the edge a neighbouring strand. Meticulous care is given so that no air gap is created between the two individual strands: (b) the strand of tape is then very carefully pressed onto the film, to prevent any air bubbles from forming underneath it.

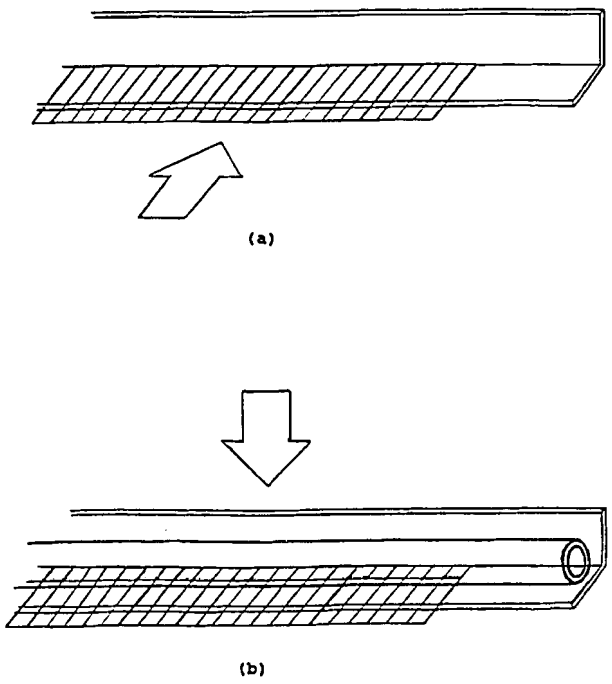

Figure 3.7: Mounting of the Gold-Film onto the Plexiglass Pipe: (a) the edge of the film is pushed up against an L-bar, as shown. The exposed double-sided adhesive tape is facing up; (b) the plexiglass pipe is then pushed down, along the side of the L-bar, until it touches the double-sided adhesive tape, and preliminary adhesive contact is made. This way, the contact line between the two is parallel to the longitudinal axis of the pipe and the film's edge.

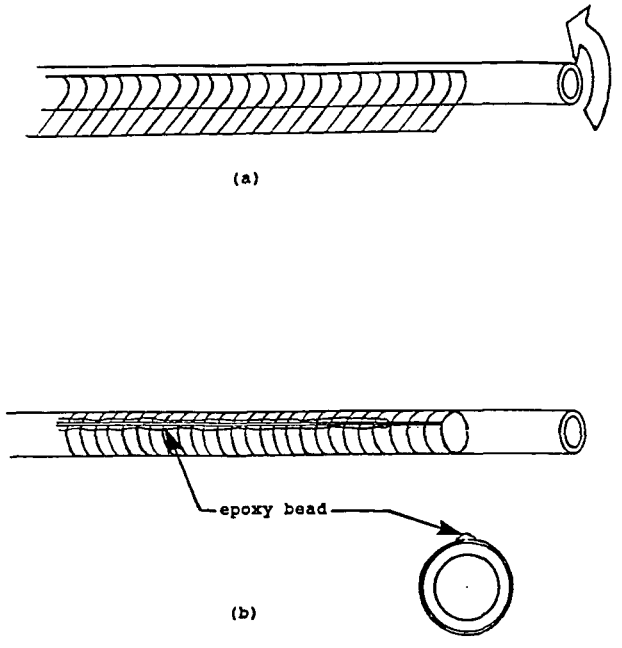

Figure 3.8: Wrapping of the Gold Film Around the Pipe: (a) the pipe and film are moved over to a nearby rubber mat. The film is firmly wrapped around the pipe, by carefully rolling the latter over the former, as shown. The pipe is pressed, manually, onto the film as it is being rolled. This prevents air bubbles from being created between the pipe and film and also ensures strong adhesive contact between the two; (b) once the film is completely wrapped around the pipe, a long bead of epoxy is applied over the seam (the gap between the two long edges of the gold-film). The epoxy glue ensures that the film will not unwrap from the pipe during the period of its use.

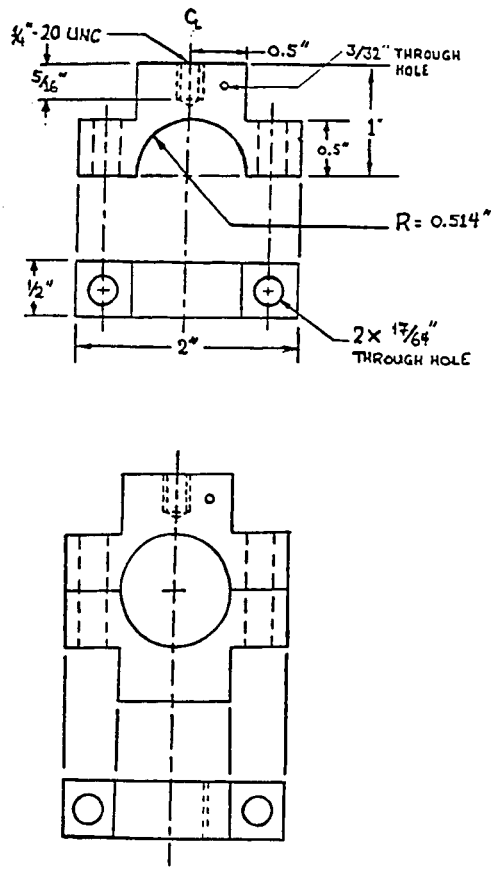

Figure 3.9: Design of the Copper Electrodes

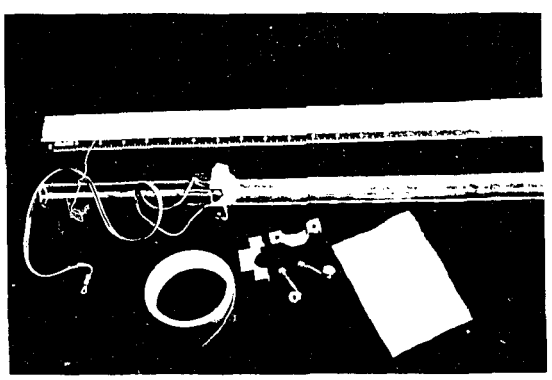

Figure 3.10: The Copper Electrode and its Constituent Parts; shown in the photograph: a scale in inches (top); an electrode fully installed onto a test section (middle); and, bottom row, from left to right, 1 roll of 3M scotch brand electrical tape, a disassembled electrode, and one bag of thermally conductive epoxy.

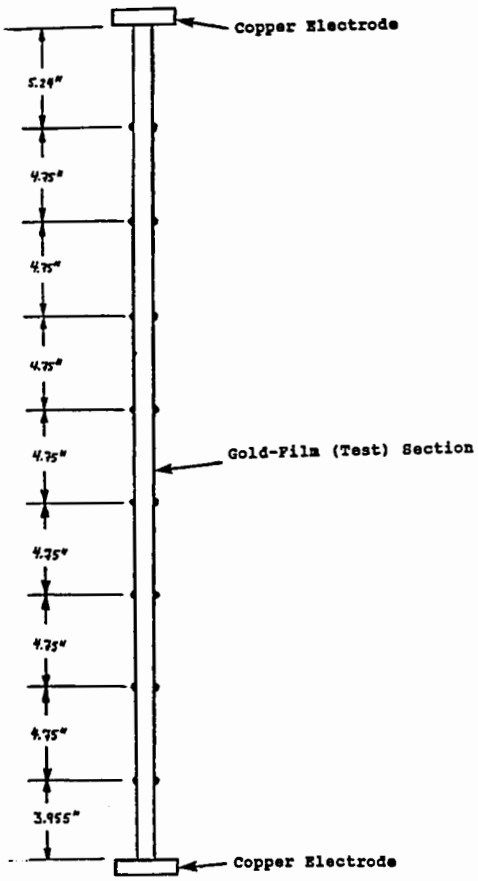

Figure 3.11: Location of Thermocouples on Gold Film (Test) Section

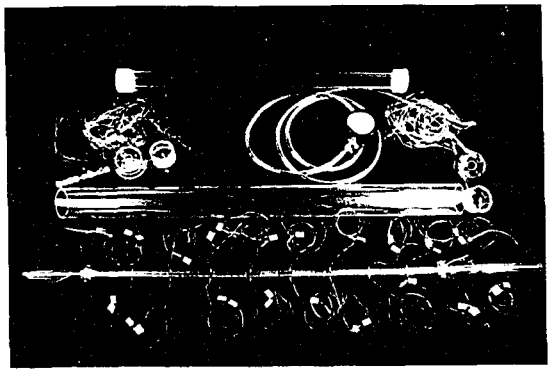

Figure 3.12: Photograph of the Test Section and Vacuum Chamber, Disassembled; shown in the photograph: top, the thermocouple cage; second row from top, left to right, (i) lexan cap (inlet) with vacuum fittings, adjoining thermocouple wires, and supporting collar for thermocouple connectors, (ii) lexan cap (outlet) with connection to the vacuum pressure gauge, adjoining thermocouple wires, and supporting collar for thermocouple connectors; second to bottom, 4" o.d. plexiglass pipe; bottom, test section no. 1.

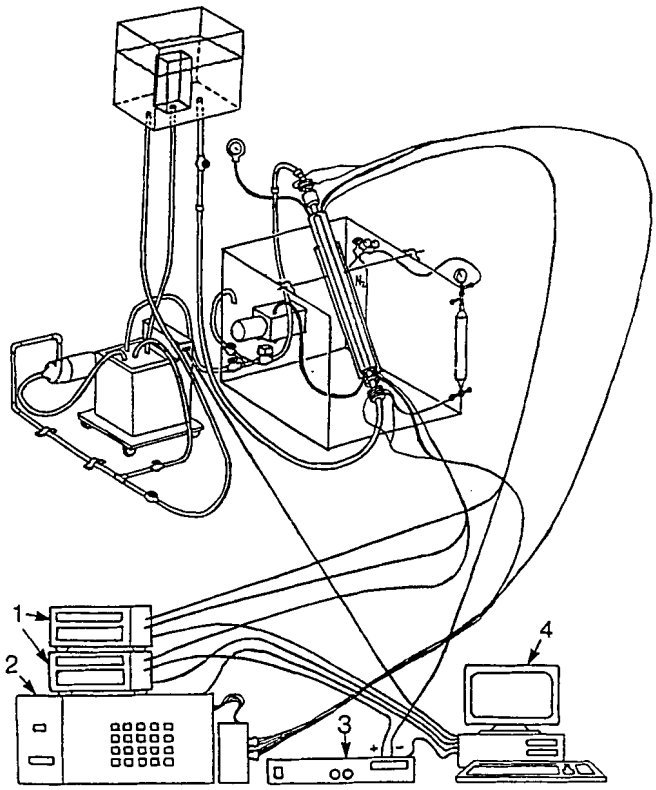

Figure 3.13: Schematic of the Control and Data Acquisition Systems; (1) multimeters; (2) data acquisition and interface system; (3) power supply; (4) computer terminal.

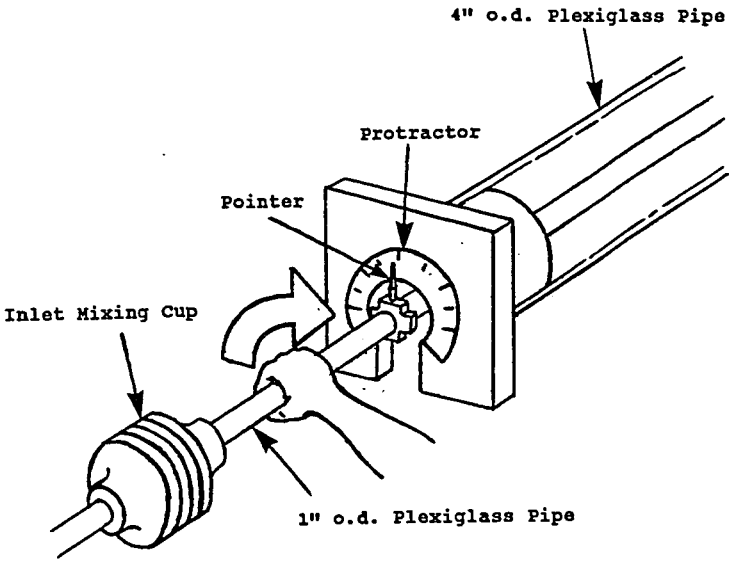

Figure 3.14(a): Indexing of the 1" o.d. Plexiglass Pipe. Rotating the entire inner tube, circumferentially, will rotate the thermocouples glued to it, as well. The tube is rotated manually, by grasping the exposed part of the 1" o.d. plexiglass pipe, as shown. The mixing cup (not shown in the figure) is being firmly held, by a second person, in order for it not to rotate along with the tube.

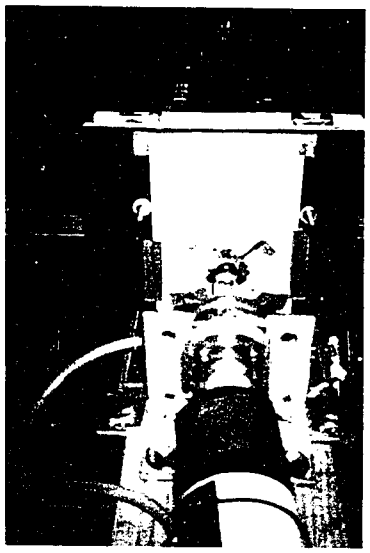

Figure 3.14(b): Photograph of the Protractor and Pointer, Situated Below the Test Section.

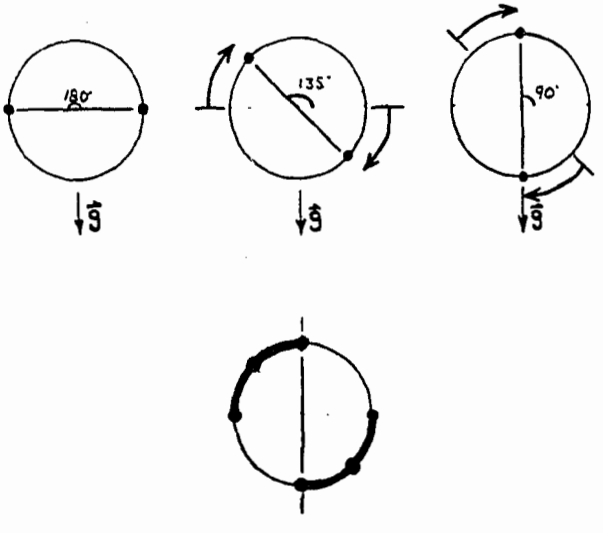

Figure 3.14(c): Indexing Sequence. *The 1" o.d. plexiglass tube is rotated, incrementally, in the sequence shown. Readings are taken after each angular increment, thereby obtaining readings at six angular positions over ½ the circumference (shown by the dots along the bold arcs in the bottom cross-section).*

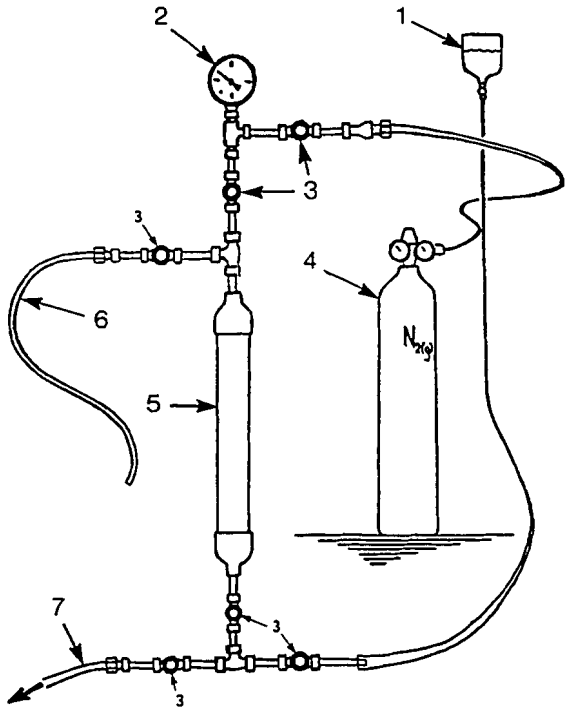

Figure 3.15: Schematic of the Dye Injection Apparatus; (1) filling cup; (2) pressure gauge; (3) needle valve; (4) pressurized nitrogen cylinder; (5) dye reservoir; (6) overflow line; (7) dye injection line (to the dye injection needle).

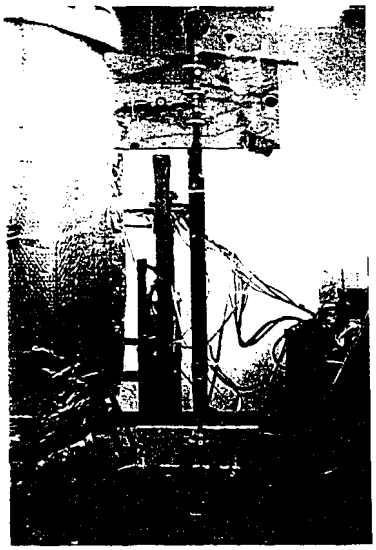

Figure 3.16: Photograph of the Dye Injection Apparatus.

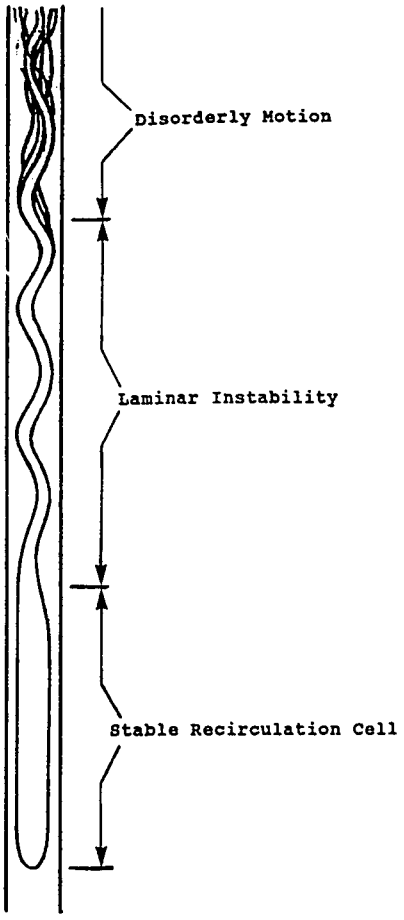

Figure 4.1: Schematic of Flow Patterns with the Test Section in the Vertical Position

APPENDIX A

RESULTS OF THE FLOW VISUALIZATION EXPERIMENTS

Numerous flow visualization experiments were conducted using test section no.2. The results of the final 35 runs are presented in this appendix.

Tables A.1 to A.5 contain the pertinent data for each run. A list of the tabulated parameters is given below.

T_{bi} : Measured Inlet Bulk Temperature, °C.

T_{bo}^{*} : Calculated Outlet Bulk Temperature, °C (See section 4.2.1).

Q : Flow Rate, cm^3/s.

α : Angle of Inclination, (measured from the horizontal).

Power: Applied Power to the Heater, Watts.

Re : Reynolds Number, Based on Diameter ($Re = \rho VD/\mu$).

Gr : Grashof Number, Based on Applied Heat Flux

$$\left(Gr = \left[\frac{g\beta\rho^2 D^4}{\mu^2 k} \right] q_w'' \right)$$

In the flow visualization experiments, the dye injection technique described in Chapter 3 was used. Photographs of the injected dye patterns are given in Figs. A.1 to

A.35. Descriptions and discussions of these results are presented concisely in Chapter 4.

Run #	T_{bi} °C	T_{bo}^{*} °C	Q cm^3/s	Power Watts	Re	$Grx10^{-5}$	Gr/Re^2
1	12.2	23.4	0.60	28.3	37.8	1.04	72.8
2	18.5	30.1	0.57	27.5	41.3	1.89	111.
3	17.6	25.5	1.85	61.4	127.2	3.30	20.4
4	20.4	30.2	0.96	39.5	72.1	2.95	56.8
5	20.2	30.9	2.33	104.0	174.9	7.95	26.0

Table A.1: Summary of Parameters for the Vertical-Tube (α = 90°) Flow-Visualization Runs.

Run #	T_{bi} °C	T_{bo}^{*} °C	Q cm^3/s	Power Watts	Re	$Grx10^{-5}$	Gr/Re^2
14	10.6	24.1	0.69	39.0	43.1	1.36	73.0
15	8.8	20.7	1.93	96.4	112.5	2.45	19.4
16	9.1	19.4	1.24	53.2	71.2	1.26	25.0
17	9.7	19.4	2.47	100.6	143.4	2.47	12.0
18	11.6	20.7	0.51	19.8	31.1	0.60	61.9
19	8.4	17.3	3.89	144.4	215.7	2.80	6.00

Table A.2: Summary of Parameters for the Horizontal-Tube (α = 0°) Flow-Visualization Runs.

Run #	T_{bi} °C	T_{bo}^{*} °C	Q cm^3/s	Power Watts	Re	Gr $x10^{-5}$	Gr/Re^2	α
6	9.5	19.7	1.02	43.8	59.4	1.09	30.9	45°
7	8.5	20.8	1.96	100.8	113.9	2.52	19.5	45°
8	10.4	22.3	0.69	34.5	41.9	1.07	60.8	45°
9	8.9	18.9	2.48	103.8	141.4	2.34	11.7	45°
10	8.8	18.4	1.50	60.0	84.9	1.30	18.0	45°
11	11.6	21.0	0.49	19.1	29.4	0.58	67.6	45°
12	9.5	19.2	3.59	145.9	207.2	3.52	8.21	45°
13	9.2	18.7	2.68	106.6	152.9	2.41	10.3	45°
20	8.3	18.2	2.52	104.4	141.4	2.16	10.8	60°
21	. 10.2	21.9	0.66	32.0	39.6	0.95	60.9	60°
22	9.7	19.7	0.93	39.1	54.2	0.99	33.6	60°
23	8.9	20.8	1.90	95.1	111.2	2.43	19.7	60°
24	8.8	18.2	1.71	67.2	96.5	1.43	15.4	60°
25	9.0	18.2	3.76	144.5	212.7	3.14	6.94	60°
33	9.9	20.7	0.82	37.3	48.4	1.02	43.4	30°
34	19.1	28.9	1.67	68.4	121.4	4.60	31.2	30°
35	10.1	19.8	2.94	119.2	172.2	3.08	10.4	30°

Table A.3: Summary of Parameters for the Tilted-Tube Flow-Visualization Runs.

Run #	T_{bi} °C	T_{bo}^{*} °C	Q cm^3/s	Power Watts	Re	Gr $x10^{-5}$	Gr/Re^2	α
26	12.6	28.5	0.36	23.9	24.1	1.17	200.	76°
27	8.9	18.7	2.24	92.2	127.4	2.04	12.6	76°
28	9.1	20.3	1.19	55.4	69.3	1.39	29.0	76°
29	9.6	19.5	3.46	144.2	200.6	3.54	8.81	76°
30	8.6	17.9	1.75	68.2	98.0	1.39	14.5	87°
31	8.8	20.9	1.30	65.7	76.0	1.69	29.3	87°
32	10.4	22.3	0.61	30.1	36.9	0.93	68.5	87°

Table A.4: Summary of Parameters for the Near-Vertical Flow-Visualization Runs.

Run #	Res. (Ohms)
1	177.61
2	177.64
3	179.24
4	177.83
5	180.09
6	176.00
7	177.73
8	175.73
9	175.16
10	176.33
11	175.47
12	179.56

Run #	Res. (Ohms)
13	178.30
14	176.19
15	177.62
16	176.39
17	178.01
18	175.41
19	179.17
20	176.67
21	175.11
22	175.41
23	177.23
24	176.40

Run #	Res. (Ohms)
25	178.97
26	175.88
27	177.32
28	176.37
29	179.39
30	176.86
31	176.87
32	176.01
33	175.37
34	176.32
35	178.38

Table A.5: Overall Electrical Resistance of the Gold-Film Heater During each Flow-Visualization Run.

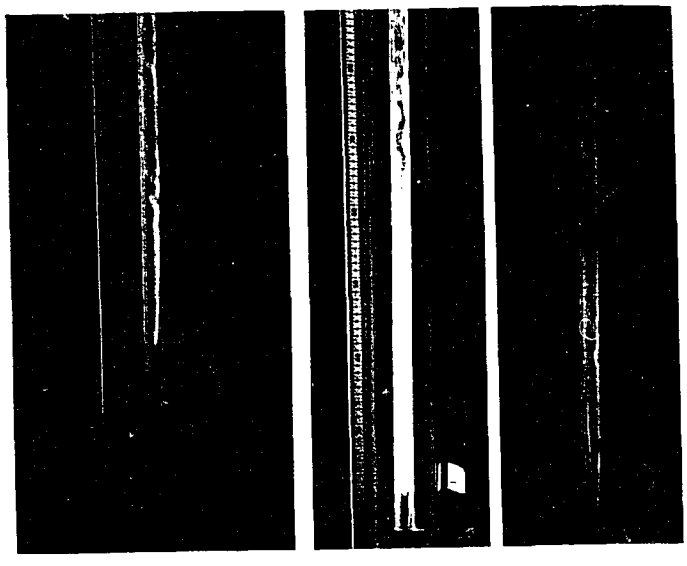

A.1 A.2(a) A.2(b)

Figure A.1 : Run #1, $Gr/Re^2 = 72.8$, $\alpha = 90°$;
A.2(a)&(b) : Run #2, $Gr/Re^2 = 111.$, $\alpha = 90°$.

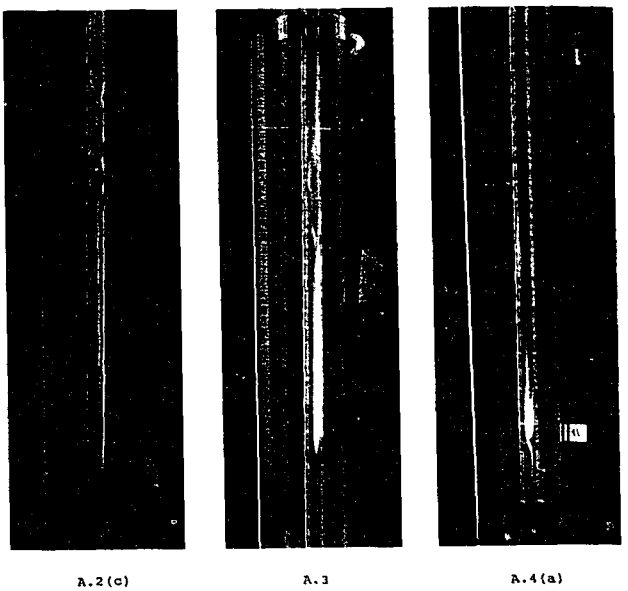

A.2(c) A.3 A.4(a)

Figure **A.2(c)** : Run #2, $Gr/Re^2 = 111.$, $\alpha = 90°$;
A.3 : Run #3, $Gr/Re^2 = 20.4$, $\alpha = 90°$;
A.4(a) : Run #4, $Gr/Re^2 = 56.8$, $\alpha = 90°$.

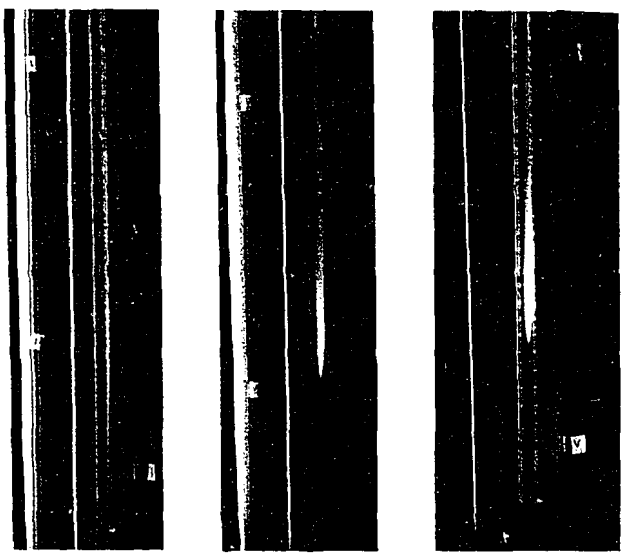

Figure **A.4(b)** : Run #4, $Gr/Re^2 = 56.8$, $\alpha = 90°$;
A.5(a)&(b) : Run #5, $Gr/Re^2 = 26.0$, $\alpha = 90°$.

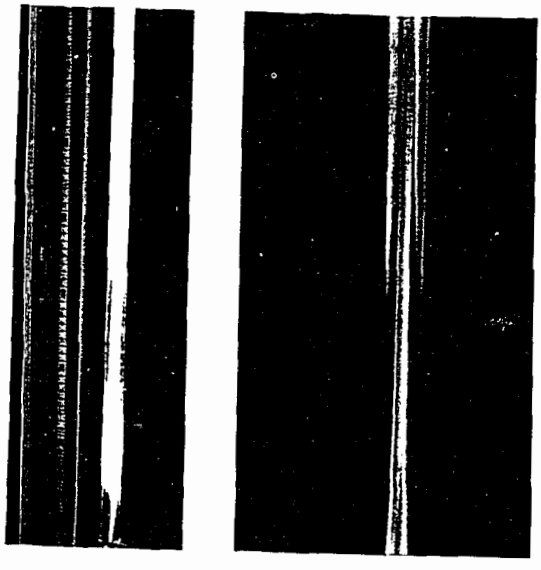

A.6(a)

A.6(b)

Figure A.6(a)&(b) : Run #14, $Gr/Re^2 = 73.0$, $\alpha = 0°$.

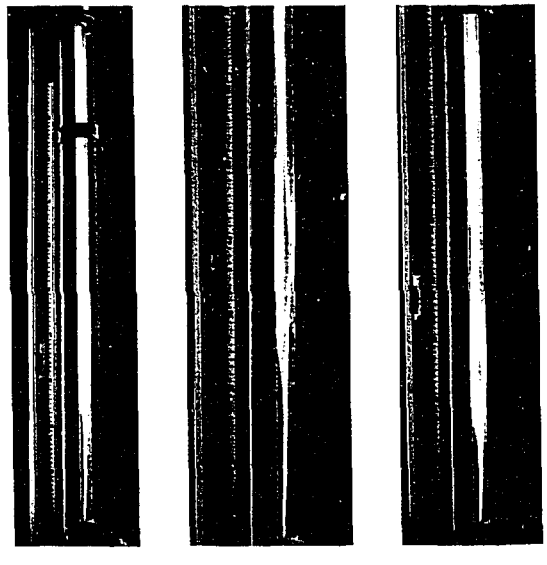

A.7(a) A.7(b) A.8(a)

Figure A.7(a)&(b) : Run #15, $Gr/Re^2 = 19.4$, $\alpha = 0°$;
A.8(a) : Run #16, $Gr/Re^2 = 25.0$, $\alpha = 0°$.

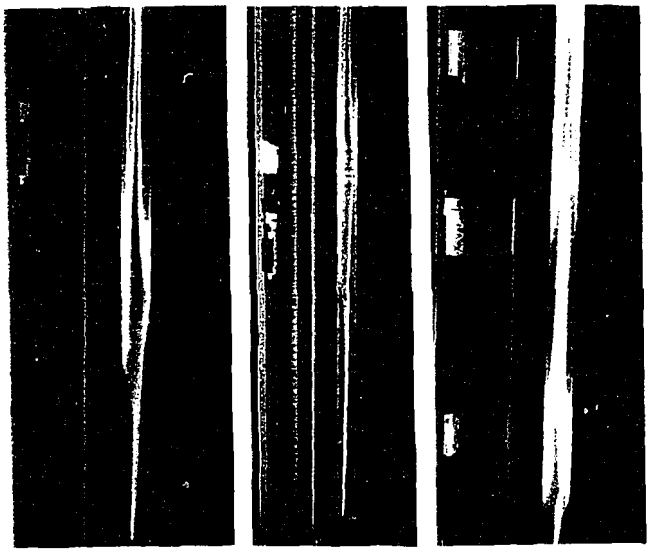

A.8(b) A.9 A.10(a)

Figure **A.8(b)** : Run #16, $Gr/Re^2 = 25.0$, $\alpha = 0°$;
A.9 : Run #17, $Gr/Re^2 = 12.0$, $\alpha = 0°$;
A.10(a) : Run #18, $Gr/Re^2 = 61.9$, $\alpha = 0°$.

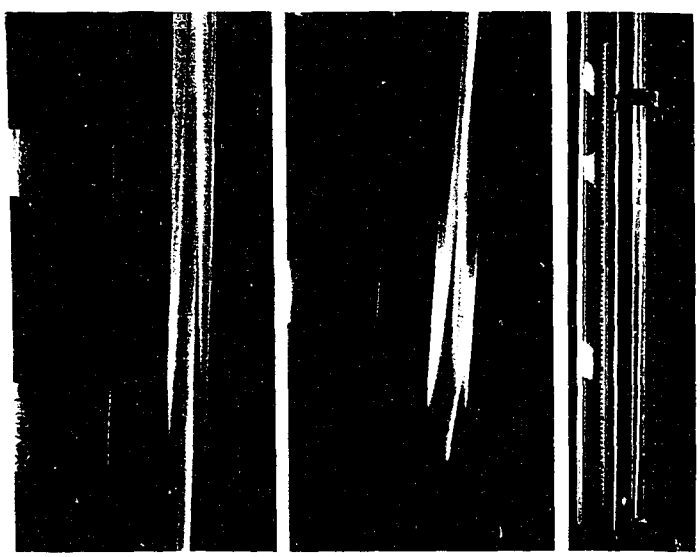

A.10(b) A.10(c) A.11

Figure **A.10(b)&(c)** : Run #18, $Gr/Re^2 = 61.9$, $\alpha = 0°$;
A.11 : Run #19, $Gr/Re^2 = 6.00$, $\alpha = 0°$.

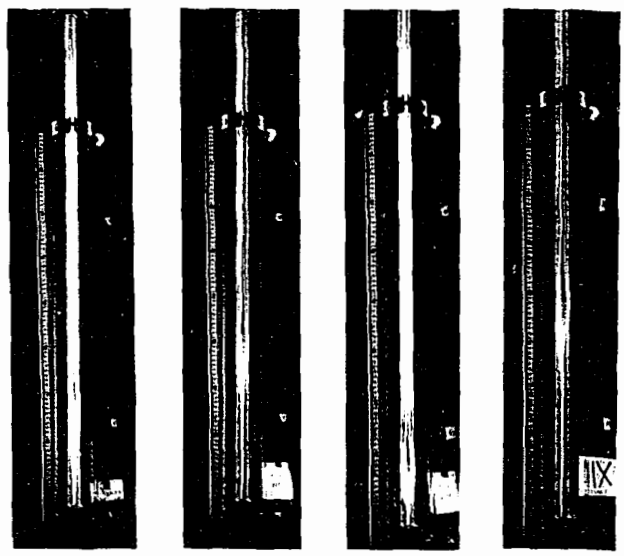

A.12 A.13 A.14 A.15

Figure **A.12** : Run #6, $Gr/Re^2 = 30.9$, $\alpha = 45°$;
A.13 : Run #7, $Gr/Re^2 = 19.5$, $\alpha = 45°$;
A.14 : Run #8, $Gr/Re^2 = 60.8$, $\alpha = 45°$;
A.15 : Run #9, $Gr/Re^2 = 11.7$, $\alpha = 45°$.

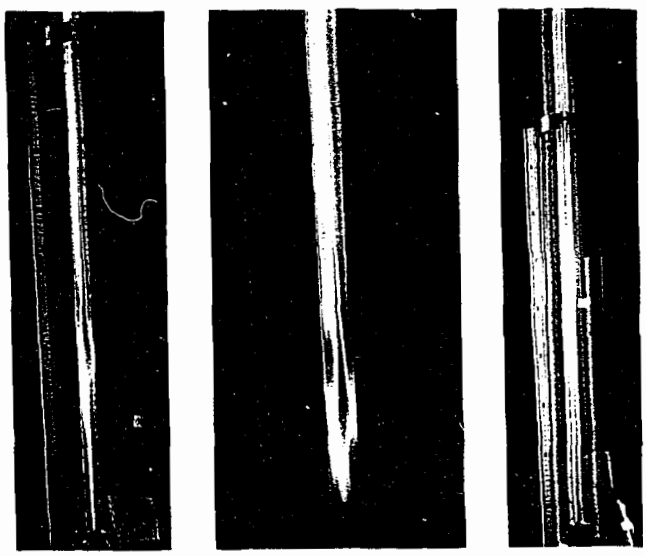

A.16 A.17 A.18

Figure **A.16** : Run #10, $Gr/Re^2 = 18.0$, $\alpha = 45°$;
A.17 : Run #11, $Gr/Re^2 = 67.6$, $\alpha = 45°$;
A.18 : Run #12, $Gr/Re^2 = 8.21$, $\alpha = 45°$.

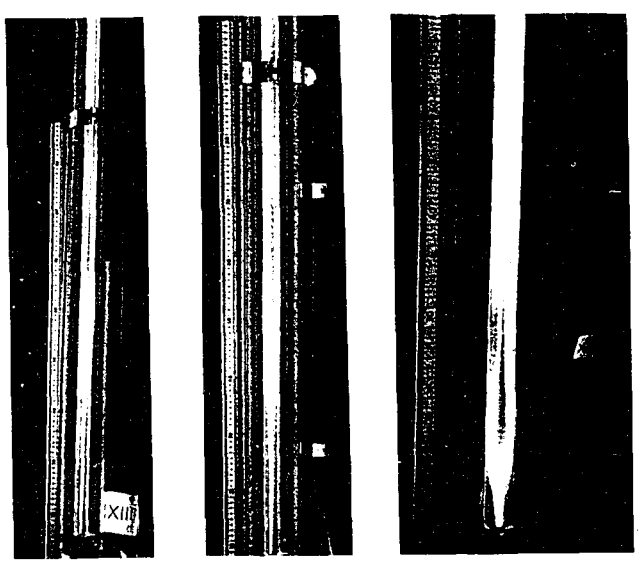

A.19 A.20 A.21(a)

Figure **A.19** : Run #13, $Gr/Re^2 = 10.3$, $\alpha = 45°$;
A.20 : Run #20, $Gr/Re^2 = 10.8$, $\alpha = 60°$;
A.21(a) : Run #21, $Gr/Re^2 = 60.9$, $\alpha = 60°$.

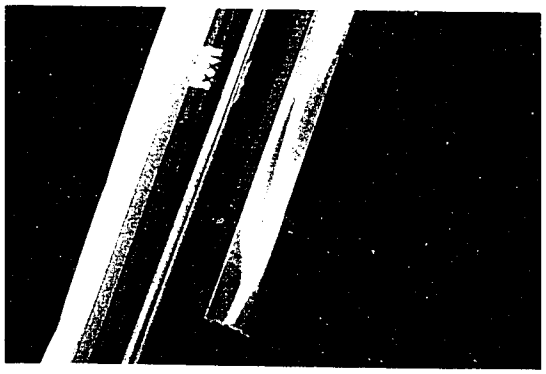

A.21(b)

A.22(a)

Figure **A.21(b)** : Run #21, $Gr/Re^2 = 60.9$, $\alpha = 60°$;
A.22(a) : Run #22, $Gr/Re^2 = 33.6$, $\alpha = 60°$.

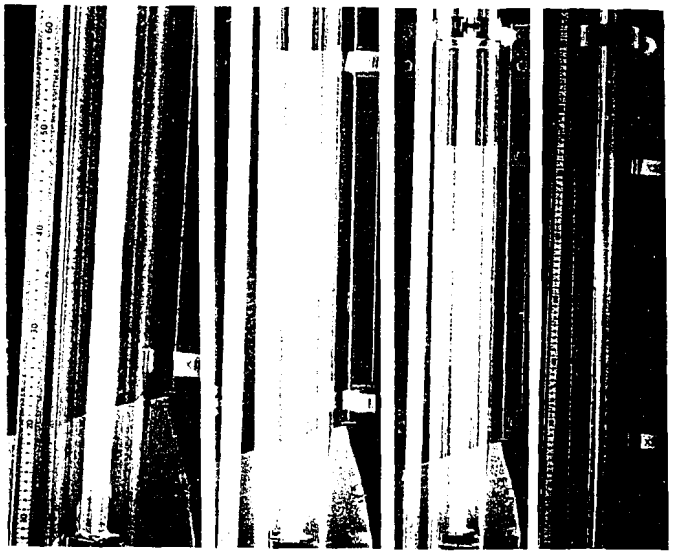

A.22(b) A.23 A.24 A.25

Figure **A.22(b)** : Run #22, $Gr/Re^2 = 33.6$, $\alpha = 60°$;
A.23 : Run #23, $Gr/Re^2 = 19.7$, $\alpha = 60°$;
A.24 : Run #24, $Gr/Re^2 = 15.4$, $\alpha = 60°$;
A.25 : Run #25, $Gr/Re^2 = 6.94$, $\alpha = 60°$.

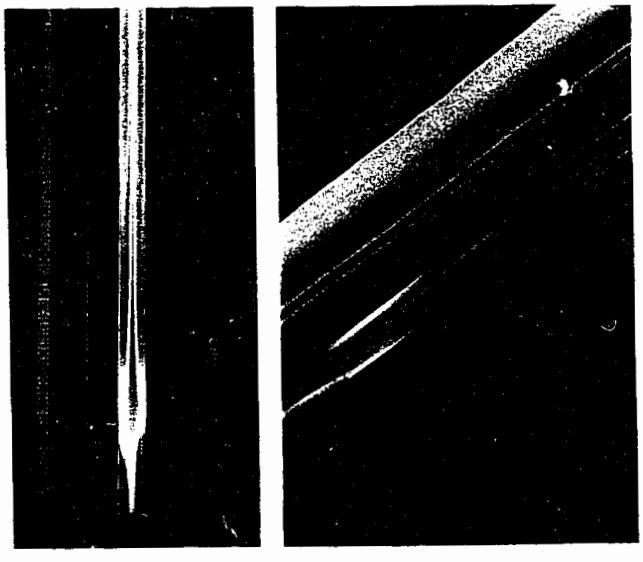

A.26(a) A.26(b)

Figure A.26(a)&(b) : Run #33, $Gr/Re^2 = 43.4$, $\alpha = 30°$.

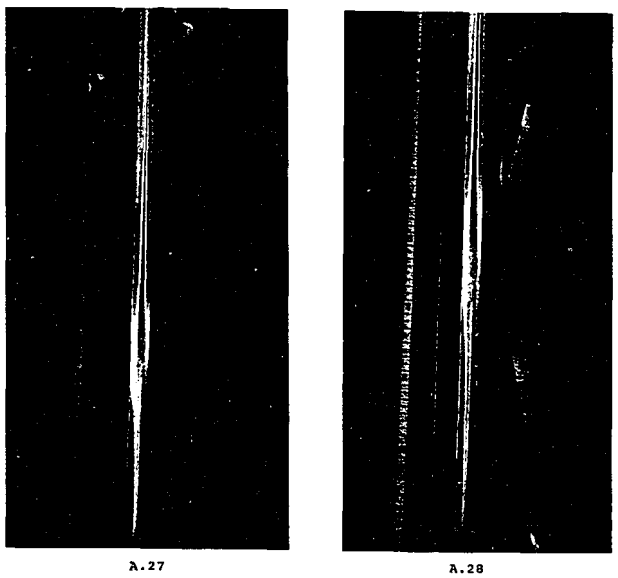

A.27 A.28

Figure A.27 : Run #34, $Gr/Re^2 = 31.2$, $\alpha = 30°$;
A.28 : Run #35, $Gr/Re^2 = 10.4$, $\alpha = 30°$.

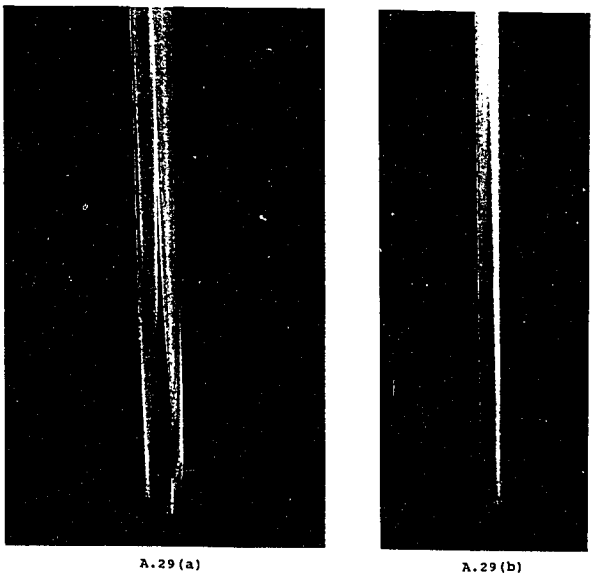

Figure A.29(a)&(b) : Run #26, $Gr/Re^2 = 200.$, $\alpha = 76°$.

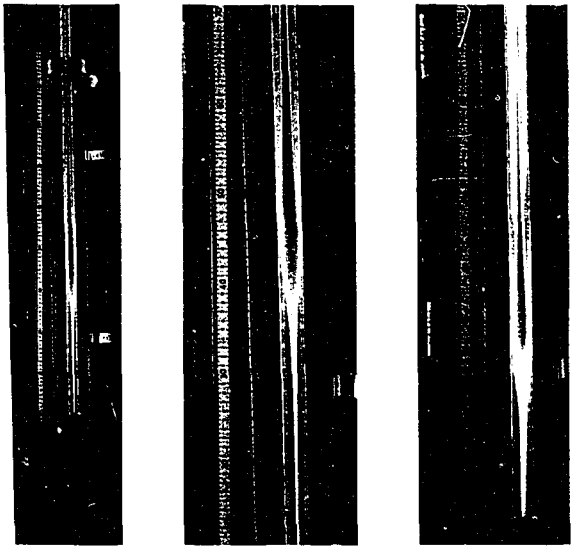

Figure **A.30(a)&(b)** : Run #27, $Gr/Re^2 = 12.6$, $\alpha = 76°$;
A.31(a) : Run #28, $Gr/Re^2 = 29.0$, $\alpha = 76°$.

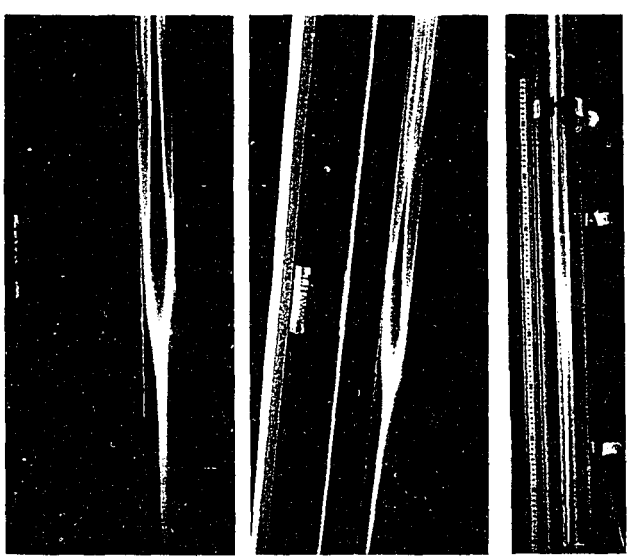

A.31(b) A.31(c) A.32

Figure A.31(b)&(c) : Run #28, $Gr/Re^2 = 29.0$, $\alpha = 76°$;
A.32 : Run #29, $Gr/Re^2 = 8.81$, $\alpha = 76°$.

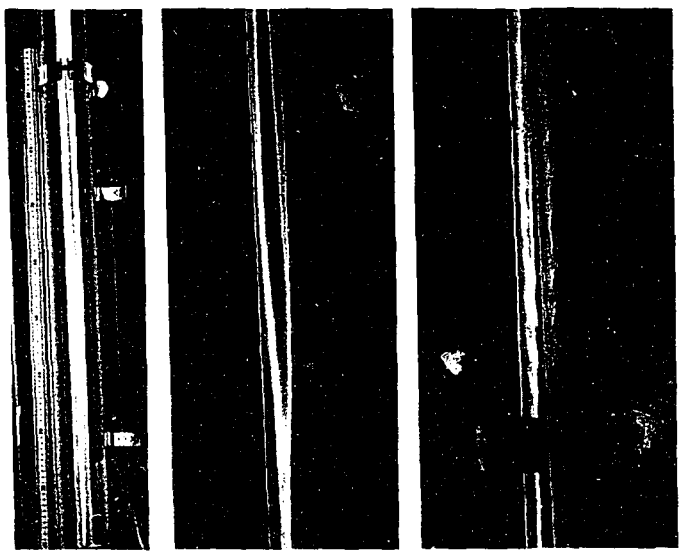

Figure A.33(a),(b)&(c) : Run #30, $Gr/Re^2 = 14.5$, $\alpha = 87°$.

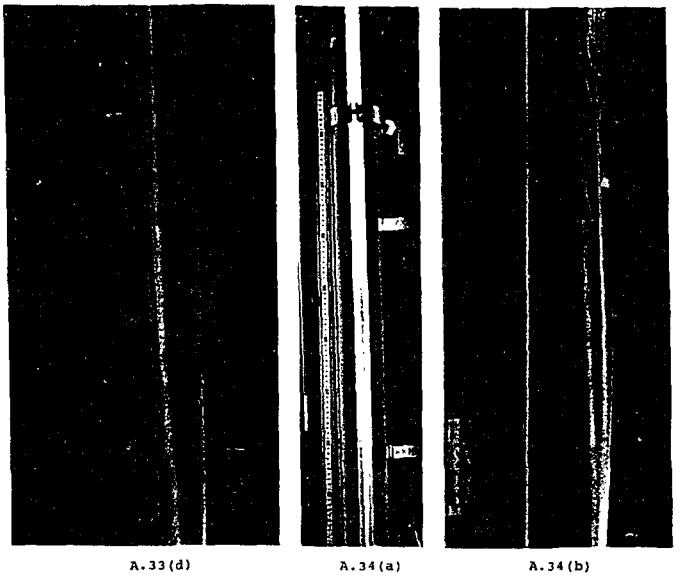

Figure **A.33(d)** : Run #30, $Gr/Re^2 = 14.5$, $\alpha = 87°$.
A.34(a)&(b) : Run #31, $Gr/Re^2 = 29.3$, $\alpha = 87°$.

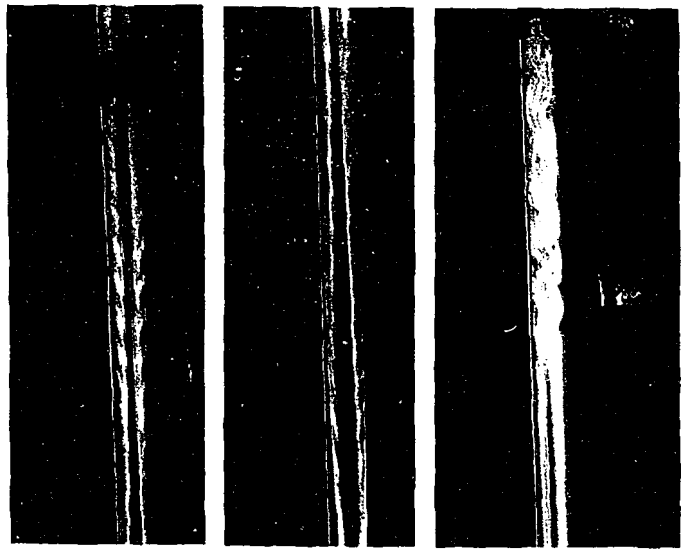

Figure A.34(d)&(c) : Run #31, $Gr/Re^2 = 29.3$, $\alpha = 87°$;
A.35(a) : Run #32, $Gr/Re^2 = 68.5$, $\alpha = 87°$.

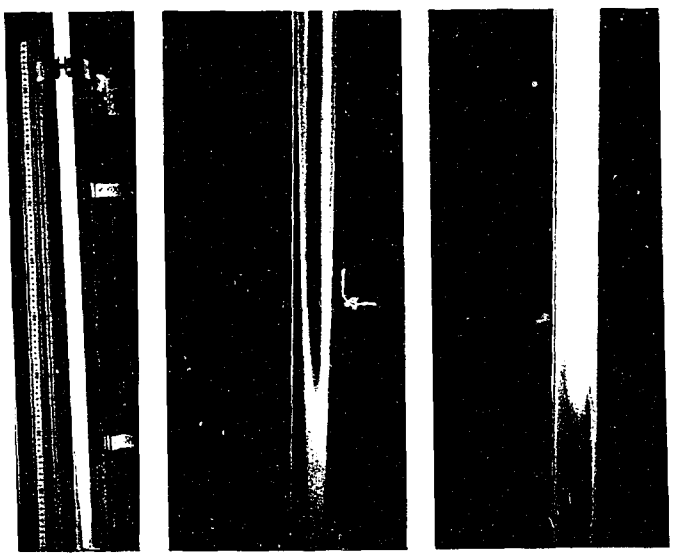

Figure A.35(b),(c)&(d) : Run #32, $Gr/Re^2 = 68.5$, $\alpha = 87°$.

APPENDIX B

RESULTS OF THE TEMPERATURE RUNS

In this Appendix, the measured and calculated data for the experimental runs using test section no. 1 are tabulated. In these runs, temperature measurements were obtained using the thermocouples attached to the gold-film heater. Flow-visualization photographs were also taken, using the dye injection technique described in Chapter 3. These photographs are given in figures B.1 to B.3.

Tables B.1 and B.6 contain the pertinent experimental data for each run. A list of the tabulated parameters is given below.

T_{bi} : Measured Inlet Bulk Temperature, °C.

T_{bo} : Measured Outlet Bulk Temperature, °C.

T_{bo}^{*} : Calculated Outlet Bulk Temperature, °C (See section 4.2.1).

Q : Flow Rate, cm^3/s.

α : Angle of Inclination, (measured from the horizontal).

V : Voltage Applied to the Gold-Film Heater, Volts.

I : Current Applied to the Gold-Film Heater, Amps.

Re : Reynolds Number, Based on Diameter ($Re = \rho VD/\mu$).

Gr : Grashof Number, Based on Applied Heat Flux

$$\left(Gr = \left[\frac{g\beta\rho^2 D^4}{\mu^2 k} \right] q''_w \right)$$

$mC_p\delta T_b$: Calculated Energy Gain of the Fluid Based on the Measured Inlet and Outlet Bulk Temperature Difference, Watts

($P_f = mC_p\delta T_b$).

VI : The Applied Power, Watts ($P_a = VI$).

%Diff: The Percent Difference Between P_a and P_f

($\%Diff = | P_a - P_f | / P_a$).

CASE#	T_{bi} °C	T_{bo} °C	Q cm^3/s	$\rho C_p \times 10^4$ $J/m^3°K$	$mC_p\delta T_b$ Watts	V Volts	I Amps	VI Watts	%Diff
38-A	8.6	17.8	2.31	4.19	89.6	131.9	0.736	97.03	7.66
38-B	8.6	18.0	2.23	4.19	87.8	131.8	0.735	96.91	9.44
38-C	8.6	18.1	2.21	4.19	88.6	131.8	0.735	96.93	8.63
39-A	8.7	17.4	2.49	4.19	91.4	131.8	0.737	97.1	5.94
39-B	8.7	17.7	2.48	4.19	93.0	131.8	0.737	97.1	4.24
39-C	8.7	17.7	2.47	4.19	92.9	131.8	0.737	97.1	4.35
40-A	8.7	17.9	2.55	4.19	98.0	133.8	0.746	99.9	1.88
40-B	8.7	17.9	2.55	4.19	97.8	133.8	0.746	99.9	2.03

Table B.1: Summary of Parameters for the Temperature Runs.

CASE #	α	T_{bo}^* °C	Re	$Grx10^{-5}$	Gr/Re^2
38-A	0°	18.61	130.7	2.10	12.29
38-B	0°	18.94	126.7	2.14	13.36
38-C	0°	19.04	125.7	2.16	13.66
39-A	45°	17.97	139.8	2.02	10.32
39-B	45°	18.05	139.5	2.04	10.46
39-C	45°	18.05	138.9	2.03	10.52
40-A	90°	18.03	143.4	2.09	10.16
40-B	90°	18.03	143.4	2.09	10.16

Table B.2: Angle of Inclination, Calculated Outlet Bulk Temperature, and Non-Dimensional Parameters of the Temperature Runs.

	CASE #38-A		CASE #38-B		CASE #38-C	
Location, z/L	Temp. °C θ= 90°	Temp. °C θ= 270°	Temp. °C θ= 45°	Temp. °C θ= 225°	Temp. °C θ= 0°	Temp. °C θ= 180°
0.093	37.44	34.24	35.73	34.53	34.17	35.14
0.205	39.85	34.61	37.65	34.99	35.12	35.90
0.317	41.44	35.12	39.47	35.52	36.05	36.75
0.429	43.10	35.90	40.36	36.25	37.02	37.45
0.541	44.23	36.47	41.77	36.91	37.75	38.33
0.653	45.02	36.52	42.19	37.02	38.23	38.72
0.765	44.94	38.04	41.84	38.39	37.53	40.14
0.877	47.54	37.89	44.82	38.06	40.03	39.85

Table B.3: Temperature Readings of Run #38.

	CASE #39-A		CASE #39-B		CASE #39-C	
Location, z/L	Temp. °C θ= 0°	Temp. °C θ= 180°	Temp. °C θ= 45°	Temp. °C θ= 225°	Temp. °C θ= 90°	Temp. °C θ= 270°
0.093	33.36	34.31	34.50	34.36	35.14	33.96
0.205	34.07	34.77	35.69	34.72	36.87	34.25
0.317	34.79	35.46	36.58	35.19	38.11	34.84
0.429	35.85	36.27	37.36	35.88	39.40	35.75
0.541	36.41	37.02	38.17	36.50	40.09	36.41
0.653	36.96	37.33	38.73	36.91	40.58	36.65
0.765	36.45	38.90	38.24	38.59	40.12	38.34
0.877	38.85	38.78	40.78	38.55	42.40	38.44

Table B.4: Temperature Readings of Run #39.

	CASE #40-A		CASE #40-B	
Location, z/L	Temp. °C θ= 90°	Temp. °C θ= 270°	Temp. °C θ= 0°	Temp. °C θ= 180°
0.093	34.85	35.74	34.63	35.69
0.205	36.49	37.00	36.21	37.01
0.317	37.69	38.23	37.39	38.29
0.429	38.93	39.30	38.71	39.46
0.541	39.48	40.00	39.26	40.11
0.653	39.98	40.16	39.71	40.25
0.765	39.33	41.74	39.06	41.83
0.877	41.55	41.58	41.23	41.69

Table B.5: Temperature Readings of Run #40.

Case #	Res. (Ohms)
38-A	179.23
38-B	179.34
38-C	179.34
39-A	178.93
39-B	178.93
39-C	178.95
40-A	179.28
40-B	179.33

Table B.6: Overall Electrical Resistance of the Gold-Film Heater During each Temperature Run.

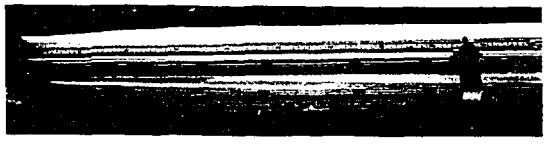

B.1(a)

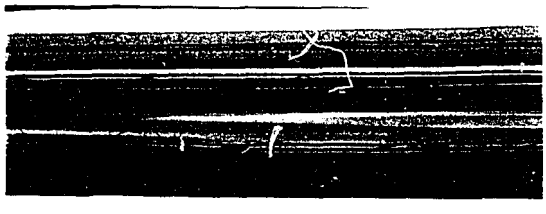

B.1(b)

Figure B.1: Horizontal-Tube (α=0°), Temperature Run #38; (a) large view; (b) close-up.

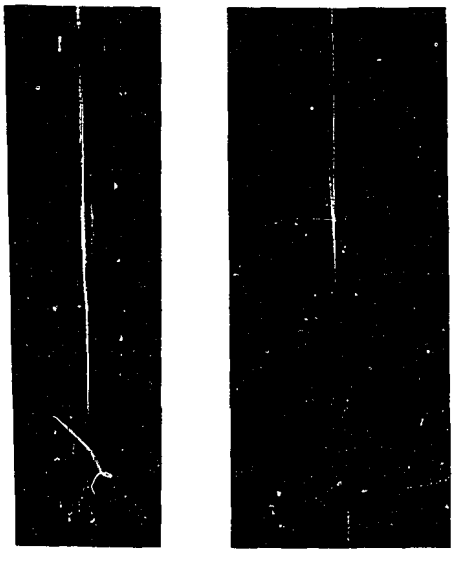

B.2(a) B.2(b)

Figure B.2: Inclined-Tube (α=45°), Temperature Run #39; (a) large view; (b) close-up.

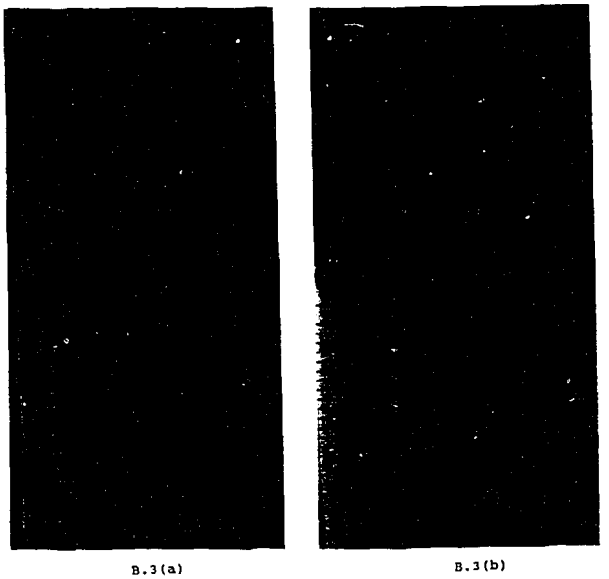

B.3(a) B.3(b)

Figure B.3: Vertical-Tube (α=90°), Temperature Run #40; (a) recirculation cell; (b) laminar instability.

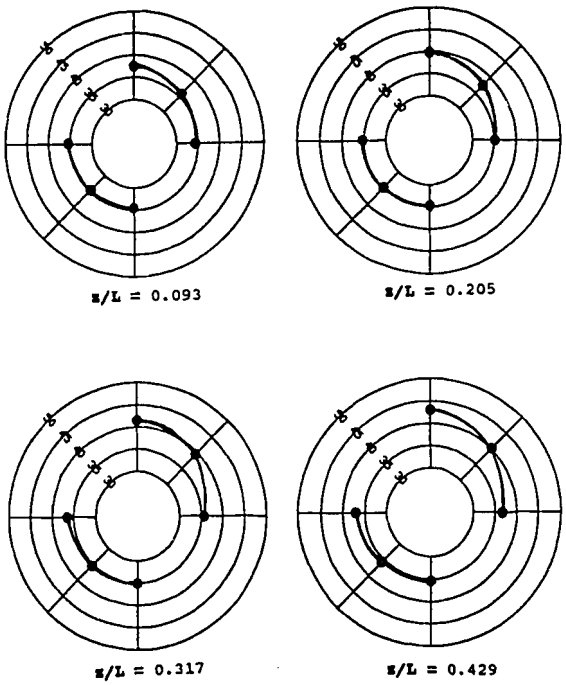

On the radial axis, are plotted the temperature readings (in °C).

z : Axial distance from the inlet plane of the heated section of the tube.
L : Total length of the heated section of the tube.

Figure B.4(a): Polar Plots of the Temperature Readings of Run #38.

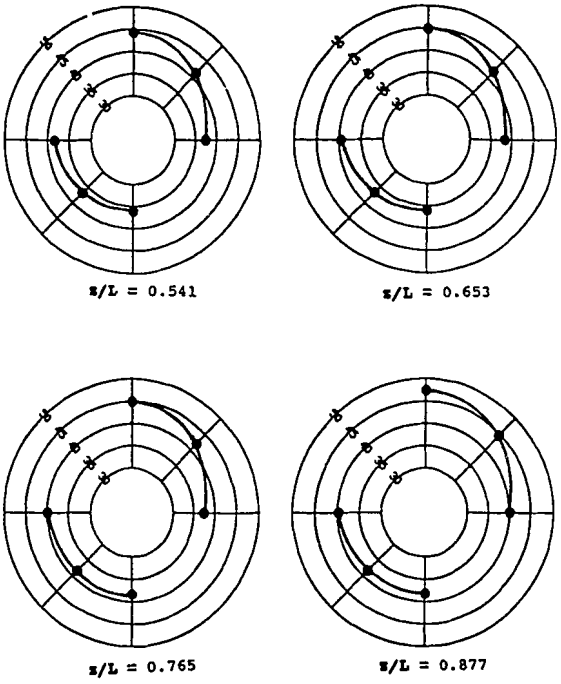

Figure B.4(b): Polar Plots of the Temperature Readings of Run #38

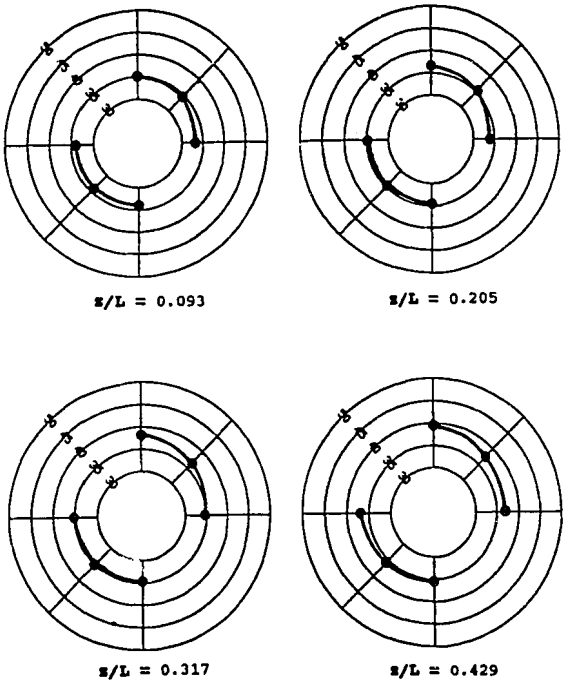

On the radial axis, are plotted the temperature readings (in °C).

z : Axial distance from the inlet plane of the heated section of the tube.
L : Total length of the heated section of the tube.

Figure B.5(a): Polar Plots of the Temperature Readings of Run #39

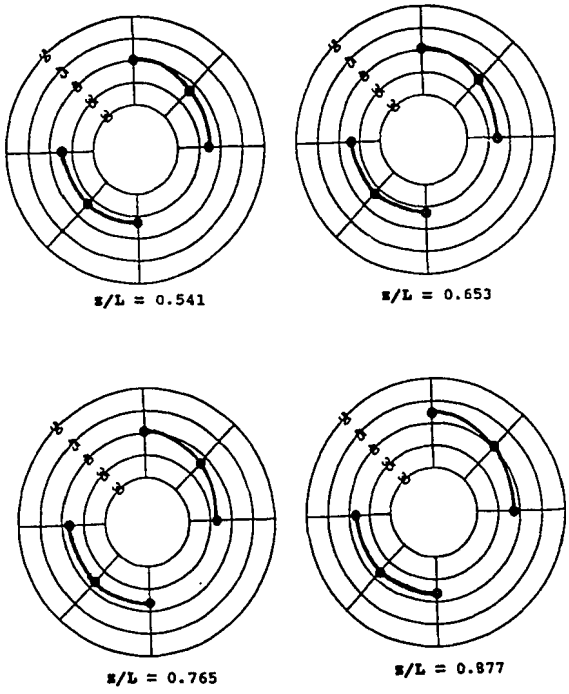

Figure B.5(b): Polar Plots of the Temperature Readings of Run #39

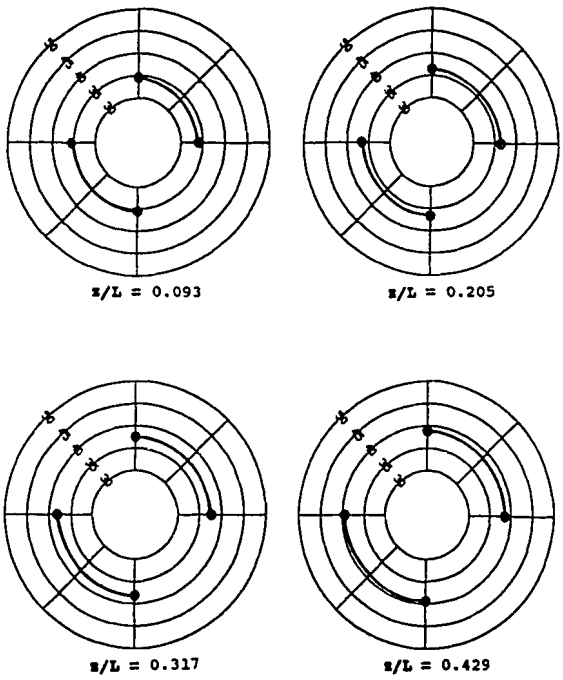

On the radial axis, are plotted the temperature readings (in °C).

z : Axial distance from the inlet plane of the heated section of the tube.
L : Total length of the heated section of the tube.

Figure B.6(a): Polar Plots of the Temperature Readings of Run #40.

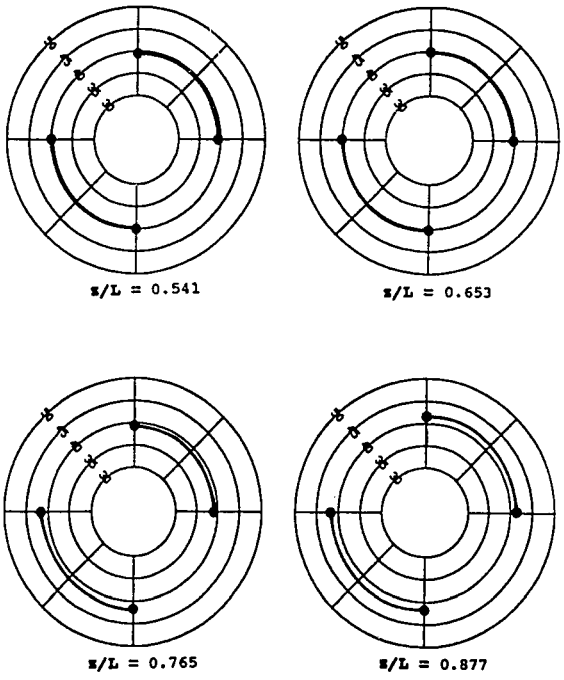

Figure B.6(b): Polar Plots of the Temperature Readings of Run #40

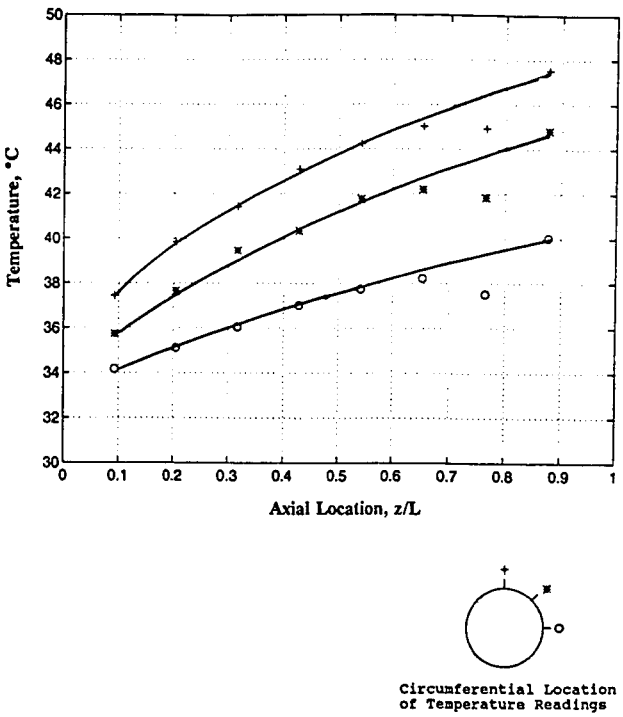

Figure B.7(a): Graph of Temperature Readings versus Axial Location for Run #38.

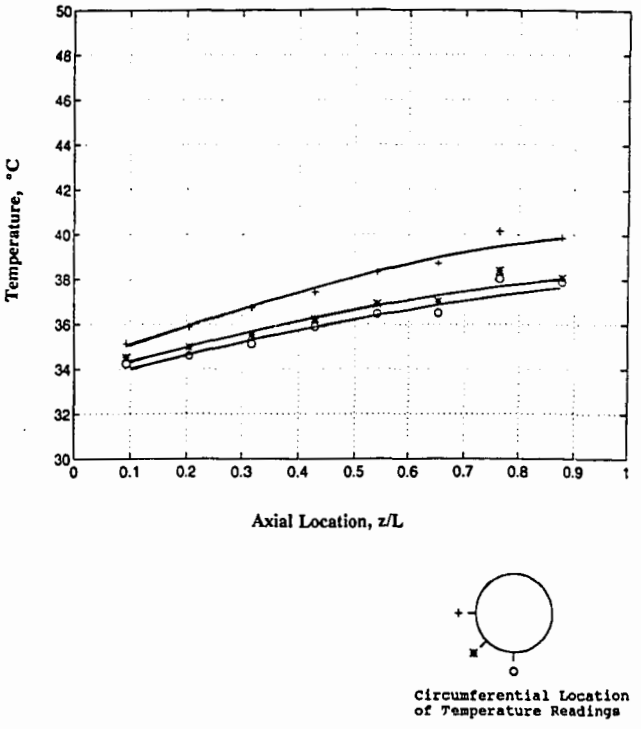

Figure B.7(b): Graph of Temperature Readings versus Axial Location for Run #38.

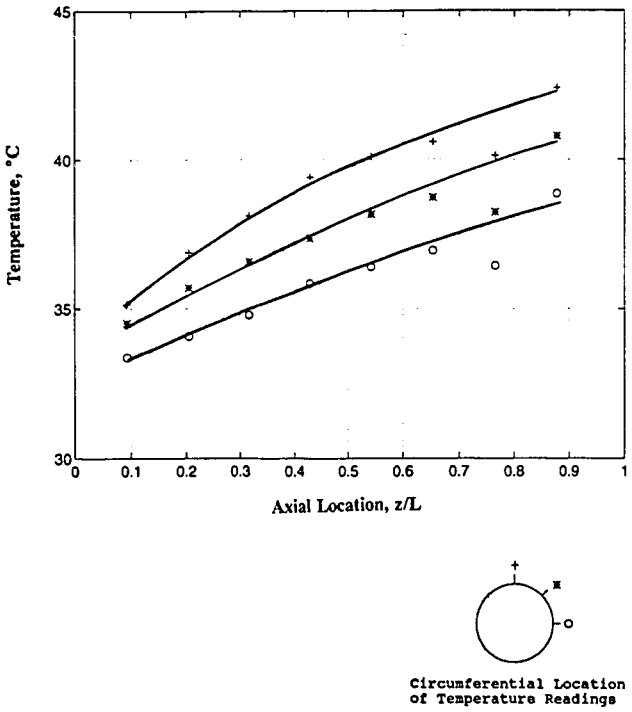

Figure B.8(a): Graph of Temperature Readings versus Axial Location for Run #39.

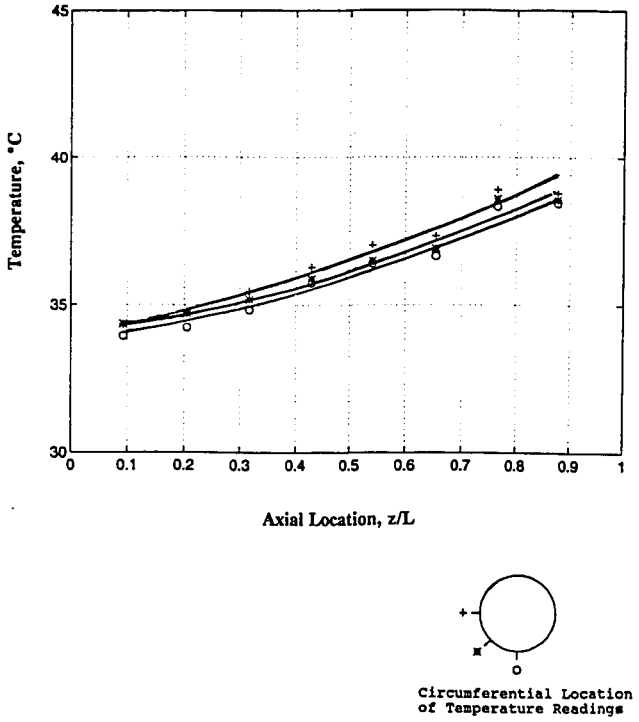

Figure B.8(b): Graph of Temperature Readings versus Axial Location for Run #39.

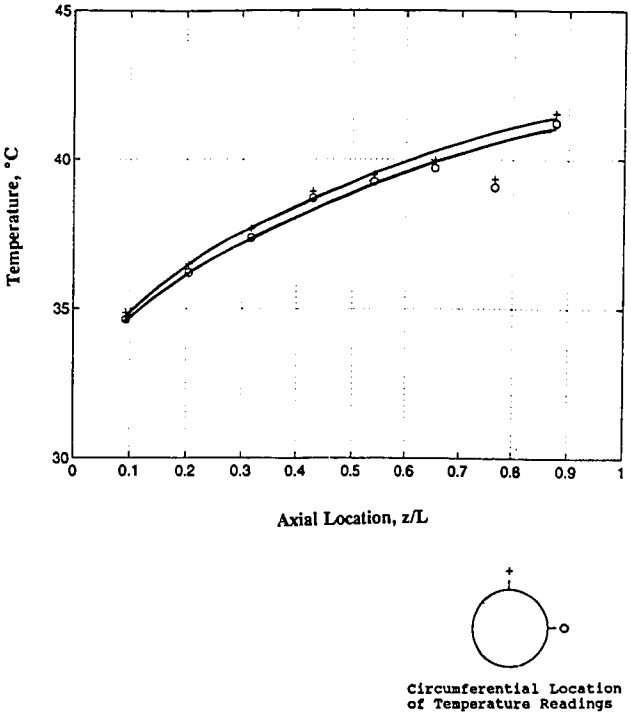

Figure B.9(a): Graph of Temperature Readings versus Axial Location for Run #40.

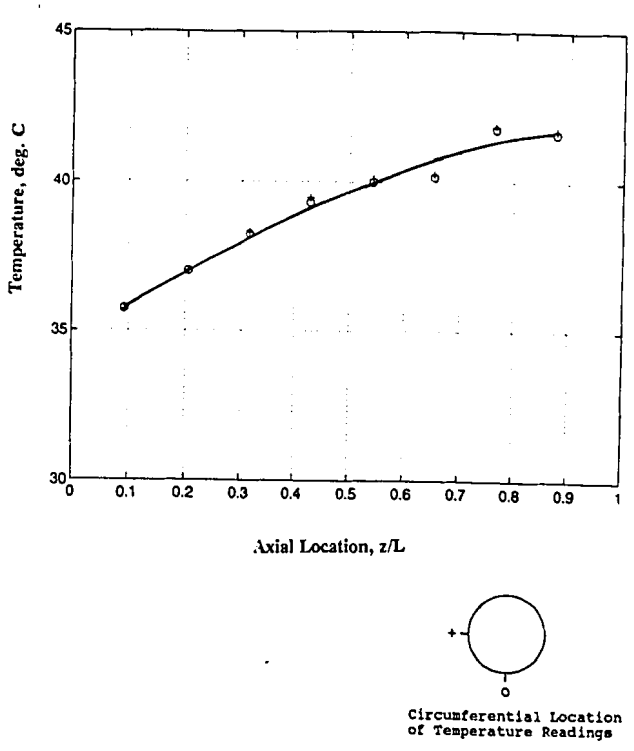

Figure B.9(b): Graph of Temperature Readings versus Axial Location for Run #40.